# EFFECTS OF INTERACTIONS IN MESOSCOPIC SYSTEMS

DIMITRY M. GANGARDT

# EFFECTS OF INTERACTIONS IN MESOSCOPIC SYSTEMS

FINAL PAPER

SUBMITTED IN PARTIAL FULFILLMENT OF THE REQUIREMENTS
FOR THE DEGREE OF DOCTOR OF SCIENCE

## DIMITRY M. GANGARDT

# ACKNOWLEDGMENT

# Contents

# List of Figures

# Abstract

In this thesis the effects of interactions between electrons in mesoscopic systems are studied. One part is devoted to the study of mesoscopic super-conductors in which the size of the system is comparable to both coherence length and London penetration depth. In recent experiments performed on small aluminium disks the jumps of magnetisation as a function of external magnetic field were observed. We show that these jumps are due to the penetration of the magnetic field into the sample in the form of vortices and determine the number of vortices by solving the Ginzburg-Landau equations in some geometries analytically at the dual point and in the London regime. In both cases the resulting expressions for magnetisation are in good qualitative agreement with the experimental results. Magnetisation curves at the dual point are in good quantitative agreement with experiments, since this regime is relevant for the most experimental situations. The Ginzburg-Landau equation in the London regime can be used to study the topology of magnetic field profile. Each solution can be classified by the set of topological numbers (index), the number of vortices being one of them. The topological study of the solutions of the Ginzburg-Landau equations is not specific to the London regime and can be extended to other experimentally relevant regimes as well as to the more complicated geometries of the sample.

Another part of this work deals with an interacting electrons in mesoscopic conductors. In parallel to the recent studies of such systems we study the localization in the Hilbert space of Tomonaga-Luttinger model. For the standard version of this model, the states are found to be extended in the basis of Slater determinants, representing the eigenstates of the non-interacting system. The linear dispersion which leads to the fact that these eigenstates are extended is replaced by one with random level spacings modeling the complicated one-particle spectra of realistic models. The localization properties of the eigenstates are studied. The interactions are simplified and an effective one-dimensional Lloyd model is obtained. The effects of many-body energy correlations are studied numerically. The eigenstates of the system are found to be localized in Fock space for any strength of the interactions, but the localization is not exponential.

1

# List of Symbols

$\vec{A}$      - vector potential

$a$      - inverse radius of a sample in units of $\sqrt{2}\lambda$

$\vec{B}$      - magnetic induction

$B_0$      - magnitude of magnetic induction in the center of the sample

$B_M$      - Meissner term of the magnetic induction

$B_V$      - vortex contribution to the magnetic induction

$B_{\bar{V}}$      - anti-vortex (image) contribution to the magnetic induction

$C_k$      - probability amplitude of the effective one-dimensional tight binding model

$D(z)$      - Vandermonde determinant

$d$      - vortex distance from the center in polygonal configuration

$E_n$      - $n$-th one-particle energy level

$E_{(\lambda)}$      - energy of excitation $(\lambda)$

$\mathcal{E}_k$      - effective on-site energy in the tight-binding model

$F$      - free energy

$F_S, F_N$      - free energy of super-conductor, normal metal

$\mathcal{F}$      - super-conductor free energy difference between finite and zero magnetic field

$G$      - Gibbs free energy

$G_S, G_N$      - Gibbs free energy of super-conductor, normal metal

$\mathcal{G}$      - super-conductor Gibbs free energy difference between finite and zero magnetic field

$g_{(l)}$      - number of group elements in the class $(l)$

$\vec{H}$      - magnetic field

$H_c, H_{c1}, H_{c2}$      - critical magnetic fields

$H_e$      - magnitude of external magnetic field

$H_n$      - matching field for entrance of $n$-th vortex

$\hat{H}$      - total Hamiltonian

$\hat{H}_0$      - non-interacting Hamiltonian

$\hbar = h/2\pi$      - Planck constant

$I_n(x)$      - modified Bessel functions of first kind

$\vec{j}$      - current density

$K_n(x)$      - modified Bessel functions of second kind

$M$      - magnetisation

| | | |
|---|---|---|
| $N, n$ | - | number of vortices |
| $\mathcal{N}$ | - | demagnetisation factor |
| $N_M, N_m, N_s$ | - | number of maxima, minima, saddle points |
| $N_{sb}$ | - | number of saddle points on the boundary |
| $\hat{n}$ | - | unit vector normal to the surface of the sample |
| $P$ | - | permutation, inverse participation ratio |
| $R$ | - | radius of the sample |
| $r, \theta$ | - | polar coordinates |
| $S_N$ | - | symmetric group of $N$ elements |
| $S_{(l)}$ | - | totally symmetric function |
| $s_l(z)$ | - | power sum |
| $\hat{U}$ | - | interaction part of the total Hamiltonian |
| $V$ | - | hopping matrix element in the tight-binding model |
| $V_m$ | - | interaction matrix element |
| $z, \bar{z}$ | - | complex coordinates |
| $x$ | - | ratio of the distance from the center and the radius of the sample |
| $\alpha, \beta$ | - | coefficients in the expansion of the Ginzburg-Landau free energy |
| $\alpha(n)$ | - | power in the scaling ansatz for the free energy of $n$ vortices |
| $\Gamma$ | - | the curve separating the paramagnetic and diamagnetic regions |
| $\Delta$ | - | one-particle level spacing |
| $\delta$ | - | thickness of the magnetic field profile near the boundary of the sample |
| $\kappa$ | - | Ginzburg-Landau parameter |
| $\lambda$ | - | London penetration depth |
| $(\lambda)$ | - | a partition |
| $\xi$ | - | correlation length, localization length |
| $\phi_0 = hc/2e$ | - | flux quantum |
| $\chi$ | - | phase of the order parameter; Euler-Poincaré characteristic |
| $\chi_{(l)}^{(\lambda)}$ | - | character of irreducible representation of $S_N$ |
| $\Psi_{(\lambda)}(z)$ | - | totally anti-symmetric function |
| $\psi$ | - | order parameter of the Ginzburg-Landau theory |
| $\Omega$ | - | cross-section of the super-conducting sample |
| $\partial\Omega$ | - | boundary of the super-conducting cross-section $\Omega$ |

# Chapter 1

# Introduction

The present Ph.D. manuscript is devoted to the study of effects of interactions between electrons in mesoscopic systems. Recent developments in technology opened the possibility to carry out experimental research on systems of small (submicron) size, such that the geometric shape of the boundaries plays an important role in the physics of such systems. This systems still have a large number of atoms, so they cannot be considered microscopic. On the other hand, the small size of these systems allows for quantum phase coherence of electron wave functions to play an important role in their physics. Such systems are said to be mesoscopic, examples are the quantum dots or small superconducting grains of size comparable to the coherence length of electronic wave-functions (quantum dot) or superconucting order parameter (superconductors). In these systems the interactions between electrons are important, since it leads to effects such as finite life-time of electrons in a quantum dot or it is responsible for the onset of superconductivity in a superconductors. In this work we study the combined effects of interactions and finite size and geometry on the observable physical quantities. In order to achieve this goal the usual theoretical approaches to the interacting systems, such as perturbation theory, non-perturbative methods and exact solutions when applied to the mesoscopic systems are modified in order to take into account the finite geometry and the discreteness of the spectrum of the mesoscopic systems. Our research was motivated by the recent experimental and theoretical observation of non-trivial effects of interactions in mesoscopic systems. One of them is the discontinuous behavior of magnetization of a type II superconductor which can be attributed to the sudden appearance of the vortex inside the sample. It is worth mentioning here that the vortex interactions plays an important role even in the case of infinite system and it remains essential for the vortices in a mesoscopic sample. Another interesting problem considered in this Ph.D. thesis is related to the existence of the quasiparticle excitations in small conductors and their stability as compared to the Landau Fermi liquid theory which is the main theoretical tool to describe the properties of macroscopic conductors. Mapping the interacting system onto a problem of hopping on an effective lattice we study the life-time of a quasiparticle within the framework of Anderson localization.

The study of magnetic behavior of small superconductors was triggered by recent experiments [1, 2] where the magnetization of small aluminum disks was measured. It has been observed that instead of going to zero abruptly at the critical field as in the bulk type I superconductors or decreasing smoothly down to zero as in the type II materials, the magnetization of the disks shows a series of discontinuous jumps, see Fig. 1.1. The periodicity of these jumps
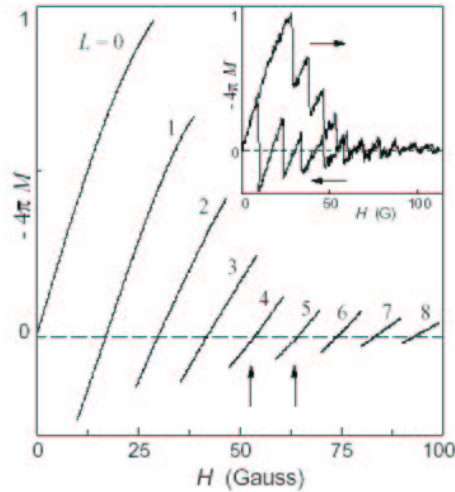
Figure 1.1: Magnetizations of Al disk of radius $R = 120\mu$m at T=0.5 K. Inset shows magnetization response when the field is swept up continuously from zero to high fields and then back to zero, as the arrows indicate.

for low fields corresponds to the entrance of additional quantum flux into the sample and indicates the appearance of an additional vortex inside the samples the magnetic field reaches a certain critical value. There is no controversy between the observation of vortices and the fact that aluminum is a type I superconductor. It has been known for a long time [3, 4] that thin films made of type I superconducting material can show the type II behavior such as stable vortex phase. At each value of the external field the true equilibrium corresponds to a certain vortex number, while states with different vortex number are metastable, separated from the equilibrium state by an energy barrier. When the external field is varied the system chooses the equilibrium state with different number of vortices which results in discontinuous jumps of magnetization. When the direction of the field sweep is reversed one observes the hysteretic behavior of the magnetization with the possibility of the paramagnetic magnetization (paramagnetic Meissner effect). This is to be compared to the diamagnetic behavior of a superconductor in the thermodynamic limit. In the more recent experiments [5] more fine transitions within the same number of vortices were reported. The vortices can form a giant vortex in the center of the disk as well as different geometrical patterns, Fig. 1.2. The structural transition between these geometrical patterns is driven also by the external magnetic field and shows the same hysteretic behavior as the transition between the states with different number of vortices.

The hysteretic behavior is the manifestation of the metastability: thermodynamically unfavorable states are very robust and can persist for hours at temperatures less than $T_c = 1.3K$ so the transition to the other state depends on the field sweep direction. To explain these experiments several numerical and analytical computations were performed. These computations are based on the phenomenological Ginzburg-Landau theory. Though the Ginzburg-Landau theory is formally valid only close to the transition, the numerical results [6, 7] based on this is theory were in remarkably good agreement with experimentally observed magnetization curves deep inside the superconducting phase. These works have revealed physical
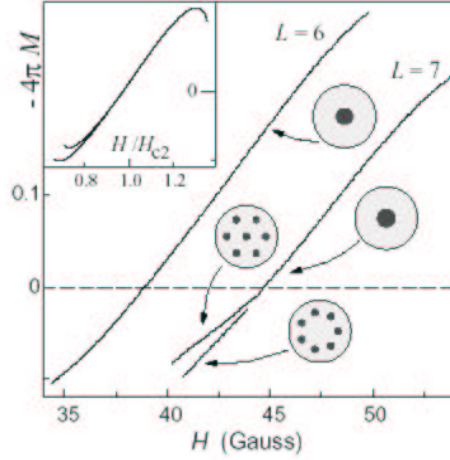
Figure 1.2: Structural transitions for seven vortices. The drawings show schematically the expected distribution of magnetic flux for different branches of the magnetization curve.

phenomena that play an important role in such systems, like the role of surface barriers for vortex nucleation and hysteresis [8, 9, 10]; the interplay between vortex-vortex and vortex-edge interactions that explains vortex structures in mesoscopic disks [9, 8]; the transition between a giant multiple vortex state and a state with several vortices carrying a unit quantum of flux [11].

The thickness of disks in the experiments is small compared to both coherence length and penetration depth, so the order parameter and vector potential can be considered as constant across the thickness and the system is effectively two dimensional. Analytical studies of the Ginzburg-Landau equations in two-dimensional systems require the use of various approximations since, in general, exact solutions can not be found due to the non-linearity. One approach is to neglect the nonlinear quartic term assuming $|\psi| \ll 1$, and to decouple them by supposing that the magnetic field inside the sample is equal to the applied field $H_e$. This approach describes correctly the super-conducting-normal phase boundary [12, 13, 14, 15, 16], but fails to explain the behavior of the sample deep inside the super-conducting state, where the order parameter is large and the quartic term is important. In the linearized theory, the order parameter profile is given by the solution of Scrëdinger-like equation for an effective charge -2$e$ particle. In the disk geometry the eigenfunctions of this equation are classified according to their angular momentum $m$, which represents the number of vortices or the winding number of the order parameter phase. For each value of $m$ the magnitude of the corresponding eigenfunction has a minimum at the origin, so all the vortices are situated at the center of the disk [16] therefore one can not study the role of surface barriers, the interaction between vortices, and the fragmentation of a giant vortex into unit vortices. The critical field for the entrance of the first vortex is obtained form the equality of the eigenenergies for $m = 0$ and $m = 1$ states. Since these energies are certain functions of the external flux $\Phi = \pi R^2 H_e$, the condition on $\Phi$ makes the first entrance field to scale as inverse square of the disk radius. This is to compare with the experimentally observed scaling of the first entrance field as $1/R$. In the vicinity of the upper critical field [16] the linearized theory

6

agrees quantitatively with the experimental results, since in this regime the vortices occupy a big part of the sample so the order parameter is small. The superconductivity remains at the boundaries and the upper critical field is essentially the surface critical field for a mesoscopic disk. The non-linear term is therefore important for the physics of the superconductor and must be taken into account when temperatures and magnetic fields are far below its critical values and the number of vortices is small. We shall describe other analytical methods which describe at least approximately the non-linearity of Ginzburg-Landau equations later on in this introduction. Now we pass to the second problem studied in this Ph.D. work, that of quasiparticle life-time in a mesoscopic conductor.

The validity of the quasiparticle concept is important for effective one-particle description of the physical properties of mesoscopic conductors and it has been a subject of recent experimental [17] and theoretical works [18, 19, 20, 21, 22, 23, 24]. The central problem is the possibility to describe the low energy excitations of small electronic systems, such as quantum dots as a superposition of few-particle states which behave as a single particle with a finite life-time, the picture which is valid for the macroscopic conductors and is the basis of the Landau Fermi liquid theory. For a mesoscopic conductor there appears an additional energy scale: the spacing of one particle levels, which is zero for macroscopic systems. The excitations containing more than one particle also have discrete spectrum, which prohibits the application of the Fermi Golden Rule for the calculation of the life-time. The problem is to determine the range of interactions and excitation energies for which the quasiparticle picture is valid for a finite size conductor. For this purpose the mapping of the Hilbert space of interacting electrons onto an effective lattice was introduced in [20] and the problem of quasiparticle life-time was considered within the framework of the Anderson localization [25]. Each site of the effective lattice represents the eigenstate of the non-interacting system (the Slater determinant of one-particle orbitals) and the bonds represent the interaction matrix elements. The states connected by interactions are organized in generations according to the number of particle-hole pairs excited form the Fermi vacuum. Introducing the concept of the distance between the Slater determinants according to the number of occupied one-particle orbitals the effective model is tight binding, since the interactions have finite range and couple only the states belonging to generations, whose particle-hole content is not very different. Similar models appeared earlier in the studies of the scattering of a proton by heavy nuclei [26]. The authors of [20] make several approximation, namely they neglect the transitions to the states of the same generation and to the generation with the smaller number of pairs, since the number of such transitions is much smaller than the number of transitions to the next generation with additional electron-hole pair. In this approximation the effective lattice have no closed loops and have structure of the tree (Cayley tree). Each site on the Cayley tree has $K + 1$ neighbors and $K$ is the branching number. In the many-body context the branching number is related to the energy $\epsilon$ of the initial particle excited above the Fermi sea. The Anderson hamiltonian, used to study the localization transition is characterized by the diagonal (on-site) energies distributed randomly with the typical value $W$ and the off-diagonal hopping amplitude $V$. These two energies can be combined into the dimensionless parameter $Z = W/V$ which measures the strength of the disorder. The Cayley tree model provides the exact solution of the localization problem. It was studied [27] using the self-consistent equation for the self-energy of the Green's function. This is essentially the mean-field approach which is exact above the upper critical dimension. The effective dimension of the Caley tree lattice is infinite, since the number of sites grows exponentially with the size of the system,

and the self-consistent equation is exact. Studying the fixed points of this equation the localization transition for the value of parameter $Z = Z_c \approx K \ln K$ was found. For the disorder parameter $Z$ above this value the discontinuity of the self-energy across the real axis is zero, which results in the point-like spectrum and the wave-functions are exponentially localized in the range of localization length. For small disorder the wave-functions are extended and the self-energy has a finite discontinuity across the imaginary axis. The criterion for the localization given above is valid when the energy of the eigenstate is in the center of the energy band. For weaker disorder the states with energies in the band center are extended and those close to the band edge remain localized, defining the mobility edge $E_c$ separating the two regions of the spectrum. The mobility edge for the Cayley tree lattice was studied in [28] and the it was shown that the localization length as a function of energy diverges when the mobility edge is approached from below with critical exponent $\nu = 1$. The study of the conductivity on the Cayley tree composed of one-dimensional random scatterers [29] predicted the critical exponent for the conductivity to be $s = 2$. Using the results of the scaling approach to the localization [30] and the fact that the mean field theory is exact on the Cayley lattice it was argued in [31] that the upper critical dimension for the localization transition is four. It is interesting [27] that though the states are extended for the disorder less than the critical value $Z < K \ln K$ they are not extended uniformly over the whole tree. A typical state occupies an infinite random subtree, formed by a small fraction of the whole tree. To delocalize the system completely the disorder must satisfy $Z < K$.

These results were used in [20] to predict the appearance of a quasiparticle picture in a mesoscopic conductor. The existence of quasiparticles with finite life-time corresponds to the extended regime in a many-body system, while in the opposite localized regime the initially introduced particle is coupled by interactions to a small number of states and has no definite life-time. Using the relation between the energy of the particle above the Fermi level $\epsilon$ and the branching number $K$ the many-body system is in the localized regime for a particle energy below the lower threshold $\epsilon^{**} = \Delta\sqrt{g/\ln g}$, where $\Delta$ is the one-particle level-spacing and $g$ is dimensionless conductance, i.e. conductance in units of $e^2/\hbar$. Due to the existence of two different delocalized regimes it was shown that until the excitation energy $\epsilon$ reaches another critical value $\epsilon^* = \Delta\sqrt{g} > \epsilon^{**}$ the states are not completely delocalized, i.e. they do not mix large number of non-interacting states, but rather a small portion of them, corresponding to a subtree of the whole lattice. The quasiparticle picture is valid, therefore, for excitations with energy above $\epsilon^*$.

Recently the system of interacting particles was studied numerically [22, 23] and analytically [21, 32, 24] from the point of view of localization in the Hilbert space. The inverse participation ratio and the spectral statistics were computed as a function of interactions between the particles. The inverse participation ratio is the fourth power of amplitude of the wave-function on some particular site summed over all sites of the lattice. It is designed to characterize the degree of the localization: for localized system the wave-function is peaked around one site, so the inverse participation ratio is finite, while for an extended wave-function the site amplitude is roughly an inverse square root of the total number of sites and the inverse participation ratio vanishes in the thermodynamic limit. The spectral statistics is also sensitive to the localization behavior: for a localized system the energy levels are distributed independently according to the Poisson law, while for an extended system there exist strong correlations between the levels (level repulsion) given by the Wigner-Dyson distribution. Using these criteria it was observed that the choice of the type of the lattice affects the localization-delocalization transition point. The spectral statistics and the properties of

eigenstates such as inverse participation ratio were shown to be sensitive to the type of the lattice. It was doubted that the actual transition and the properties of states in the delocalized phase can be accounted for properly using the pure tree-like structure of the lattice. The Cayley tree model with a large branching number was studied by super-symmetry methods in [21] and the existence of the special, not completely delocalized, phase between $\epsilon^{**}$ and $\epsilon^*$ was not confirmed. It was found there that the states are strongly correlated above the threshold $\epsilon > \epsilon^{**}$. The Cayley tree model was questioned in [32]. Taking into account the possibility of closed loops on the lattice using the random-matrix theory no delocalization transition was observed, rather the participation ratio and spectral width of the eigenstates of the interacting system exhibited a smooth crossover from almost localized to delocalized states. In the analytical study [24] of the perturbation series convergence for the self-energy it was claimed in that the infinite tree-like lattice used in [20] may be inadequate for description of the quasiparticle decay. So, the study of the Anderson localization on effective lattice with different structure representing the many-body Hilbert space, especially the structure of the extended stateson this lattice would certainly be of interest.

Now we discuss the methods we used in order to deal with interacting mesoscopic systems described above. To find an approximate solutions to the Ginzburg-Landau equations and to calculate the thermodynamical properties of small superconducting discs and cylinders we employed two approaches. These approaches are valid in different regimes of a superconductor, namely they depend on the value of the dimensionless Ginzburg-Landau parameter $\kappa = \lambda/\xi$, defined as the ratio of the two fundamental lengths: the London penetration depth $\lambda$, describing the spatial variations of the magnetic field and the correlation length $\xi$ describing the order parameter. For type I superconductor $\kappa$ is less than $1/\sqrt{2}$ and for type II $\kappa$ is greater than this critical value. The difference between the two types of superconductors can be rephrased in terms of vortex interactions. For type I the vortices attract each other, so no stable one-vortex configuration can be observed in such materials. For type II the vortex-vortex interactions are repulsive and the bulk materials the vortices appear in stable triangular lattice configuration, the Abrikosov lattice. The special value $\kappa = 1/\sqrt{2}$ is called the dual point and corresponds to the non-interacting vortices for an infinite system. At this particular value of the parameter the equations in an infinite plane reduce to first order differential equations that can be decoupled [33, 34, 35] and the expression for the Ginzburg-Landau free energy is particularly simple. At the dual point the existence of vortices can be demonstrated analytically [36]. For aluminum, which was used in the experiments $\lambda = 70$ nm and $\xi = 250$ nm, so $\kappa = 0.28$ and aluminum is a genuine type I superconductor. However, $\kappa$ depends on the sample thickness and characteristic type II behavior was observed experimentally [4] in thin films of type I superconductors. It is known [3] that for thin sample the effective penetration depth is $\lambda^2/d$, where $d$ is the thickness. Using the fact that the effective Ginzburg-Landau parameter of aluminum disk used in the experiments is larger than its bulk value we try the approach valid at the dual point when $\kappa$ takes the special value $1/\sqrt{2}$. It is based on an exact result for the free energy of infinite superconductor described by two-dimensional Ginzburg-Landau equations. To apply this result to a disk of finite size we observe that the solution valid for an infinite plane approximates very well the order parameter and the magnetic field in the inner region of the disk. For the disk boundary a simple variational ansatz can be used to find the contribution of this domain to the total free energy of the sample. Assuming thermodynamical equilibrium, the matching fields (critical fields corresponding to the entrance of the $n$-th vortex) are obtained from the minimization of the free energy with respect to the number of vortices. We study the Ginzburg-Landau free energy not only at

the dual point $\kappa = 1/\sqrt{2}$ but also in its vicinity where vortices start to interact weakly [37]. Taking into account non-linear effects, our calculations describe the magnetic response of the sample as its size changes, providing an understanding of the non-linear Meissner effect and of the multi-vortex state. We also study non-equilibrium vortex configuration in order to determine the interaction between a vortex and edge currents.

A second approach is to use the London equation which can be derived from the Ginzburg-Landau equations by supposing that $|\psi| = 1$ everywhere except on a finite number of isolated vortex locations where $|\psi| = 0$. Many theoretical results have been derived from the London equation, such as discrete nucleation of flux lines in a thin cylinder [38, 39] or in a thin disk [3, 40], the existence of surface energy barriers [41, 42], and the computation of polygonal ring configurations of vortices in finite samples [43, 44]. London's equation is valid rigorously when the parameter $\kappa$ goes to infinity, *i.e.* for extreme type II super-conductors in which vortices are indeed point-like. Despite the fact that in the experiments $\kappa$ is of order of unity, we resort to the London limit due to the simplicity of the resulting equations which enables us to study the topological properties of different vortex configurations unsensitive to the vortex size. We believe that the topological properties obtained in this limit remain valid for the whole range of the Ginzburg-Landau parameter. Using known results [38] for the magnetization of an infinite cylinder with a circular cross-section, we derive, in the mesoscopic regime, closed expressions for the magnetic field and the free energy that are suitable for analytical calculations. The equilibrium magnetization is curve is obtained through the minimization of the free energy and the series of matching fields are calculated. The metastable states can be also studied within the London regime. We obtain the energy barrier for a vortex to reach the sample center (Bean-Livingston barrier) and study the vortex nucleation in the sample. The paramagnetic Meissner state can then be explained using a simple scenario for the hysteretic behavior of the magnetization, involving the appearance and the disappearance of this surface barrier.

Once the existence of metastable states established, a criterion to classify them is required. The number of vortices is a simple topological number but it is not precise enough to distinguish between all different type of states. An attempt to classify different vortex configurations was done in [45]. In this work the uniform magnetic field distribution was assumed and order parameter was expanded in eigenstates of linearized Ginzburg-Landau equation belonging to different values of angular momentum $m$. The solution was found by minimizing the Ginzburg-Landau functional with respect to the coefficients of this expansion in the restricted subspace defined by finite set of angular momentum values. Including more angular momentum components to this set the transitions from the giant vortex state to different ring-like configurations of vortices were observed, so this set of integers was proposed as classifying numbers to characterize a given metastable vortex state. However it is not obvious to relate them to the geometric features of a given pattern. A more geometrical path is followed here to present a topological description of vortex patterns. Our study is based on an analogy between a configuration of vortices and a dynamical system, obtained by interpreting the super-conducting current as the local (phase-space) velocity of a particle. The Hamiltonian of the associated dynamical system turns out to be the magnetic field. We shall show that a configuration of vortices can be characterized by the critical points of the magnetic field (or equivalently the points where the current vanishes). The number of critical points of a given type (maxima, minima, saddle-points) will provide a natural set of topological invariant integers associated with a configuration. This geometrical analysis reveals the existence of structural transitions between states with the *same* number of vortices: indeed,

the number and the nature of the critical points can vary abruptly when the applied field exceeds some specific values, provoking topological phase transitions. For a simple polygonal configuration of vortices, we calculate the corresponding transition fields. These topological changes are in fact best visualized considering the geometrical properties of special closed curve $\Gamma$, first introduced in [46], which is everywhere orthogonal to the current lines and which passes through the critical points of the system. Any structural change affecting the critical points, will manifest itself in a topological change of the shape of $\Gamma$. This curve thus provides an efficient and elegant tool to characterize vortices patterns and to understand qualitatively the topological transitions between different configurations. It must be mentioned that it is the curve $\Gamma$ which separates the inner paramagnetic and outer diamagnetic regions of a superconducting sample and exists for any value of the Ginzburg-Landau parameter. In particular at the dual point discussed earlier it defines the boundary region of the sample and allows to obtain an analytic expression for the free energy. Having described the methods for calculation of the properties of mesoscopic superconductors we pass to the methods we used for the study of quasiparticles in mesoscopic conductors.

To deal with the interacting ballistic conductors we adopted the approach used in [20] and applied the analogy between hopping of particles on a real space lattice and the interactions matrix elements between the states of non-interacting system. The goal is to study localization in the many-body Hilbert space of a system for which the properties of the extended states are known exactly without any assumptions on the structure of the effective lattice. To this end we considered the one-dimensional interacting systems [47] and we choose the chiral Tomonaga-Luttinger model due to its simplicity and the possibility to find the eigenstates for any strength of interactions by bosonization [48]. The transformation from the non-interacting fermionic to the interacting bosonic basis is given by the irreducible characters of the permutation group and a numerical algorithm can be implemented to diagonalize the interacting Hamiltonian. We used this transformation to compute numerically the inverse participation ratio of the bosonic eigenstate in the non-interacting basis we found that that the eigenstates are extended. This can be attributed to the fact that due to the linearity of the one particle energy-momentum relation the non-interacting eigenstates are degenerate. The interactions lift this degeneracy mixing the Slater determinants into coherent superpositions which are described by the bosonic quantum numbers. Thus the bosonic eigenstates of the full interacting model can be viewed as a generalization of the extended Bloch states in the tight-binding models with degenerate on-site energies. We employed this analogy to find the possible mechanism which would lead to the localization of the interacting states.

It is well known that the linearization of the dispersion is the required to solve the Tomonaga-Luttinger model [48]. In analogy to the disordered systems a random dispersion was introduced into the Tomonaga-Luttinger model to study the properties of its eigenstates as a function of the disorder. It is expected to model a system where the single particle spectrum is complicated. The question we address is whether this model exhibits localization, since the randomness introduced into the dispersion leads to randomness of the diagonal matrix elements of the many-body Hamiltonian analogous to the diagonal disorder introduced into tight-binding Anderson models.

We found that the states remain localized in the basis of Slater determinants, i.e. resemble the states of the non-interacting systems. To obtain this result the special properties of the interaction matrix were used, i.e. its non-zero elements are concentrated along the diagonal so the interactions are in some sense of short range. This enable us to map the interacting problem into one-dimensional localization model similar to the exactly solvable Lloyd model

[49]. The difference is that the parameters of the diagonal disorder derived from the random dispersion are position-dependent. Introducing a position dependent localization length we obtain a non-exponential localization of the eigenstates. The dependence of the localization length on the energy of the excitation is then studied in the weak and strong coupling regimes.

Our presentation is organized as follows. In chapter 2, some basic features of the Ginzburg-Landau theory of super-conductivity are recalled. In chapter 3 the dual-point solution for an infinite system is modified to take into account the effects of the boundary. This description is then applied to study the thermodynamics of the mesoscopic super-conductors in different geometries such as infinite cylinder and thin mesoscopic disk. The magnetization curves are obtained and compared with the exact numerical solutions of the Ginzburg-Landau equations. In chapter 6 the case of the infinite cylinder is studied using the London limit of Ginzburg-Landau equations. The topological aspects of the analytical solutions are of main importance since the topological description remains valid for the general $\kappa$. In chapter 9 we review some known facts about the standard Tomonaga-Luttinger model. We describe the structure of the Hilbert space as an effective lattice and discuss the bosonization solution in this context. In chapter 10 we introduce randomness into the dispersion law of the Tomonaga-Luttinger model and simplify the interaction matrix. Then we solve the resulting model with assumption of independence of the on-site energies. Chapter 11 is devoted to the study of relevance of the correlations between the energies. In chapter 12 we present the conclusions on our studies of the mesoscopic superconductors and localization in the Hilbert space of the Tomonaga-Luttinger model. The results are discussed and further investigations are proposed. The appendices provide the mathematical details of the calculations.

# Chapter 2

# The Ginzburg-Landau theory of super-conductivity

We recall here some basic features of the Ginzburg-Landau theory and define our notations. The order parameter $\psi$ is a complex number defined by its magnitude and phase:

$$\psi = |\psi|e^{i\chi} \tag{2.1}$$

As in the general theory of second order phase transitions one writes down the free energy as an expansion in powers of the order parameter and its gradient:

$$F_S = F_N + \int \alpha |\psi|^2 + \frac{\beta}{2}|\psi|^4 + \frac{\hbar^2}{4m}\left|\vec{\nabla}\psi\right|^2, \tag{2.2}$$

where the integration is performed over the volume of the sample and we omit the volume element in what follows. Here $F_N$ is the free energy in the normal state (i.e. for $\psi = 0$); $\beta$ is a positive coefficient independent of the temperature and $\alpha$ is a function of the temperature given by

$$\alpha \sim (T - T_c), \quad \alpha > 0 \tag{2.3}$$

so $\alpha$ is positive above the transition and negative below. The coefficient of the gradient term implies that the particles has mass $2m$. Here the mass $m$ is identified with the mass of the electron, since as we know from the microscopic BCS theory Cooper pairs consist of two electrons. However this choice is not crucial for the following discussion and we use it as convention.

Now we consider our system in magnetic field described by the vector potential $\vec{A}$ satisfies $\vec{\nabla} \times \vec{A} = \vec{B}$, where $\vec{B}$ is the local magnetic induction. When a magnetic field is present the expression (2.2) has to be modified in two ways. Firstly, the magnetic field energy density $B^2/8\pi$ must be added to the free energy density. Secondly, the gradient term has to be changed so as to satisfy the requirement of the gauge symmetry:

$$\vec{\nabla}\psi \rightarrow \left(\vec{\nabla} - \frac{2ie}{\hbar c}\vec{A}\right)\psi SGinzbu \tag{2.4}$$

Thus we have the following basic expression for the free energy of a super-conductor:

$$F_S(B) = F_N(0) + \int \frac{B^2}{8\pi} + \alpha|\psi|^2 + \frac{\beta}{2}|\psi|^4 + \frac{\hbar^2}{4m}\left|\left(\nabla - \frac{2ie}{\hbar c}\vec{A}\right)\psi\right|^2 \tag{2.5}$$

where $F_N(0) = F_N$ is the free energy of the sample in the normal state in the absence of the magnetic field. It must be emphasized that the coefficient $2ie/\hbar c$ in th expression is not arbitrary (in contrast to the above-mentioned conventional choice of the $\hbar^2/4m$). The doubling of the electron charge is due to the Cooper effect; this coefficient could not be fond by purely phenomenological means.

In a homogeneous sample, with no magnetic field, the order parameter $\psi$ is independent of the coordinates. Then the expression (2.2) reduces to

$$F_S - F_N = \alpha V |\psi|^2 + \frac{\beta V}{2} |\psi|^4. \tag{2.6}$$

where $V$ is the volume of the sample. For $T > T_c$ the minimum is obtained for $\psi = 0$ as expected in the absence of the super-conductivity. In the super-conducting phase (for $T < T_c$) the non-trivial solution

$$|\psi|^2 = -\alpha/\beta \tag{2.7}$$

appears and the free energy reaches its minimum:

$$F_S - F_N = -V\alpha^2/2\beta. \tag{2.8}$$

This value can be related to the thermo-dynamical critical magnetic field by the following argument. The condition for the super-conducting transition at external field $H_e = H_c$ is the equality of the Gibbs free energies $G_S(H_c) = G_N(H_c)$, where we express the free energy as a function of the external magnetic field $H_e$ rather than the magnetic induction $B$ by means of the Legendre transform

$$G = F - \frac{H_e}{4\pi} \int B. \tag{2.9}$$

Since the magnetic field can exist only at the boundary of a macroscopic super-conductor its free energy is the same as for zero magnetic field: $G_S = F_S$. On the other hand the magnetic field penetrates completely the normal metal $B = H_e$, neglecting small magnetism of these materials, and the Gibbs free energy of the normal metal is given by $G(H_e) = F_N - VH_e^2/8\pi$. Therefore

$$F_N - F_S = V\alpha^2/2\beta = \frac{VH_c^2}{8\pi} \tag{2.10}$$

This expression sets the energy units of the Ginzburg-Landau free energy functional.

In a more general situation th solutions minimizing the Ginzburg-Landau functional are found by independent variation of the fields $\psi$, $\psi^*$ and $\vec{A}$. Varying the integral (2.5) with respect to $\psi^*$ and integrating by parts the term $\left(\vec{\nabla}\psi - (2ie/\hbar c)\vec{A}\psi\right) \nabla\psi^*$, we find

$$\delta F_S = \int \left[-\frac{\hbar^2}{4m}\left(\nabla - \frac{2ie}{\hbar c}\vec{A}\right)^2 \psi + \alpha\psi + \beta|\psi|^2\psi\right]\delta\psi^* + \frac{\hbar^2}{4m}\int\left(\nabla\psi - \frac{2ie}{\hbar c}\vec{A}\psi\right)\delta\psi^* \cdot d\vec{S} \tag{2.11}$$

where the first integral is taken over the volume and the second – over the surface of the system. Therefore we obtain one condition for the stationarity of the Ginzburg-Landau functional:

$$-\frac{1}{4m}\left(-i\hbar\vec{\nabla} - \frac{2e}{c}\vec{A}\right)^2 \psi + \alpha\psi + \beta|\psi|^2\psi = 0. \tag{2.12}$$

Varying the functional with respect to $\psi$ gives the complex conjugate equation. Now we vary the integral (2.5) with respect to $\vec{A}$ to obtain the Maxwell equation of electrodynamics:

$$\vec{\nabla} \times \vec{B} = \frac{4\pi}{c}\vec{j} \qquad (2.13)$$

where the current density is

$$\vec{j} = -\frac{ie\hbar}{2m}(\psi^*\vec{\nabla}\psi - \psi\vec{\nabla}\psi^*) - \frac{2e^2}{mc}|\psi|^2\vec{A}. \qquad (2.14)$$

The equations (2.12)-(2.13) form the complete set of Ginzburg-Landau equations. The boundary conditions on the solutions of these equations are found from the condition that the surface integral in the variation of $\delta F_S$ is zero. Thus it follows from (2.11) that

$$\hat{n} \cdot \left(\nabla\psi - \frac{2ie}{\hbar c}\vec{A}\psi\right) = 0 \qquad (2.15)$$

where $\hat{n}$ is the normal vector at the surface of the system. As a result of this condition the normal component of the current (2.14) is also zero as can be seen by multiplying the boundary condition (2.15) by $\psi^*$ and subtracting from it the complex conjugate expression. The boundary conditions on the magnetic field depends on the particular geometry of the sample and will be discussed in what follows.

In order to obtain the characteristic length scales of the Ginsburg-Landau equations we consider first the solution of (2.12) in the absence of the magnetic field in a situation when $\psi$ varies smoothly in the space. In the linear approximation the equation (2.12) is

$$\frac{\hbar^2}{4m}\nabla^2\psi + \alpha\psi = 0 \qquad (2.16)$$

which defines the typical length, the correlation length $\xi^2 = \hbar^2/4m\alpha$ over which $\psi$ varies. The second characteristic length related to the space variations of the magnetic field is obtained by substituting the value (2.7) for the order parameter to the second Ginzburg-Landau equation (2.13) and taking the curl operation on both sides. In this way one obtains the London equation:

$$\nabla^2\vec{B} = \frac{8\pi e^2}{mc^2}\frac{\alpha}{\beta}\vec{B} = \vec{B}/\lambda^2 \qquad (2.17)$$

which defines the second characteristic length, the London penetration depth $\lambda^2 = mc^2\beta/8\pi e^2\alpha$. Both characteristic lengths diverge at the transition as can be seen from the expression (2.3) for $\alpha(T)$. The two characteristic lengths $\lambda$ and $\xi$ appear as phenomenological parameters. Their ratio $\kappa = \lambda/\xi$ is called the Ginzburg-Landau parameter. Now we show that it is the only dimensionless parameter which describes the super-conductor. To this end we make the following change of units:

$$r \to \sqrt{2}\lambda r, \quad \vec{B} \to \frac{H_c}{\sqrt{2}\kappa}\vec{B}, \quad \vec{A} \to \frac{\hbar c}{2\sqrt{2}e\lambda}\vec{A}, \quad |\psi|^2 \to \frac{H_c^2}{4\pi}|\psi|^2, \quad F/V \to \frac{H_c^2}{8\kappa^2\pi}F/V$$
$$(2.18)$$

which amounts to measuring lengths in units of $\lambda\sqrt{2}$, the magnetic field in units of $\phi_0/4\pi\lambda^2$ and the vector potential in units of $\phi_0/2\sqrt{2}\pi\lambda$, where the flux quantum $\phi_0$ is given by $\phi_0 = hc/2e$. The order parameter is rescaled by its value for homogeneous system in the absence

of magnetic field (2.7) and the density of Ginzburg-Landau free energy $F/V$, is measured in units of $H_c^2/8\kappa^2\pi$ where $H_c$, the thermodynamic field, satisfies $H_c = \kappa\phi_0/2\sqrt{2}\pi\lambda^2$.

Since we are interested in variation of the free energy with magnetic field we can subtract the constant energy of the super-conductor for homogeneous system without magnetic field $F_S(0) = -\alpha/2\beta = H_c^2/4\pi$ and define $\mathcal{F} = F_S(B) - F_S(0)$. In the dimensionless form it is given by

$$\mathcal{F} = \int \frac{B^2}{2} + \kappa^2 \left(1 - |\psi|^2\right)^2 + \left|(\vec{\nabla} - i\vec{A})\psi\right|^2 \quad , \tag{2.19}$$

The Ginzburg-Landau equations (2.12)-(2.13) become

$$-(\vec{\nabla} - i\vec{A})^2\psi = 2\kappa^2\psi(1 - |\psi|^2) \tag{2.20}$$
$$\vec{\nabla} \times \vec{B} = 2\vec{j} \tag{2.21}$$

The current density is now given by $\vec{j} = \mathrm{Im}(\psi^*\vec{\nabla}\psi) - |\psi|^2\vec{A}$ and is related to the super-fluid velocity $\vec{v}_s$ by

$$\vec{v}_s = \vec{j}/|\psi|^2 = \vec{\nabla}\chi - \vec{A} \tag{2.22}$$

Outside the super-conducting sample, $\psi = 0$. The boundary condition (2.15) on the surface of the super-conductor in dimensionless form are

$$\hat{n} \cdot (\vec{\nabla} - i\vec{A})\psi = 0. \tag{2.23}$$

The London fluxoid is the quantity $\left(\vec{v}_s + \vec{A}\right)$, that is identical to $\vec{\nabla}\chi$. Since $\chi$ is the phase of the univalued function $\psi$, the circulation of the London fluxoid along a closed contour $\mathcal{C}$ is quantized [41, 50]:

$$\oint_{\mathcal{C}} (\vec{v}_s + \vec{A}) \cdot \vec{dl} = \oint_{\mathcal{C}} \vec{\nabla}\chi \cdot \vec{dl} = 2\pi n \tag{2.24}$$

The integer $n$ is the winding number of the phase of the system along the contour $\mathcal{C}$ and is a topological characteristic of the system.

In this study, the super-conducting sample is either an infinite cylinder or a thin disk, with cross-section of radius $R$, placed in an external magnetic field parallel to its axis. When the variation of the order parameter and magnetic field in axial direction is small the system can be regarded as effectively two-dimensional. For infinite cylinder the order parameter and magnetic field are uniform due to the translational symmetry along the axis. The situation of magnetic disks encountered in the experiments must be analyzed more carefully. The flux lines deviate a ditance of order $R$ over the effective screening length $\lambda_e$. The expression of the effective screening length is unknown in the general case. In the limit of large $R$ it is given by $\lambda^2/d$ [51, 40]. For a finite and small enough $R$ we assume that the condition $R \ll \lambda_e$ holds, so the flux lines are straight in the vicinity of the sample and the magnetic field is independent of the position along the axis. For the order parameter the thikness must be compared to the correlation length $\xi \sim 250$nm. In the experiments the thickness $d$ is of order 70nm and the relation $d < \xi$ is satisfied. In what follows we write down directly the two-dimensional Ginzburg-Landau energy functional (2.19) for the Ginzburg-Landau free energy per unit length in the axial direction. The integral are performed over the surface $\Omega$, the circular area of radius $R$, perpendicular to the axis. Since the radius of the cross-section, $R$, is an important parameter, we define the dimensionless quantity: $a = \lambda/\sqrt{2}R$; $a$ is supposed to be small compared to 1 (typically $a \sim 1/10$ in the experiments) unless stated otherwise. The flux created by the external and uniform magnetic field $H_e$ (expressed in units of $\phi_0/4\pi\lambda^2$)

through the cross section $\pi R^2$ of the sample is equal to $\pi R^2 H_e \phi_0 / 4\pi\lambda^2 = H_e\phi_0/2a^2$. The flux $\phi_e$, in units of the flux quantum $\phi_0$, is thus given by:

$$\phi_e = \frac{H_e}{2a^2} \tag{2.25}$$

We emphasize that, in the units we have chosen, the flux $\phi_b$ of a magnetic field $\vec{B}$ through a surface $\Omega$ is obtained via the following formula:

$$\phi_b = \frac{1}{2\pi}\int_\Omega \vec{B}\cdot \vec{dS} = \frac{1}{2\pi}\oint_{\partial\Omega}\vec{A}\cdot \vec{dl} \tag{2.26}$$

An extra factor $1/2\pi$ appears here because $B$ is given in units of $\phi_0/4\pi\lambda^2$, the surface in units of $2\lambda^2$ and the flux in units of $\phi_0$.

The Gibbs free energy $G$ obtained from $F$ via a Legendre transformation (2.9) reads in the dimensionless form:

$$G = F - H_e\int_\Omega B = F - H_e 2\pi\phi_b = F - 4\pi a^2 \phi_e\phi_b \tag{2.27}$$

In a normal sample, $\psi = 0$ and $B = H_e$. Therefore, the Gibbs free energy $G_N$ of a normal sample is given by:

$$G_N = F_N - H_e\int_\Omega B = F_N - 2\pi a^2 \phi_e^2 \tag{2.28}$$

At thermodynamic equilibrium, the super-conductor selects the state of minimal Gibbs free energy. The quantity that we are interested in, and which is measured in experiments, is the magnetisation $M$ of the super-conductor due to the applied field given by $4\pi M = B - H_e$. It is obtained, at thermodynamic equilibrium and up to a constant equal to the super-conducting condensation energy, from the difference of the (dimensionless) Gibbs energies

$$\mathcal{G} = G_S - G_N = \mathcal{F} + 2\pi a^2 \phi_e^2 - 4\pi a^2 \phi_e\phi_b \tag{2.29}$$

using the thermodynamic relation [41]:

$$-M = \frac{1}{2\pi}\frac{\partial \mathcal{G}}{\partial \phi_e} \tag{2.30}$$

These are the basic quantities and notation which we use in the following sections.

# Chapter 3

# Dual point of the Ginzburg-Landau equations

We now study the particular case of the dual point, defined by $\kappa = 1/\sqrt{2}$. At this value the non-linear second-order differential equations for $\psi$ and $\vec{A}$ can be reduced to first-order ones. Since we consider a geometry of a long cylinder or a thin disk the system under considerations are essentially two-dimensional. In two dimensions we have the following mathematical identity:

$$\left| (\vec{\nabla} - i\vec{A})\psi \right|^2 = |\mathcal{D}\psi|^2 + \vec{\nabla} \times \vec{j} + B|\psi|^2 \tag{3.1}$$

where $\vec{j}$ is the current density and the operator $\mathcal{D}$ is defined as $\mathcal{D} = \partial_x + i\partial_y - i(A_x + iA_y)$. Using this identity at $\kappa = 1/\sqrt{2}$ the free energy (2.19) of a two dimensional domain $\Omega$ can be written as [34, 52]:

$$\mathcal{F} = \int_\Omega \left( \frac{1}{2} \left( B - 1 + |\psi|^2 \right)^2 + |\mathcal{D}\psi|^2 \right) + \oint_{\partial\Omega} (\vec{j} + \vec{A}) \cdot \vec{dl} \tag{3.2}$$

The second integral over the boundary of the domain $\Omega$ results from the Stokes theorem. If we suppose that the domain $\Omega$ is infinite and super-conducting at large distances [34], i.e. $|\psi| \to 1$ at infinity, then the boundary integral in (3.2) is identical to the fluxoid. Using the quantization property (2.24), we obtain

$$\mathcal{F} = 2\pi n + \int_\Omega \left( \frac{1}{2}(B - 1 + |\psi|^2)^2 + |\mathcal{D}\psi|^2 \right) \tag{3.3}$$

The free energy is thus minimum when Bogomol'nyi equations [34] are satisfied, that is when,

$$\mathcal{D}\psi = 0 \tag{3.4}$$
$$B = 1 - |\psi|^2 \tag{3.5}$$

These two equations can be decoupled and one obtains that $|\psi|$ is a solution of the second-order nonlinear equation

$$\nabla^2 \ln |\psi|^2 = 2 \left( |\psi|^2 - 1 \right) \tag{3.6}$$

This equation is related to the Liouville equation. It was proven that this equation as well as (3.4, 3.5) admit families of vortex solutions [36]. For infinite systems, it can be shown that each vortex carries one flux quantum and that the winding number $n$ is equal to the number

18

of vortices in the system. Thus, the total free energy results only from the boundary term in (3.2) and is a purely topological number:

$$\mathcal{F} = 2\pi n \quad .$$

(3.7)

The free energy is proportional to the number of vortices: at the dual point, vortices do not interact with each other [34, 37].

## 3.1 Finite size systems

In a finite system with boundaries, vortices do not interact with each other at the dual point but they are repelled by the edge currents. Therefore, at thermodynamic equilibrium, all vortices collapse into a giant vortex state. Since the super-conductor under discussion has a circular cross-section, this giant vortex (or *multi-vortex*) is located at the center and the system is invariant under cylindrical symmetry. In a *finite* size mesoscopic super-conductor at the dual point, the boundary integral, in (3.2), can not be identified with the fluxoid because $|\psi|$ is in general different from 1 on the boundary of the system. This quantity is no more a topological integer but a continuously varying real number. The two terms of (3.2) can not, therefore, be minimized *separately* to obtain the optimal free energy. In [52], we found a method to circumvent this difficulty: if the system is invariant under cylindrical symmetry, *i.e.* all the vortices are at the center of the disk, then the current density has only an azimuthal component $\jmath_\theta$. The current $\jmath_\theta$ has opposite signs near the center (where the vortex is located) and at the edge of the disk (where Meissner currents oppose the penetration of the external field). Hence, there exists a circle $\Gamma$ on which $\jmath_\theta$ vanishes [52]. Along $\Gamma$, we have

$$\vec{\jmath} + \vec{A} = \vec{\jmath}/|\psi|^2 + \vec{A} = \vec{\nabla}\chi \quad \text{and therefore} \quad \oint_\Gamma \left(\vec{\jmath} + \vec{A}\right) \cdot \vec{dl} = 2\pi n$$

(3.8)

The domain $\Omega$ can thus be divided into two sub-regions, $\Omega = \Omega_1 \cup \Omega_2$, such that the boundary between $\Omega_1$ and $\Omega_2$ is the circle $\Gamma$. By convention, we call $\Omega_1$ the bulk and the annular ring $\Omega_2$ the boundary region (see Fig. 3.1).

Numerical solutions of the Ginzburg-Landau equations in a two dimensional super-conductor, with cylindrical symmetry, clearly show the separation of the sample cross-section into two distinct subdomains. In Fig. 3.2, we have plotted the order parameter and the magnetic field in a cylinder of radius $R = 10\lambda\sqrt{2}$ with one vortex at the center. These two quantities vary only near the center and near the edge: there is a whole intermediate region in which $|\psi|$ and $B$ remain almost constant. When the system is large enough, these constant values are, to an excellent precision, identical to the asymptotic values of $|\psi|$ and $B$ in an infinite system. The current vanishes for a value of $r$ for which $\frac{dB}{dr} = 0$, and this determines the radius of the circle $\Gamma$. In Fig. 3.2, this corresponds approximately to $r \simeq 5.5$, though practically, the circle $\Gamma$ can be placed anywhere in the saturation region where the current is infinitesimally small.

Although the Bogomol'nyi equations (3.4, 3.5) do not minimize the Ginzburg-Landau free energy [53], we notice that the behaviour of $|\psi|$ and $B$ in the bulk sub-domain $\Omega_1$ is still given by the relation $B = 1 - |\psi|^2$,(3.5) which, as shown in Fig. 3.3, represents indeed an excellent approximation. Thus, using (3.2) and (3.8), we conclude that at the dual point the free energy of $\Omega_1$ can be calculated as that of an infinite domain, namely

$$\mathcal{F}(\Omega_1) = 2\pi n$$

(3.9)

19
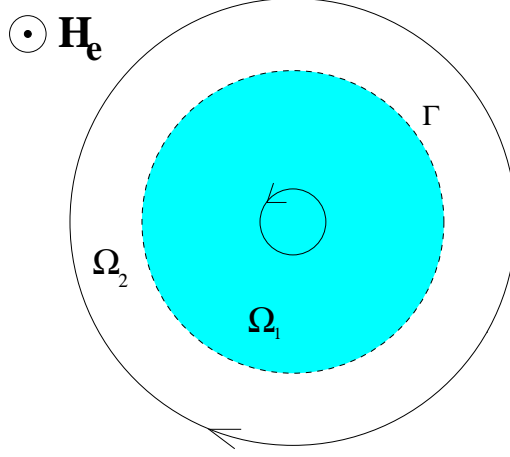
Figure 3.1: The sample cross-section is divided into two subdomains by the circle $\Gamma$. The arrows indicate the direction of the current.
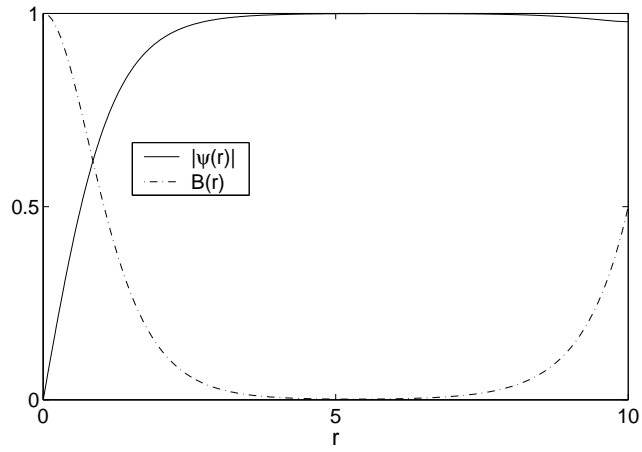


Figure 3.2: Behaviour of the order parameter and the magnetic field at the dual point for a cylinder of radius 10 $\lambda\sqrt{2}$ containing one vortex.
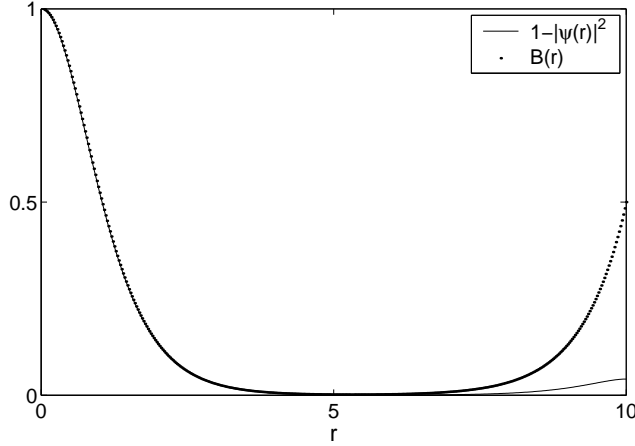
Figure 3.3: Comparison between $B$ and $1 - |\psi|^2$ in a cylinder of radius $10\ \lambda\sqrt{2}$ containing one vortex.

We also emphasize that the flux in $\Omega_1$ is quantized and one has:

$$\frac{1}{2\pi}\int_{\Omega_1} B = n \tag{3.10}$$

To calculate $\mathcal{F}(\Omega_2)$, the identity (3.2) valid at the dual point is of no use anymore, since $|\psi|$ is in general different from 1 at the boundary, and the boundary integral in (3.2) can not be identified to the fluxoid. We therefore have to go back to the definition (2.19) of the Ginzburg-Landau free energy which becomes at the dual point:

$$\mathcal{F}(\Omega_2) = \int_{\Omega_2} \frac{B^2}{2} + (\nabla|\psi|)^2 + |\psi|^2|\vec{\nabla}\chi - \vec{A}|^2 + \frac{(1-|\psi|^2)^2}{2} \tag{3.11}$$

The assumption of cylindrical symmetry implies that $\chi = n\theta$ where $\theta$ is the polar angle and $n$ the number of vortices present at the center of the disk. Examining again Fig. 3.2, we observe that in $\Omega_2$, the order parameter and the magnetic field vary from their values on the edge to their saturation values over a region of width $\delta$, which is of order 1 in units of $\lambda\sqrt{2}$[1] The length $\delta$ therefore represents the typical distance over which the integrand in (3.11) has a non negligible value.

With the help of this observation, we shall estimate $\mathcal{F}(\Omega_2)$ using a variational Ansatz: we shall consider that the modulus of the order parameter has a constant value $\psi_0$ over a ring of width $\delta$, included in $\Omega_2$ and that $\vec{A}$ and $\vec{B}$ decay exponentially with a characteristic length $\delta$ from their boundary value to their bulk value. Clearly, our approximation will be valid only if the width of $\Omega_2$ is large enough compared to 1. We first remark that our Ansatz is compatible with the boundary condition (2.23), which reduces here to $d\psi/dR = 0$ and that it allows us to neglect the curvature term $(\nabla|\psi|)^2$ in (3.11). To evaluate the term proportional to the

---

[1]Indeed, one has for a thick system $\delta \simeq \lambda$ at the dual point. For a thin film of thickness $d$, $\delta \simeq \lambda^2/d$ in the London limit [3]. Since we are considering a mesoscopic regime in which $d \simeq \lambda$, both expressions indicate that $\delta$ is of order 1.

super-fluid velocity $v_s(r)$ (2.22), we first notice that, due to the Meissner effect, it decreases from the boundary at $r = R$ with a behaviour well described by

$$v_s(r) = v_s(R)e^{-(R-r)/\delta} \tag{3.12}$$

with $v_s(R) = a(n - \phi_b)$. To obtain the last equality we used that the boundary value of the vector potential is $\vec{A}(R) = a\phi_b\hat{u}_\theta$, where $\phi_b$ is the total flux through the system. Hence, for a constant amplitude $\psi_0$ of the order parameter, we have

$$\frac{1}{2\pi}\mathcal{F}(\Omega_2) = \frac{\delta}{2a}\left(\psi_0^2 v_s^2(R) + (1 - \psi_0^2)^2\right) + \frac{1}{2\pi}\int_{\Omega_2}\frac{B^2}{2} \tag{3.13}$$

The magnetic contribution in (3.11) is obtained from the typical magnitude $\bar{B}$ of the magnetic field in $\Omega_2$ determined using (2.26) and (3.10) as

$$\phi_b = \frac{1}{2\pi}\int_\Omega B = \frac{1}{2\pi}\int_{\Omega_1}B + \frac{1}{2\pi}\int_{\Omega_2}B = n + \frac{\delta}{a}\bar{B} \tag{3.14}$$

Thus, using the fact that $B^2$ decrease exponentially with a characteristic length $\delta/2$, we estimate the contribution of the magnetic energy to $\mathcal{F}(\Omega_2)$ as being:

$$\frac{1}{2\pi}\int_{\Omega_2}\frac{B^2}{2} = \frac{\delta}{2a}\frac{\bar{B}^2}{2} = \frac{a}{4\delta}(n - \phi_b)^2 \tag{3.15}$$

After substituting this expression into (3.13) we minimize $\mathcal{F}(\Omega_2)$ with respect to $\psi_0$. The optimal variational value of $\psi_0$ is given by:

$$\psi_0^2 = \begin{cases} 1 - \frac{1}{2}v_s^2(R) = 1 - \frac{a^2}{2}(n - \phi_b)^2 & \text{if } |a(n - \phi_b)| \leq \sqrt{2} \\ 0 & \text{if } |a(n - \phi_b)| > \sqrt{2} \end{cases} \tag{3.16}$$

Inserting these expressions in (3.13), we obtain the variational free energy $\mathcal{F}(\Omega_2)$:

$$\frac{1}{2\pi}\mathcal{F}(\Omega_2) = \begin{cases} Av_s^2(R) - Bv_s^4(R) & \text{if } |a(n - \phi_b)| \leq \sqrt{2} \\ \frac{\delta}{2a} + \frac{1}{4a\delta}v_s^2(R) & \text{if } |a(n - \phi_b)| > \sqrt{2} \end{cases} \tag{3.17}$$

with $A$ and $B$ defined by

$$A = \frac{\delta}{2a}\left(1 + \frac{1}{2\delta^2}\right)$$
$$B = \frac{\delta}{8a} \tag{3.18}$$

The total free energy of the mesoscopic super-conductor containing $n$ vortices, at the dual point, is thus:

$$\frac{1}{2\pi}\mathcal{F}(n, \phi_b) = n + \begin{cases} Av_s^2(R) - Bv_s^4(R) & \text{if } |a(n - \phi_b)| \leq \sqrt{2} \\ \delta/2a + v_s^2(R)/4a\delta & \text{if } |a(n - \phi_b)| > \sqrt{2} \end{cases} \tag{3.19}$$

This energy is the sum of two contributions:

(i) a *bulk* term proportional to $n$ which is a topological quantity at the dual point.

(ii) A *boundary* term, reminiscent of the well-known 'Little and Parks' free energy [41] (this boundary term can be given a geometric interpretation in terms of a geodesic curvature [52, 54]).

## 3.2 A cylinder at the dual point

We now apply the relations (3.19) to the simple case of an infinitely long super-conducting cylinder of radius $R > \lambda$, lying in an external field $H_e$ directed along its axis. There are two contributions to the total flux $\phi_b$: the flux of $n$ vortices present at the center of the sample and a fraction of the applied flux $\phi_e$ localized near the boundary and proportional to $\lambda/R$ (due to the Meissner effect). Hence,

$$\phi_b = n + 2a\phi_e \quad \text{with} \quad \phi_e = \frac{H_e}{2a^2} \tag{3.20}$$

The exact numerical coefficient in front of the term $a\phi_e$ does not affect the result of our calculation; we take it equal to 2, the value obtained in the London limit [38]. The total free energy, using (3.19) and the fact that $v_s(R) = -2a^2\phi_e$, is given by

$$\frac{1}{2\pi}\mathcal{F}(n, \phi_b) = n + \begin{cases} 4a^4 \left( A\phi_e^2 - 4a^4 B \phi_e^4 \right) & \text{if} \quad a^2|\phi_e| \leq 1/\sqrt{2} \\ \frac{\delta}{2a} + \frac{a^3}{\delta}\phi_e^2 & \text{if} \quad |a^2|\phi_b| > 1/\sqrt{2} \end{cases} \tag{3.21}$$

Using (2.27) and (3.21), the Gibbs free energy, $\mathcal{G}(n, \phi_e)$, of a cylinder containing $n$ vortices at the dual point is given by:

$$\frac{1}{2\pi}\mathcal{G}(n, \phi_e) = n \left( 1 - 2a^2\phi_e \right) + P(\phi_e) \tag{3.22}$$

where $P(\phi_e)$ is a polynomial in $\phi_e$ that does not depend on $n$. Hence, all the curves $\mathcal{G}(n, \phi_e)$ meet at

$$\phi_c = \frac{1}{2a^2} \tag{3.23}$$

For values of $\phi_e$ less than this critical value, the free energy is minimized if there are no vortices. At $\phi_e = \frac{1}{2a^2}$ all vortices are nucleated simultaneously and the sample becomes normal. This value corresponds to a critical applied field $H_e$ which is equal to 1 in our units, or restoring the units back, and recalling that $\kappa = 1/\sqrt{2}$

$$H_e = \frac{\phi_0}{4\pi\lambda^2} = \frac{\phi_0}{2\sqrt{2}\pi\lambda\xi} \tag{3.24}$$

This is precisely the formula for the thermodynamic critical field of a super-conductor [41] (which, for a cylindrical super-conductor with $\kappa \leq \frac{1}{\sqrt{2}}$, is the same as the upper critical field). The magnetisation $M$ of the cylinder satisfies the linear Meissner effect:

$$-M = \frac{1}{2\pi}\frac{\partial \mathcal{G}(n, \phi_e)}{\partial \phi_e} = H_e(1 - ca) \quad \text{with} \quad c = 4 - \delta\left(1 + \frac{1}{2\delta^2}\right) \ . \tag{3.25}$$

The macroscopic result [41] is $-M = H_e$; the finite-size correction to the susceptibility is proportional to $R^{-1}$.

Thus, the well-known results for an infinite super-conducting cylinder can easily be retrieved from the dual point approach. We now proceed to the study of the magnetic response of a thin disk.

## 3.3 A mesoscopic disk at the dual point

To model the experimental sample of [1, 2], we consider a mesoscopic disk of thickness $d$ smaller than $\xi$ and $\lambda$. Because the disk is very thin, we take the order parameter and the magnetic field to be constant across the thickness $d$ of the sample [52]. This enables us to study the disk as an effective two-dimensional system. However, unlike the case of a long cylindrical sample, strong demagnetisation effects are present in a thin disk. The value of $B$ near the edge of the disk is larger than the applied field $H_e$ because geometric demagnetisation effects induce a distortion of the flux lines [8]. Hence the continuity condition $B(R) = H_e$ (3.20) valid for a long cylinder does not apply to describe a thin disk.

In order to find a more suitable choice for the boundary condition for a thin disk, we notice that the higher value of the magnetic field at the boundary, a feature which has been obtained from numerical computations [51], results from a demagnetisation factor $\mathcal{N}$ close to one, such that [41] $H = \frac{H_e}{1 - \mathcal{N}}$ in the Meissner phase. The flux lines are distorted by the sample and they pile up near the edge of the disk. To describe this, we shall thus take as boundary condition for a thin disk, the expression proposed in [52], which consists in taking the potential-vector at the edge of the disk equal to its applied value, *i.e.*

$$\vec{A}(R) = \phi_e a \hat{u}_\theta \tag{3.26}$$

or

$$\phi_b = \phi_e \tag{3.27}$$

Again, this relation does not mean that the field $B$ is uniform and equal to its external strength. A more refined value for the boundary condition could have been obtained by using the expression $\mathcal{N} \simeq 1 - \frac{\pi}{2}\frac{d}{R}$ in the limit $d \ll R$ of a flat disk. Then, $H \simeq \frac{2R}{\pi d}H_e$ or equivalently $\phi_b \simeq \frac{4\delta}{d}\phi_e$. But, since $\delta \simeq d$, we shall use for convenience the simpler boundary condition given above.

Substituting $v_s(R) = a(n - \phi_e)$ in (3.19), the free energy $\mathcal{F}(n, \phi_e)$ of a thin disk containing $n$ vortices is found to be

$$\frac{1}{2\pi}\mathcal{F}(n, \phi_b) = n + \begin{cases} Aa^2(n - \phi_e)^2 - Ba^4(n - \phi_e)^4 & \text{if} \quad a|(n - \phi_e)| \leq \sqrt{2} \\ \frac{\delta}{2a} + \frac{a}{4\delta}(n - \phi_e)^2 & \text{if} \quad a|(n - \phi_e)| > \sqrt{2} \end{cases} \tag{3.28}$$

and the corresponding Gibbs free energy is obtained using (2.29). In our previous work [52], we obtained an expression which can be retrieved from (3.28) by taking $\delta = 1$ and by neglecting the magnetic energy as well as the $a^3$ term. Despite these crude approximations, our analytical results agreed satisfactorily with experimental data, though they could not describe neither the behaviour of a disk with a radius smaller than $\lambda$ and $\xi$, nor its behaviour when $R$ is increased. We apply our present approach to a thin disk with a radius $R$ much smaller than $\xi$, and then we consider the case $R > \xi$.

### 3.3.1 Fractional fluxoid disk and Non-Linear Meissner Effect

We now consider a disk small enough so that no vortices can nucleate *i.e.* its radius $R$ is less than $\xi$ (such a system is sometimes called a *fractional fluxoid* disk [6]). If there are no vortices, the domain $\Omega_1$ is empty and $\Omega = \Omega_2$. Since the radius of $\Omega$ is small with respect to both $\lambda$ and $\xi$, we can no more use the expression (3.28) for the free energy, but we can assume that the amplitude $|\psi|$ of the order parameter has a uniform value $\psi_0$ all over the disk and
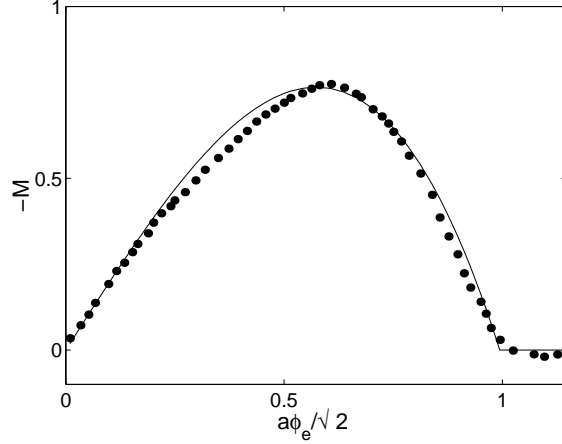
Figure 3.4: Magnetisation of a fractional fluxoid disk. Comparison between the experimental measurements [56] (for $R = 0.31 \mu m$) and the theoretical curve taken from the expression (3.30).

that the magnetic field equals the external applied field $B = H_e$. Moreover, in the absence of vortices $\vec{\nabla}\chi = 0$ and we can choose the Landau gauge $A(r) = rB/2$. Starting from (3.11), and after minimizing the free energy with respect to $\psi_0$, we find the difference between the free energies of the super-conducting and the normal states to be:

$$\frac{\mathcal{G}}{2\pi} = \frac{\phi_e^2}{4}\left(1 - \frac{a^2}{4}\phi_e^2\right) \quad \text{if} \quad a\phi_e \leq \sqrt{2}$$

$$\frac{\mathcal{G}}{2\pi} = 0 \quad \text{otherwise} \tag{3.29}$$

From (2.30) we deduce the magnetisation $M$ of the sample:

$$-M = \frac{1}{2\pi}\frac{\partial \mathcal{G}}{\partial \phi_e} = \frac{1}{2}\left(\phi_e - \frac{a^2}{2}\phi_e^3\right) \quad \text{if} \quad a\phi_e \leq \sqrt{2}$$

$$M = 0 \quad \text{otherwise} \tag{3.30}$$

The curve representing this magnetisation is a cubic. The upper critical field is $\phi_e = 1/a$, i.e. $H_e \propto R^{-1}$; this scaling agrees with the linear analysis of [16] in the limit $R \ll \xi$. The transition between the super-conducting phase and the normal phase is of second order. In Fig. 3.4, we plot the relation (3.30) for $-M$ as a function of the external flux $\phi_e$. The dots represent the experimental points obtained from [2]. The analytical curve has been scaled so that the maximum value of the magnetisation and the critical flux coincide with the corresponding experimental data.

### 3.3.2 Mesoscopic disk with vortices

We now consider a disk with $R \geq \xi$. The Gibbs free energy difference $\mathcal{G}(n, \phi_e)$ of the disk with $n$ vortices is given by (2.29). The entrance field $H_n$ of the $n$-th vortex is obtained by

25

solving the equation $\mathcal{G}(n, \phi_e) = \mathcal{G}(n - 1, \phi_e)$ which, using (3.28), reduces to

$$\frac{2}{\delta} = a(1 + \frac{1}{2\delta^2}) \left( (n - 1 - \phi_e)^2 - (n - \phi_e)^2 \right) - \frac{a^3}{4} \left( (n - 1 - \phi_e)^4 - (n - \phi_e)^4 \right) \qquad (3.31)$$

Using the following change of variable

$$\phi_e = n - \frac{1}{2} + \frac{y}{2a} \qquad (3.32)$$

we obtain an equation for $y$

$$\frac{2}{\delta} = (1 + \frac{1}{2\delta^2})y - \frac{y^3}{8} \qquad (3.33)$$

(a term $a^2/8$ has been neglected in comparison to 1). The solution of (3.33) that satisfies $y \geq 0$ (because $\phi_e \geq 0$) depends on the value of the parameter $\delta$. One can show that the polynomial $P(y) = (1 + \frac{1}{2\delta^2})y - \frac{y^3}{4} - \frac{2}{\delta}$ always has a positive root. We retain only the smaller positive root $y_0$ of (3.33) because in thermodynamic equilibrium, the system always chooses the state with minimal Gibbs free energy. Restoring the usual units, and using (3.32), the nucleation fields are found to be:

$$\begin{aligned} H_1 &= y_0 \frac{\phi_0}{2\pi\sqrt{2}R\lambda} + \frac{\phi_0}{2\pi R^2} \\ H_{n+1} &= H_1 + n\frac{\phi_0}{\pi R^2} \end{aligned} \qquad (3.34)$$

When the applied field $H_e$ lies between $H_n$ and $H_{n+1}$, the disk contains exactly $n$ vortices and its magnetisation is calculated using (2.30). In Fig. 3.5, we have plotted the magnetisation of a mesoscopic disk with $R = 10\lambda\sqrt{2}$ both from exact numerical solutions of the Ginzburg-Landau equations and from the expression (2.30). The agreement is very satisfactory. For larger values of the number $n$ of vortices, a discrepancy between the theoretical and the numerical expressions appears which results from the interaction between the vortices and the edge currents that we have neglected until now.

The expression (3.19) is also in good agreement with previous experimental and numerical results [1, 6]. A non-linear Meissner behaviour still exists before the nucleation of the first vortex as well as between successive jumps. The field $H_1$ of nucleation of the first vortex scales as $R^{-1}$. The transition between a state with $n$ vortices to a state with $(n + 1)$ vortices is of first order since the entrance of a new vortex induces a jump in the magnetisation. These jumps are of constant height and have a period $\frac{\phi_0}{\pi R^2}$. If we use the experimental values of [1] for $R$ and $\lambda$ we obtain a value for the period of the jumps which is in very good agreement with the experimental value.

If $R$ is smaller than a threshold value, the system is a fractional fluxoid disk with a second order phase transition. If $R \simeq 1$, a vortex can nucleate in the disk and a first order transition occurs. When $R$ increases, the number of jumps increases (as $R^2$). These qualitative changes of behaviour with increasing $R$, which are the important features obtained from the present model, have been indeed observed in experiments carried out on disks of different sizes. In an earlier study [52], we obtained satisfactory values for the nucleation fields but the fractional fluxoid disk, and the different regimes obtained by increasing $R$ could not be explained because we neglected subdominant terms that are retained here.

It has been observed experimentally that the period and the height of the jumps cease to be constant when the number of vortices increases. These effects are related both to

26
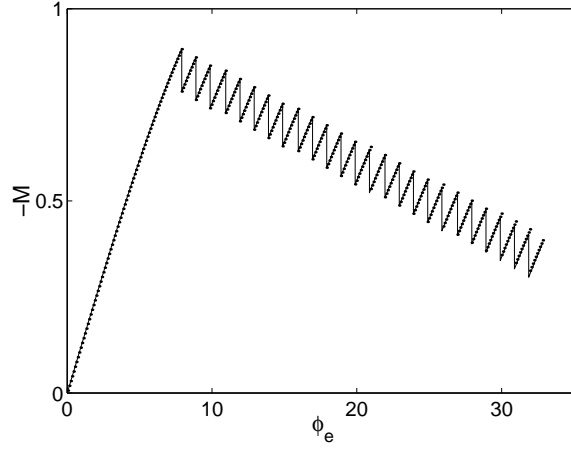
Figure 3.5: Behaviour of the magnetisation of a disk with radius 10 $\lambda\sqrt{2}$, at the dual point. Dots represent the numerical solution and the solid curve the expression (2.30) together with (3.19). The only free parameter $\delta$ has been taken to $\delta = 0.76\lambda$.

interactions between the vortices and between vortices and edge currents. The purpose of the next section is to take into account these interactions and to obtain a better estimate for the free energy and the magnetisation of a mesoscopic disk.

# Chapter 4

# Weakly interacting vortices in the vicinity of the dual point

So far we have obtained analytical expressions for the free energy and the magnetisation of a thin super-conducting disk *at the dual point*. When the Ginzburg-Landau parameter has the special value, $\kappa = 1/\sqrt{2}$, vortices do not interact. This fact, discussed in [34, 37], implies that the bulk free energy does not depend on the location of the vortices. However, when $\kappa$ is away from the dual point, the vortices start interacting among themselves; therefore the bulk free energy ceases to be a purely topological integer $n$ and the vortex interaction energy must be taken into account. Because of this interaction the vortices are no longer necessarily placed at the center of the disk: in an equilibrium configuration, the cylindrical symmetry can be broken and the optimal free energy may correspond to geometrical patterns such as regular polygons, polygons with a vortex at the center, or even rings of polygons [9, 44, 55]. It is the competition between the interaction amongst vortices and the interaction between vortices and edge currents that determines the shape of the equilibrium configuration.

Analytical studies were mostly carried out in the limit $\kappa \to \infty$ and were based on the London equation [38, 40, 44] for which vortices are point-like and have a hard-core repulsion [41]. We shall study a regime where $\kappa$ is slightly different than $1/\sqrt{2}$, *i.e.* a regime where vortices interact *weakly*. We shall determine, to the leading order in $(\kappa - 1/\sqrt{2})$, the interaction energy of the vortices.

## 4.1 The interaction energy

In order to obtain an estimate for the free energy of a system of interacting vortices, we have solved numerically the Ginzburg-Landau equations for a cylindrically symmetric infinite system with $n$ vortices located at the center (these equations are explicitly written in Appendix A). The free energy per vortex is plotted in Fig. 4.1 as a function of $\kappa$, for $n = 1, 2, 3, 5$ and 10. At the dual point, the free energy per vortex is equal to 1 and is independent of $n$: all the curves pass through this point. When $\kappa$ is different from $\frac{1}{\sqrt{2}}$ the interaction between the vortices changes the value of the free energy. One can deduce from figure 6 that vortices attract each other for $\kappa$ less than $\frac{1}{\sqrt{2}}$ while they repel each other when $\kappa \geq \frac{1}{\sqrt{2}}$.

From our numerical results we observed that in the vicinity of the dual point, the free
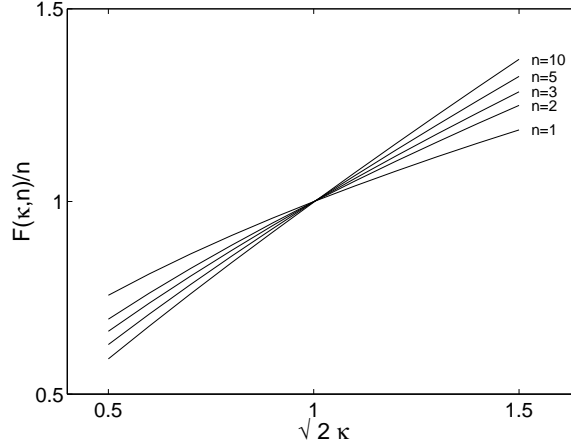
Figure 4.1: Behaviour of the free energy per vortex $F/n = \mathcal{F}/2\pi n$ as a function of $\sqrt{2}\kappa$ for different values of $n$, the number of vortices. At the self-dual point $\sqrt{2}\kappa = 1$, the energy $\mathcal{F}(n) = n\mathcal{F}(1)$ so that the interaction energy between the vortices vanishes identically.

energy $\mathcal{F}(\kappa, n)$ satisfies the following scaling behaviour:

$$\frac{1}{2\pi}\mathcal{F}(\kappa, n) = n(\kappa\sqrt{2})^{\alpha(n)} \tag{4.1}$$

We note that the relation (4.1) is exact at the dual point. For $n = 1$, $\mathcal{F}(\kappa, 1)$ is nothing but the self energy $\mathcal{U}_S$ of a vortex. In the vicinity of the dual point we can write:

$$\frac{1}{2\pi}\mathcal{F}(\kappa, 1) = 1 + \alpha(1)(\kappa\sqrt{2} - 1) \tag{4.2}$$

The values of the function $\alpha(n)$, as determined from numerical computations, for $n$ ranging from 1 to 30 are given in the following table

| n | $\alpha(n)$ | n | $\alpha(n)$ | n | $\alpha(n)$ |
|---|---|---|---|---|---|
| 1 | 0.417 | 11 | 0.785 | 21 | 0.841 |
| 2 | 0.544 | 12 | 0.794 | 22 | 0.845 |
| 3 | 0.613 | 13 | 0.802 | 23 | 0.847 |
| 4 | 0.658 | 14 | 0.809 | 24 | 0.850 |
| 5 | 0.690 | 15 | 0.815 | 25 | 0.853 |
| 6 | 0.715 | 16 | 0.821 | 26 | 0.855 |
| 7 | 0.734 | 17 | 0.826 | 27 | 0.857 |
| 8 | 0.750 | 18 | 0.830 | 28 | 0.859 |
| 9 | 0.764 | 19 | 0.834 | 29 | 0.860 |
| 10 | 0.775 | 20 | 0.838 | 30 | 0.862 |

We can now derive an approximation for the free energy of a $n$ vortices configuration located at the center of the disk and for $\kappa$ close to $1/\sqrt{2}$. Since this configuration is cylindrically symmetric, one can again use the circle $\Gamma$ to separate the system into two subdomains $\Omega_1$
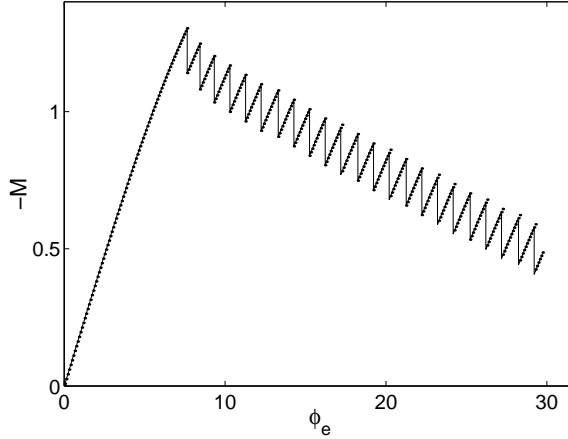
Figure 4.2: Magnetisation curve of a disk of radius 10 $\lambda\sqrt{2}$, as a function of the applied field for $\kappa\sqrt{2} = 0.9$. Dots represent the numerical solution and the solid curve the expression (2.30) together with (4.4, 4.1). The only free parameter $\delta$ has been taken to $\delta = 0.76\lambda$.

and $\Omega_2$ and then estimate separately the two contributions to the total free energy. From our numerical scaling result, we deduce a formula for the bulk free energy of a finite system which is valid for $\kappa$ close to the dual point. Expanding (4.1) in the vicinity of the dual point, we obtain:

$$\frac{1}{2\pi}\mathcal{F}(\Omega_1) = n + (\kappa\sqrt{2} - 1)n\alpha(n) \qquad (4.3)$$

and the boundary contribution, obtained via a variational Ansatz is now given by:

$$\frac{1}{2\pi}\mathcal{F}(\Omega_2) = \begin{cases} Av_s^2(R) - B(\kappa)v_s^4(R) & \text{if} \quad |a(n - \phi_e)| \le 2\kappa \\ \kappa^2\delta/a + v_s^2/4a\delta & \text{if} \quad |a(n - \phi_e)| > 2\kappa \end{cases} \qquad (4.4)$$

where $A$ is still given by the relation (3.18) while $B(\kappa)$ is now given by $B(\kappa) = \delta/16a\kappa^2$.

The magnetisation curve of Fig. 4.2 shows both the numerical results and a plot of the magnetisation deduced from (4.4) using (2.30). We notice that the magnetisation of a meso-scopic disk is modified when the interactions between vortices are taken into account. The period and the amplitude of the jumps are not constant anymore; besides, the non-linearity of the curve between two successive jumps is enhanced. These important features of the $M - H_e$ curve were observed in previous experimental and numerical results [1, 56]. Here we have shown that these features are a consequence of vortex interactions.

## 4.2 The energy of a large multi-vortex

In the limit of very large number of vortices $n \to \infty$ some analytical results can be obtained from a simple Ansatz for the solutions of Ginzburg-Landau equations. We observe that the numerical solution to the equations (2) for $n = 30$, shown on the Fig. 4.3 is close to the rectangular shape for both $f(r) = |\psi(r)|^2$ and $B(r)$. Therefore it would be plausible to approximate both functions in the limit $n \to \infty$ by simple expressions. Using the notations
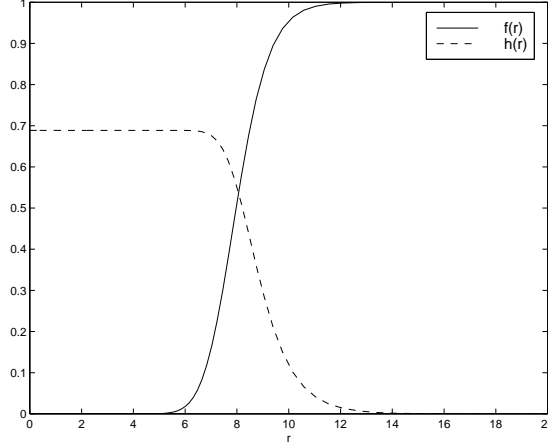
Figure 4.3: The function $f(r)$ and $h(r)$ for $n = 30$ and $\sqrt{2}\kappa = 1.5$.

of Appendix A we write

$$f(r) = \begin{cases} 0 & r < a \\ 1 & r > a \end{cases} \quad , \qquad B(r) = \begin{cases} B_0 & r < b \\ 0 & r > b \end{cases} \quad . \tag{4.5}$$

The solutions depend on three parameters: $a$, the "radius of the vortex", $b$, the "radius of magnetic field penetration" and $B_0 = B(0)$, the value of the magnetic field at $r = 0$. The approximate function $p(r)$, related to the super-fluid velocity $p = rv_s$, is therefore

$$p(r) = \begin{cases} \frac{B_0 b^2}{2}(1 - r^2/b^2) & r < b \\ 0 & r > b \end{cases} \tag{4.6}$$

In order to find three parameters $a$, $b$ and $B_0$ the following equations are used:

- Flux quantization

$$\int_0^\infty r\,dr\,B(r) = n = p(0) = \frac{B_0 b^2}{2} \tag{4.7}$$

- Identity (A.15) of Appendix A, true for an value of $\kappa$.

$$\int_0^\infty r\,dr\,B^2(r) = \frac{B_0^2 b^2}{2} = \kappa^2 \int_0^\infty r\,dr\,\left(1 - f^2(r)\right) = \frac{\kappa^2 a^2}{2} \tag{4.8}$$

- Identity (A.10) of Appendix A that follows from the integration of the Maxwell equation (A.3)

$$B_0 = 2\int_0^\infty \frac{dr}{r}\,p(r)f^2(r) = \frac{B_0 b^2}{2}\int_a^b \frac{dr}{r}(1 - r^2/b^2) = \frac{B_0 b^2}{2}\left[2\log\frac{b}{a} - \left(1 - \frac{a^2}{b^2}\right)\right] \tag{4.9}$$

Using (4.7) and (4.8) the last equation can be rewritten in terms of $B_0$ only. Let us define $X = B_0/\kappa$. In terms of this variable we have

$$\frac{\kappa}{n} = \frac{1}{X}\log\frac{1}{X^2} + \left(X - \frac{1}{X}\right) \tag{4.10}$$

31
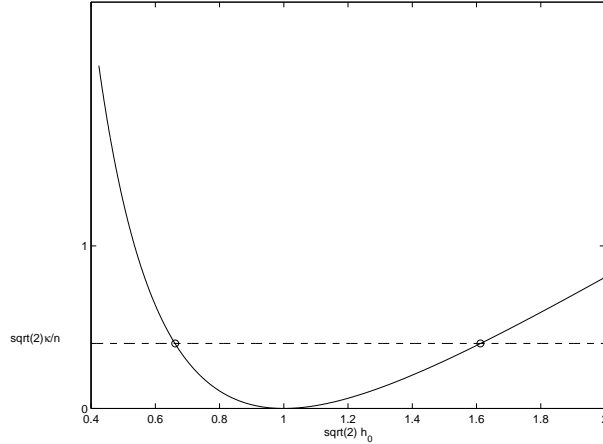
Figure 4.4: Graphical solution to the equation (4.10). Two solutions are shown

This is the (transcendental) equation to determine $X$ as function of $\kappa$. The right hand side is shown on Fig. 4.4 as a function of $X$. There are always two solutions to (4.10) for each value of $\sqrt{2}\kappa/n$. The solution $X(\kappa) > 1$ is to be chosen when $\kappa < 1/\sqrt{2}$ and $X(\kappa) < 1$ for $\kappa > 1/\sqrt{2}$. One interesting consequence of the relation (4.10) is that in the limit $n \to \infty$ for fixed $\kappa$ one finds $X \to 1$. The exact way of approaching this value can be deduced from the Taylor expansion up to the second order of the function in the rhs of (4.10) near $X$ that yields $X \approx 1 \pm \sqrt{\kappa/2n}$ in the limit $n \to \infty$. The sign is determined by the value of $\kappa$, whether it is less/greater than $1/\sqrt{2}$.

The free energy is found from the expression (A.16):

$$\frac{1}{2\pi}F = \kappa^2 \int_0^\infty r\,dr\,\left(1 - f^2(r)\right) = \frac{\kappa^2 a^2}{2} = \frac{B_0^2 b^2}{2} \tag{4.11}$$

It can be rewritten as

$$\frac{1}{2\pi}F(\kappa)/n = \frac{B_0^2 b^2}{2} = X(\kappa, n)\sqrt{2}\kappa \tag{4.12}$$

which in the limit $n \to \infty$ has the form (4.1) with $\alpha = 1$. This gives us the limit $\alpha(n \to \infty) = 1$ consistent with the numerical values in section 4.1. The comparison with numerical values for the energy per vortex $F/2\pi n$ is shown on Fig. 4.5. The relative error goes to zero as $\propto 1/\sqrt{n}$, but for specific values of $n$ it decreases slowly from 20% to 8%. It is however important that the expression (4.12) gives qualitative understanding of the stability of vortices: for $\sqrt{2}\kappa > 1$ one sees that $X(\kappa, n)$ is *increasing* function of $n$ so the energy per vortex $F/n$ *grows* with $n$ and the multi-vortex is unstable with respect to decomposition to $n$ vortices, while for $\sqrt{2}\kappa > 1$ one finds that $X(\kappa, n)$ is *decreasing* function of $n$ so the energy per vortex $F/n$ *diminishes* with $n$ and the multi-vortex is stable.

## 4.3 Two-vortex interaction energy

The exponent $\alpha(n)$ in the relations (4.1) or (4.3) allows to describe the interacting potential between vortices. It is interesting to compare the result (4.1) with the energy of $n$ vortices
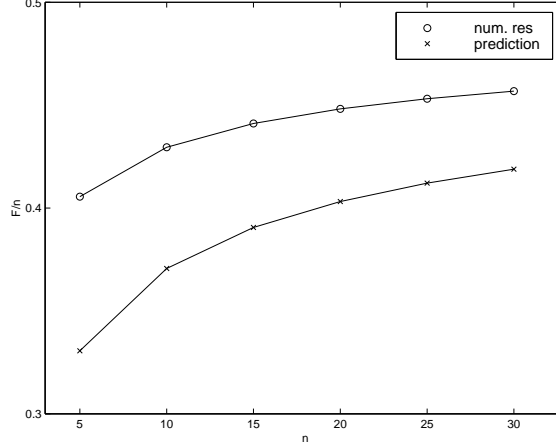
Figure 4.5: Energy per vortex $F/n$ as a function of vorticity $n$ for $\sqrt{2}\kappa = 2$.

obtained by assuming a two-body interaction. In this case the energy of the whole system of $n$ vortices can be written as a sum of two terms

$$\frac{1}{2\pi}\mathcal{F} = n\mathcal{U}_S + \frac{n(n-1)}{2}\mathcal{U}_I(0) \tag{4.13}$$

where $\mathcal{U}_S$ represents, as noted before, the self-energy of a vortex and $\mathcal{U}_I$ the two body interaction potential. Using the data of [37], we can estimate these two energies to the leading order in $(\kappa\sqrt{2} - 1)$. We obtained:

$$\mathcal{U}_S = 1 + \beta_1(\kappa\sqrt{2} - 1) \quad \text{with} \quad \beta_1 \simeq 0.4 \tag{4.14}$$

$$\mathcal{U}_I(r) = \beta_2(\kappa\sqrt{2} - 1)\min\left(1, \exp(-C(r - \frac{1}{\kappa}))\right) \tag{4.15}$$

with $\beta_2 \simeq \frac{1}{4}$ and $C \simeq \frac{1}{2}$. From this analysis, and assuming only two-body interaction, we derive an approximate value for the free energy of a configuration with $n$ vortices placed at the same point:

$$\frac{1}{2\pi}\mathcal{F}(\kappa, n) = n\mathcal{U}_S + \frac{n(n-1)}{2}\mathcal{U}_I(0) \simeq n + (\kappa\sqrt{2} - 1)n\left(\beta_1 + \beta_2\frac{n-1}{2}\right) \tag{4.16}$$

If we compare this relation to the previous expression (4.3) we find that instead of the sublinear function $\alpha(n)$ we have a linear behaviour $\beta_1 + \frac{n-1}{2}\beta_2$. Hence, the function $\alpha(n)$ takes into account not only two-body interactions among vortices but also multiple interactions which are present for values of $\kappa$ around the dual point unlike the large $\kappa$ limit where only the two-body contribution remains.

33

# Chapter 5

# Free energy of a system without cylindrical symmetry

In this section, we calculate the energy at the dual point of a system with only one vortex that is not located at the center of the disk. Such a configuration is not in thermodynamic equilibrium and its free energy can be related to a surface energy barrier (analogous to the classical Bean-Livingston barrier in the London limit). We first show that even when the cylindrical symmetry is broken, the system can still be separated into bulk and edge domains.

## 5.1 Bulk and edge domains. The curve $\Gamma$

We have seen in section 3.1 that when one or more vortices are located at the center of the disk, there exists a circle $\Gamma$ on which the current vanishes identically. This circle allowed us to define a bulk and an edge domain and to identify the bulk energy with the fluxoid.

If all the vortices are not placed at the center of the disk (*i.e.* the configuration is not cylindrically symmetric) there is in general no curve of zero current. However the curve $\Gamma$ has now the following property: at each point $M$ of $\Gamma$ the current $\vec{\jmath}$ is normal to $\Gamma$. The existence of such a curve is shown by the following argument. Consider a disk with only one vortex $V$ situated at a point different from the center of the disk. Take a line segment joining the vortex $V$ to the closest point $S$ on the boundary of the disk (see Fig. 5.1). The component of the current density normal to the $VS$ segment changes its sign when one goes from $V$ to $S$. Hence, there exists a point $M$ along this segment where the current either vanishes or is parallel to $VS$. To draw the curve $\Gamma$ we start from $M$ in a direction orthogonal to the $VS$ segment, and then $\Gamma$ is constructed via infinitesimal steps by imposing that at a point $M' = M + dM$, very close to $M$, the direction of $\Gamma$ is orthogonal to the direction of the current at $M'$.

Although we lack a general proof, we believe on topological grounds that for vortices at arbitrary positions, there always exists a $\Gamma$ curve which is everywhere orthogonal to the current (one should note that $\Gamma$ does not necessarily have only one connected component). In [57], we shall present a numerical construction of $\Gamma$. In the sequel of this work we assume that $\Gamma$ exists, that it encircles all the vortices, and consists of one or many simple closed curves. We shall call the curve $\Gamma$ *the separatrix*.

Using $\Gamma$, the domain $\Omega$ can be decomposed in two regions $\Omega_1$ and $\Omega_2$ such that:
(i) $\Omega_1 \bigcup \Omega_2 = \Omega$ ;
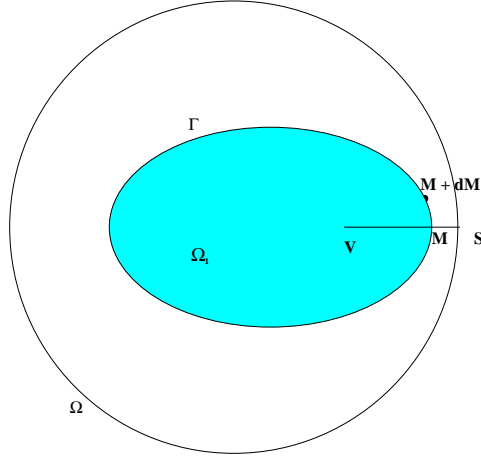
Figure 5.1: The separation of a system without cylindrical symmetry in two subdomains by a curve $\Gamma$.

(ii) $\Omega_1$ contains all the vortices ( $\Omega_1$ may have multiply connected components);

(iiii) $\Omega_2$ contains the edge of the disk;

(iv) the separatrix $\Gamma$ is the boundary between $\Omega_1$ and $\Omega_2$ and is everywhere normal to the current density.

The remarkable property of the separatrix implies that along $\Gamma$ one can write:

$$\oint_\Gamma (\vec{\jmath} + \vec{A}) \cdot \vec{dl} = \oint_\Gamma \left( \frac{\vec{\jmath}}{|\psi|^2} + \vec{A} \right) \cdot \vec{dl} = \oint_\Gamma \vec{\nabla}\chi \cdot \vec{dl} \tag{5.1}$$

since along $\Gamma$, $\vec{\jmath} \cdot \vec{dl} = 0$. Since the separatrix is the boundary of $\Omega_1$, the property (5.1) ensures that the total magnetic flux through $\Omega_1$ is quantized. Hence, at the dual point, we can again use the method of Bogomoln'yi and find the free energy of $\Omega_1$ to be a purely topological number, just as for an infinite domain, even if the cylindrical symmetry is broken.

## 5.2 Free energy of one vortex: the surface energy barrier.

As before, we estimate the contribution $\mathcal{F}(\Omega_2)$ to the total free energy via a variational Ansatz, taking the modulus of the order parameter to be constant. To obtain a qualitative result for the surface energy barrier we neglect the magnetic energy so that, at the dual point, we have:

$$\begin{aligned}
\frac{1}{2\pi}\mathcal{F}(\Omega_2) &\approx \int_{\Omega_2} |\psi|^2 |\vec{\nabla}\chi - \vec{A}|^2 + \frac{(1 - |\psi|^2)^2}{2} \\
&\approx \frac{\delta}{2a} \left( \psi_0^2 \langle v_s^2 \rangle + (1 - \psi_0^2)^2 \right)
\end{aligned} \tag{5.2}$$

where

$$\langle v_s^2 \rangle = \int \frac{d\theta}{2\pi} |\vec{\nabla}\chi - \vec{A}(R)|^2 \tag{5.3}$$

is the super-fluid velocity square averaged over the boundary of the disk. As before, we have replaced the integral over $\Omega_2$ by a line integral along the boundary of the sample (*i.e.* the

35
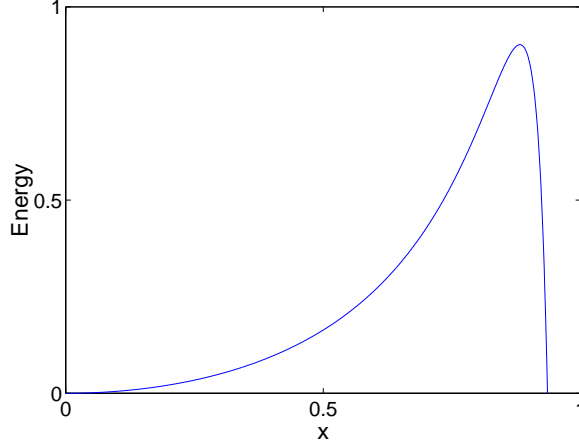
Figure 5.2: Confining energy of a vortex inside a disk due to edge currents.

disk of radius $R$) multiplied by an effective length $\delta$. The function $\chi$ appearing in (5.2) is the phase of the order parameter, and the vector potential is taken, as before, to its value on the boundary of the sample. Optimizing (5.2) with respect to $\psi_0$ we find that:

$$\psi_0^2 \;=\; 1 - \frac{\langle v_s^2 \rangle}{2} \tag{5.4}$$

$$\frac{1}{2\pi}\mathcal{F}(\Omega_2) \;=\; \frac{\delta}{2a}\left(\langle v_s^2 \rangle - \frac{\langle v_s^2 \rangle^2}{4}\right) \tag{5.5}$$

for $\langle v_s^2 \rangle \leq \sqrt{2}$. The phase function $\chi$ and the vector potential near the edge of the disk are calculated in Appendix B. Using these results, we obtain (for n=1):

$$\frac{1}{2\pi}\mathcal{F}(\Omega_2) = \frac{\delta}{2a}\left(a(1 - \phi_e)^2 - \frac{a^3}{4}(1 - \phi_e)^4\right) + f(x, a, \phi_e - 1)\delta \tag{5.6}$$

The function $f(x, a, \phi_e - 1)$ determines the dependence of the free energy on the position $x$ of the vortex; hence, it measures the interaction energy between the edge currents and the vortex as a function of its position. It is given by

$$f(x, a, \phi_e - 1) = \frac{2ax^2}{1 - x^2}(\phi_e - 1)^2\left(1 - a^2\frac{(\phi_e - 1)^2}{1 - x^2}\right) \tag{5.7}$$

From this expression, we observe that the edge currents tend to confine the vortex inside the system. In Fig. 5.2 the surface energy as a function of the position $x$ of the vortex is plotted. According to (5.4), only the increasing part of the curve is physical. We nevertheless plot the curve defined by (5.7) in the whole range $0 \leq x \leq 1$ in order to emphasize the similarity between our result and the well-known Bean-Livingston surface barrier effect that was first derived using the London theory [42, 41].

# Chapter 6

# The London limit of the Ginzburg-Landau equations

In the London limit $\kappa \to \infty$ vortices are point-like and the amplitude of the order parameter $|\psi|$ does not vary. It can be taken to one except at the position of the vortices where it vanishes. The Ginzburg-Landau free energy (2.19) reduces to

$$\mathcal{F} = \int \left( \frac{B^2}{2} + \left| \left( \vec{\nabla} - i\vec{A} \right) \psi \right|^2 \right) d^2r \tag{6.1}$$

Using this equation and $|\psi|^2 = 1$, except at the position of the vortices, we can write

$$\left| \left( \vec{\nabla} - i\vec{A} \right) \psi \right|^2 = \left( \vec{\nabla} \times \vec{B} \right)^2 \tag{6.2}$$

so that the free energy is given by the expression

$$\mathcal{F} = \frac{1}{2} \int \left( B^2 + \frac{1}{2} \left( \vec{\nabla} \times \vec{B} \right)^2 \right) d^2r \tag{6.3}$$

which in our units is independent of $\kappa$. To obtain the equation for $B$, we notice that the phase $\chi$ is non singular except near a vortex (say at $r = 0$) where it has the property that

$$\oint \vec{\nabla}\chi \cdot \vec{dl} = 2\pi \tag{6.4}$$

on any closed contour encircling the singularity at point $r = 0$. Using Stokes theorem,

$$\oint \vec{\nabla}\chi \cdot \vec{dl} = \iint d\vec{S} \cdot \vec{\nabla} \times \vec{\nabla}\chi = 2\pi, \tag{6.5}$$

we deduce that the $\hat{z}$-component of $\vec{\nabla} \times \vec{\nabla}\chi$ equals $2\pi\delta(\vec{r})$. The equation for $B$ is then given by [1]

$$\nabla^2 B - 2B = -4\pi\delta(\vec{r}) \tag{6.6}$$

---

[1] It should be noted here that in order to obtain this equation we must be in the London limit and impose $|\psi|^2 = 1$ since starting from (2.21), we have $-\Delta h = |\psi|^2(\vec{\nabla} \times \vec{\nabla}\chi - h)$ and where $(\vec{\nabla} \times \vec{\nabla}\chi)_{\hat{z}} = 2\pi\delta_2(\vec{r})$, we must in principle take $|\psi|^2 = 0$.

This equation can be generalized to the case of $N$ vortices placed at points $\vec{r}_k$

$$\nabla^2 B - 2B = -4\pi \sum_{k=1}^{N} \delta(\vec{r} - \vec{r}_k) \qquad (6.7)$$

In the next section we shall present the solution of this equation in the particular case of a cylinder with circular cross section.

## 6.1 Solution for $N$ vortices in a circular cylinder

We shall study a circular cylinder of radius $R$. The magnetic induction and Gibbs energy of a system of $N$ vortices in this geometry has been studied first in [38]. The detailed derivation of the results is presented in the Appendix C. The solution $B(r,\theta)$ of the equation (6.7) satisfying the boundary condition $B(R,\theta) = H_e$ can be written as a sum of three terms:

$$B(r,\theta) = B_M(r) + B_V(r,\theta) + B_{\bar{V}}(r,\theta) \qquad (6.8)$$

The first term

$$B_M(r) = H_e I_0(\sqrt{2}r)/I_0(\sqrt{2}R), \qquad (6.9)$$

where $I_0(x)$ is the modified Bessel function of first kind, describes the Meissner effect in the absence of vortices. The second term is the magnetic induction of $N$ vortices placed at points $\vec{r}_k = (r_k, \theta_k)$ for $k = 1, \ldots, N$ and it is given by

$$B_V(r,\theta) = 2 \sum_{k=1}^{N} K_0(\sqrt{2}|\vec{r} - \vec{r}_k|) \qquad (6.10)$$

The third term, written with help of the modified Bessel function of first and second kind $I_n(x)$, $K_n(x)$ as

$$B_{\bar{V}}(r,\theta) = -2 \sum_{n=-\infty}^{+\infty} K_n(\sqrt{2}R) \frac{I_n(\sqrt{2}r)}{I_n(\sqrt{2}R)} \sum_{k=1}^{N} I_n(\sqrt{2}r_k) \cos n(\theta - \theta_k) \qquad (6.11)$$

ensures the boundary condition $B(R,\theta) = H_e$. We are interested in polygonal rings of vortices. For this particular configuration $r_k = d$, $\theta_k = 2\pi k/N$ and the expression for $B_{\bar{V}}(r,\theta)$ can be simplified

$$B_{\bar{V}}(r,\theta) = -2N \sum_{n=-\infty}^{+\infty} K_n(\sqrt{2}R) \frac{I_n(\sqrt{2}r)I_n(\sqrt{2}d)}{I_n(\sqrt{2}R)} \cos Nn\theta \qquad (6.12)$$

The corresponding Gibbs energy has also been obtained in [38]. The expression of the dimensionless Gibbs energy is given by

$$\mathcal{G} = \mathcal{F} - H_e \int B(\vec{r}) \, d^2r + \pi R^2 H_e^2/2 \qquad (6.13)$$

The field $B_V$ diverges at the positions of the vortices and the corresponding part of the free energy must be regularized. The singular contribution coincides with one calculated by Abrikosov [58] for the case of infinite system and is given by

$$\mathcal{F}_\infty = N\mathcal{E} + 2\pi \sum_{j \neq k} K_0(\sqrt{2}|\vec{r}_j - \vec{r}_k|) \qquad (6.14)$$

where $\mathcal{E} = 2\pi(\ln\kappa + 0.081)$ is the one-vortex energy.

The regular part of the Gibbs energy is calculated in the Appendix D. Using the expressions (6.9),(6.10) and (6.11) for the magnetic field, one obtains

$$
\begin{aligned}
\mathcal{G}_N - \mathcal{G}_0 &= N\mathcal{E} + 2\pi\sum_{j \neq k} K_0(\sqrt{2}|\vec{r}_j - \vec{r}_k|) - 2\pi H_e \sum_{k=1}^{N}\left(1 - \frac{I_0(\sqrt{2}r_k)}{I_0(\sqrt{2}R)}\right) \\
&\quad - 2\pi \sum_{n=-\infty}^{+\infty}\sum_{i,j=1}^{N} \frac{K_n(\sqrt{2}R)I_n(\sqrt{2}r_i)I_n((\sqrt{2}r_j)}{I_n(\sqrt{2}R)}\cos n(\theta_i - \theta_j)
\end{aligned}
\tag{6.15}
$$

where $\mathcal{G}_0 = \pi R H_e^2\left(\frac{R}{2} - \frac{\sqrt{2}}{2}\frac{I_1(\sqrt{2}R)}{I_0(\sqrt{2}R)}\right)$ is the Gibbs energy in the absence of vortices *i.e.* in the Meissner state. For the particular case of vortices distributed on a regular polygon of radius $d$, the previous expression (6.15) simplifies and becomes

$$
\begin{aligned}
\frac{\mathcal{G}_N - \mathcal{G}_0}{N} &= \mathcal{E} + 2\pi\sum_{l=1}^{N-1} K_0(|2\sqrt{2}d\frac{l\pi}{N}|) - 2\pi H_e\left(1 - \frac{I_0(\sqrt{2}d)}{I_0(\sqrt{2}R)}\right) \\
&\quad - 2\pi N \sum_{n=-\infty}^{+\infty} \frac{K_{Nn}(\sqrt{2}R)I_{Nn}(\sqrt{2}d)^2}{I_{Nn}(\sqrt{2}R)}
\end{aligned}
\tag{6.16}
$$

Similar expressions have been already obtained previously in [38, 59] and we shall now discuss them in the limit of a small radius $R$ in order to use the particularly elegant structure of the corresponding solutions to derive analytical expressions for the field and the energy.

# Chapter 7

# The limit of a small system

We shall now consider the limiting case where $R \ll \lambda$ for which the corresponding Gibbs free energy was obtained in [60]. In this limit the previous expressions greatly simplify. Since all the distances are given in units of $\lambda\sqrt{2}$, we can expand the expression for the magnetic induction using the expansion of the Bessel functions for small argument, so that

$$B(z, \bar{z}) - H_e = \phi_e(|z|^2 - 1) + 2\sum_{i=1}^{N} \ln\left|\frac{1 - \bar{z}_i z}{z - z_i}\right| \tag{7.1}$$

where $\phi_e = H_e R^2/2$ is the flux of the external field through the system and we use the complex notations,

$$z = \left(\frac{r}{R}\right)e^{i\theta} \quad \text{and} \quad z_k = \left(\frac{r_k}{R}\right)e^{i\theta_k} \tag{7.2}$$

together with complex conjugate $\bar{z}$ and $\bar{z}_k$. This expression for the magnetic induction is solution of the modified London equation

$$\frac{\partial^2}{\partial z \partial \bar{z}} B(z, \bar{z}) - H_e = -\pi \sum_{i=1}^{N} \delta(z - z_i)\delta(\bar{z} - \bar{z}_i) \tag{7.3}$$

which can be obtained from (6.7) for small variation of the field on the scale of $R$.

In the particular case, we shall consider from now on, of vortices distributed along a regular polygon of radius $d$, we have $r_k = d$ and for the $N$ vortices sitting on a shell, the angle $\theta_k$ of the $k$-th vortex is $\theta_k = 2\pi k/N$. Then, defining the real quantity $x = d/R \leq 1$, the relation (7.1) becomes

$$B_N(z, \bar{z}) - H_e = \phi_e(|z|^2 - 1) + 2\ln\left|\frac{1 - x^N z^N}{x^N - z^N}\right| \tag{7.4}$$

whereas the Gibbs energy (6.16) becomes

$$\frac{\mathcal{G}_N - \mathcal{G}_0}{N} = \mathcal{E}' - 2\pi\phi_e(1 - x^2) + 2\pi\ln(1 - x^{2N}) - 2\pi(N - 1)\ln x - 2\pi\ln N \tag{7.5}$$

where $\mathcal{G}_0 = \pi\phi_e^2/2$ and $\mathcal{E}' \simeq 2\pi\ln(R/\xi)$.

The relation between the radius $x$ of the polygonal configuration and the external flux $\phi_e$ is obtained by minimizing $\mathcal{G}_N(x, H_e)$ with respect to $x$ at fixed $\phi_e$, namely

$$\phi_e = \frac{N - 1}{2x^2} + \frac{Nx^{2N-2}}{1 - x^{2N}} \tag{7.6}$$
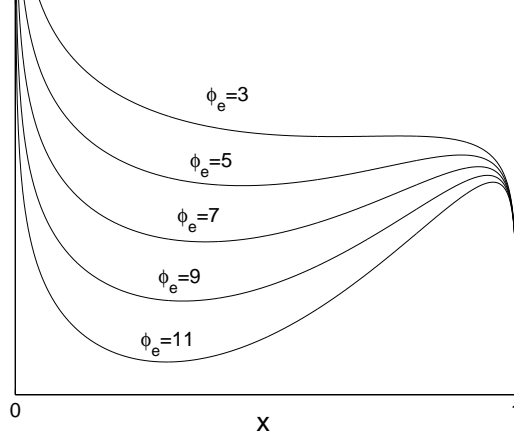
Figure 7.1: Behavior of the Gibbs energy as a function of the position $x$ of the $N = 3$ vortex shell. The maximum which exists for high enough applied field corresponds to the unstable equilibrium point for the vortex configuration and gives the height of the Bean-Livingston barrier.

## 7.1 The Bean-Livingston barrier

The relation (7.6) has, as a function of the applied flux $\phi_e$, either zero, one or two solutions. The latter case corresponds for the Gibbs energy (7.5) to the existence of a Bean-Livingston potential barrier [42] for which one solution is stable and gives the equilibrium position of the vortices while the second solution is unstable and gives the height of the potential barrier as shown in the Fig. 7.1. It should be noticed that for more than one vortex ($N > 1$), the energy $\mathcal{G}_N$ diverges logarithmically at the origin $x = 0$ due to the repulsion between the vortices.

The potential barrier disappears for low enough applied flux below a characteristic value $\phi_{min}$ given by the minimum of the function $f_N(x)$ in the rhs of (7.6) as represented in Fig. 7.2. Defining $y = x^2$, we have

$$f_N(y) \;=\; \frac{N-1}{2y} + \frac{Ny^{N-1}}{1-y^N} \tag{7.7}$$

$$f_N'(y) \;=\; -\frac{N-1}{2y^2} + \frac{N(N-1)y^{N-2}}{1-y^N} + \frac{N^2 y^{2N-2}}{(1-y^N)^2} \tag{7.8}$$

For large values of $N$, we have $y_{min}^N \simeq 1/2N$ so that

$$\phi_{min} \simeq \frac{N-1}{2\sqrt[N]{2N}} \simeq \frac{N-1}{2} \tag{7.9}$$

For $\phi_e < \phi_{min}$, there is no stable solution and then no equilibrium position for $N$ vortices exists.

## 7.2 Matching fields

By plugging the expression (7.6) into the expression (7.5), we obtain the behavior of the Gibbs energy for $N$ vortices as a function of the applied flux $\phi_e$. This expression is the counterpart,
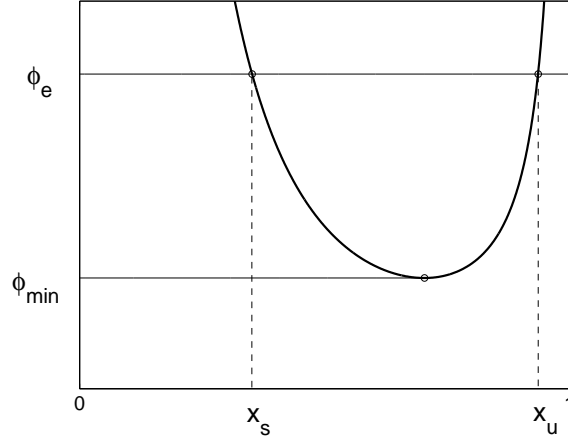
Figure 7.2: Graphical solution of equation (7.6). The curve shows the behavior of $\phi_e(x)$. The two solutions $x_s$ and $x_u$ correspond respectively to the stable and unstable positions of the vortex shell for values of the magnetic field above $\phi_{min}$.

in the London limit, of the parabolae obtained at the Bogomoln'yi point [46] for $\kappa = 1/\sqrt{2}$. For a given value $\phi_e$ of the applied field, the optimal number of vortices corresponds to the envelop of the set of curves $\mathcal{G}_N(\phi_e)$ as represented in the Fig. 7.3. The matching values $\phi_N$ are the values taken by the flux of the external field at which $\mathcal{G}_{N-1}(\phi_N) = \mathcal{G}_N(\phi_N)$. They correspond to the transition between configurations with $N-1$ and $N$ vortices respectively.

Using the relation (7.5), it is straightforward to obtain the field at which the first vortex penetrates the system; it is given by $\phi_1 = \mathcal{E}'/2\pi = \ln(R/\xi)$. This field is larger than the field at which the Bean-Livingston potential barrier disappears. For larger values of $N$, in the limit $\phi_e \gg \phi_{min}$, we approximate the relation (7.6) by $\phi_e = (N-1)/2x^2$ so that

$$\frac{\mathcal{G}_N - \mathcal{G}_0}{2\pi} \approx N\left(\phi_1 - \phi_e\right) + \frac{N(N-1)}{2}\left(1 + \ln\frac{2\phi_e}{N-1}\right) - N\ln N \qquad (7.10)$$

Equating this to the similar expression for $\mathcal{G}_{N-1}(\phi_e)$ we obtain that the matching fields for $N \to \infty$ are given by solution of the following equation

$$\phi_N = \phi_1 + \frac{N-1}{2}\left(1 + 2\ln\frac{2\phi_N}{N}\right) - \ln N + 1 + \mathcal{O}(1/N) \qquad (7.11)$$

We use the following ansatz $\phi_N = \frac{1}{2}(aN + b\ln N + c)$. Substituting it to (7.11) we obtain the coefficients

$$b = -\frac{2a}{a-2}, \qquad c = \frac{2a}{a-2}\left(1 + \phi_1 - \frac{a}{2}\right), \qquad (7.12)$$

where the coefficient $a$ satisfies the transcendental equation:

$$a = 1 + 2\ln a \qquad (7.13)$$

This equation has one obvious solution $a = 1$ which is compatible with (7.11). However from the exact numerical calculations of the matching fields using the relation (7.6) we infer that
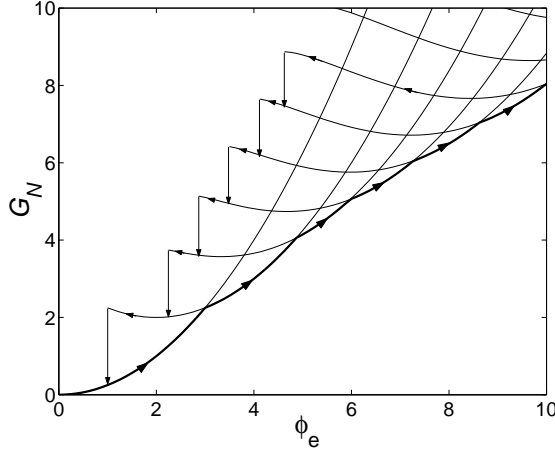
Figure 7.3: Dependence of the Gibbs energy as a function of the applied flux $\phi_e$. The equilibrium behavior of the system is described by the envelop of the curves for $\mathcal{G}_N(H_e)$. Arrows show the direction in which the magnetic flux is varied.

the second root $a \simeq 3.5129$ is realized in the solution for the matching fields. It leads to the formula

$$\phi_N = 1.76N - 2.32\ln N + 2.32\phi_1 - 1.76 + \mathcal{O}((\ln N)^2/N) \tag{7.14}$$

In the Fig. 7.4 the values of the matching fields obtained from the computed free energy are compared with our prediction. The discrepancy is attributed to the slow convergence due to the term $\mathcal{O}((\ln N)^2/N)$.

## 7.3 Magnetisation and paramagnetic Meissner effect

A paramagnetic behavior for the total magnetisation results from the existence of a high enough Bean-Livingston barrier and the long life-time of the corresponding metastable states. We propose the following scenario for the hysteretic behavior of the magnetisation when the magnetic field is increased and then swept down.

If thermal equilibrium is maintained while increasing slowly the external flux $\phi_e$, the results of the preceding section hold and the magnetisation is given by the derivative of the envelop of the curves $\mathcal{G}_N(\phi_e)$ according to the thermodynamic relation (2.30). This behavior corresponds to the upper curve in the Fig. 7.5.

When the applied field is decreased, the vortices that are already in the system are confined by the Bean-Livingston barrier and cannot escape the sample until the flux $\phi_e$ reaches a certain minimum value at which the barrier can be overcome, for instance, by the effect of thermal fluctuations. For the present discussion we use the ultimate criterion of zero barrier as a definition of the transition field.

We deducedi, from the discussion of section 7.1, that the potential barrier for $N$ vortices disappears for a characteristic field given for large $N$ by the relation (7.9), $\phi_{min} \sim (N-1)/2$. The number of vortices is then decreased by one at this field and the energy drops as shown by the arrows in Fig. 7.3. The magnetisation calculated from (2.30) is shown by the lower curve in Fig. 7.5. It shows clearly a paramagnetic behavior, although it disagrees quantitatively
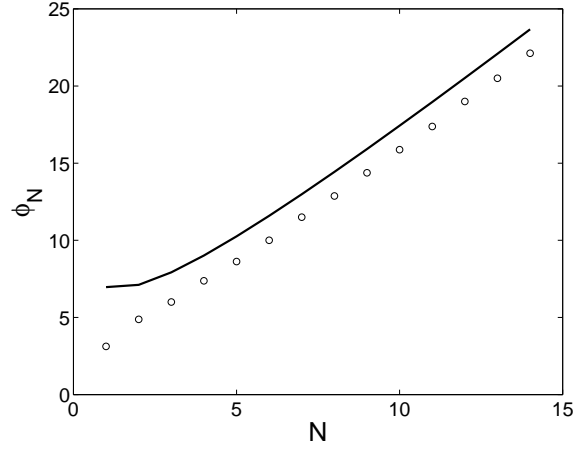
Figure 7.4: Comparison between the relation (7.14) for the matching fields $\phi_N$ and the numerical results for $\phi_1 = \ln\left(R/\xi\right) = 3$.
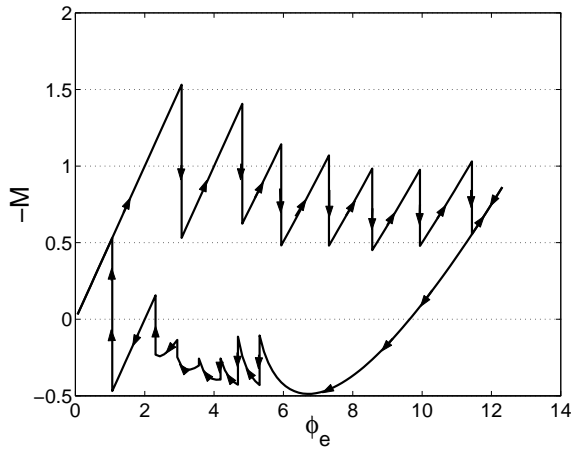


Figure 7.5: Magnetisation of the disk as a function of flux $\phi_e$ for $\phi_1 = \ln\left(R/\xi\right) = 3$. The hysteretic behavior is indicated by the arrows.

with experiments and the numerical simulations based on the exact solution of the Ginzburg-Landau equations. This discrepancy results from the rather unrealistic London limit we used for systems for which $\kappa \sim 0.3$ in order to obtain an analytic expression for the Gibbs energy. We emphasize that the system is not at thermal equilibrium but in a metastable state. It is worth noticing that for values of the parameter $\phi_1 = \mathcal{E}'/2\pi = \ln R/\xi \sim 2$, the paramagnetic Meissner effect can be observed as well for an equilibrium configuration, *i.e.* for a minimum of the Gibbs free energy. But this corresponds to $R \sim \xi$ so that the delta-like vortex approximation, crucial for the present discussion, is not justified.

# Chapter 8

# Topological phase transitions between metastable vortex patterns

Up to now, we have considered vortex configurations for which the position $x$ of the vortex ring was given by (7.6) resulting from the minimization of the energy. We shall now relax this condition and study the behavior of the metastable vortex patterns as a function of the applied magnetic flux $\phi_e$. Physically, this corresponds to a situation where $N$ vortices are pinned by a potential and remain on fixed positions.

## 8.1  An effective Hamiltonian system

When varying the field $\phi_e$, transitions in a vortex pattern with fixed number $N$ of vortices will appear. To characterize them, we shall study the behavior of the magnetic field $B$ given by (7.4). To that purpose, it is interesting first to notice that, in two dimensions, the Maxwell-Ampère equation $\vec{j} = \vec{\nabla} \times h\hat{z}$ is the Hamilton equation of a system whose generalized coordinates $(p, q)$ are the coordinates $(x, y)$ such that $j_x = \dot{x}$, $j_y = \dot{y}$ and the canonically conjugated momentum:

$$\begin{cases} \dot{p} &= -\partial_q B \\ \dot{q} &= \partial_p B \end{cases} . \tag{8.1}$$

Then, the magnetic field corresponds to the Hamiltonian of the system and the current lines are the phase space trajectories. For a Hamiltonian system, the flow can be characterized by its critical (fixed) points at which

$$\vec{\nabla} B = 0 \tag{8.2}$$

Using (8.1), we see that critical point correspond to zero velocity points such that $\vec{j} = 0$.

In such a description, a vortex corresponds to a maximum in phase-space. However there also exist in the system other critical points, such as minima and saddle-points. The number $N_M = N$ of maxima (*i.e.* vortices), $N_m$ of minima, and $N_s$ of saddles are not independent, because of the Euler-Poincare relation [61], namely the Euler-Poincaré characteristic $\chi$ is given by

$$\chi = N_M - N_s + N_m \tag{8.3}$$

The integer $\chi$ is a topological invariant and is equal to 1 for a disk thus providing a constraint between the numbers of the different types of critical points. Hence, for a system with a given number of vortices, the difference $N_s - N_m$ between saddles and minima is fixed. However,
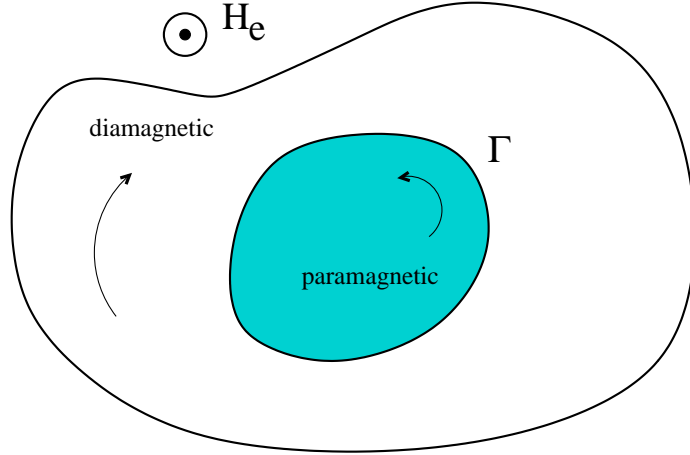
Figure 8.1: Paramagnetic and diamagnetic zones separated by the curve $\Gamma$.

each of them can vary and the set of these numbers provides a complete description of the topology of the vortex configurations, namely each topological phase can be described using this set of integers.

A different way to encode the position and the distribution of the critical points of the magnetic field in the disk is to use a special contour $\Gamma$, introduced in [46]. The curve $\Gamma$ is defined by the condition that at each point $\vec{r}$ it is perpendicular to the current density $\vec{j}(\vec{r})$. The equation of $\Gamma$ is then

$$\frac{dr}{d\theta} = r^2 \frac{\partial_r B}{\partial_\theta B} \tag{8.4}$$

To this definition we must add the requirement that $\Gamma$ must pass through the critical points at which $\vec{j}(\vec{r}) = 0$. The curve $\Gamma$ has several branches; one of them encircles all the vortices and defines a natural boundary between the diamagnetic (Meissner) domain near the boundary and the inner paramagnetic domain which includes the vortices (Fig. 8.1). An example of this curve is shown in Fig. 8.2 in the case of a disk with one vortex.

The study of the critical points and the resulting behavior of $\Gamma$ provides a complete description of the vortex states either for thermodynamic or metastable states and of the transitions between different sets of topological numbers when varying the applied field. ¿From the behavior of the curve $\Gamma$ as a function of the applied field $\phi_e$, it might be interesting to draw the analogy with the pressure exerted on a closed membrane separating two systems.

## 8.2   Topological study of a vortex ring

We now consider the simple case where all the vortices are placed on regular polygon at a distance $x$ from the center of the disk. The critical points can be classified (see Appendix E) according to their stability properties, obtained from the Hessian matrix $H_{ij} = \partial_i \partial_j h$. We review the various topological structures obtained and the transitions between them.

For a ring configuration of $N$ vortices located at the distance $x$ from the center the general

expression (7.1) for the field $B$ in circular coordinates $r$, $\theta$ reads

$$B = \phi_e(r^2 - 1) + \ln\left(\frac{1 - 2x^N r^N \cos N\theta + x^{2N} r^{2N}}{x^{2N} - 2x^N r^N \cos N\theta + r^{2N}}\right) \tag{8.5}$$

At the critical point the partial derivatives of $B$ vanish. The condition $\partial_r B = 0$ leads to

$$\phi_e r - N(x^{2N} - 1)\, r^{N-1} \frac{x^N \cos N\theta\, (r^{2N} + 1) - (x^{2N} + 1)r^N}{(1 - 2x^N r^N \cos N\theta + x^{2N} r^{2N})(x^{2N} - 2x^N r^N \cos N\theta + r^{2N})} = 0 \tag{8.6}$$

while the condition $\partial_\theta B = 0$ rewrites as

$$N r^N N\theta \frac{(1 - x^{2N})(1 - r^{2N})}{(1 - 2x^N r^N \cos N\theta + x^{2N} r^{2N})(x^{2N} - 2x^N r^N \cos N\theta + r^{2N})} = 0 \tag{8.7}$$

The solutions of equations (8.6) and (8.7) are studied in detail in Appendix E. One main feature is that one has to distinguish between the cases $N = 1$, $N = 2$ and $N > 2$ where $N$ is the number of vortices. We now describe these three cases separately.

### 8.2.1 Metastable configurations for $N = 1$

For one single metastable vortex located at distance $x$ from the center there is no other critical point for weak flux $\phi_e < \phi_m(1)$, with

$$\phi_m(1) = \frac{1 - x}{1 + x}. \tag{8.8}$$

At $\phi_e = \phi_m(1)$ a critical point appears at the point $r = 1, \theta = -\pi$. For a flux slightly above $\phi_m(1)$, this point splits into a minimum at $r < 1$, $\theta = -\pi$ and two saddle points on the boundary $r = 1$ situated symmetrically about the diameter passing through the vortex. As the flux increases the minimum moves towards the center and the saddle points approach the point $r = 1$, $\theta = 0$ each from its side. They coalesce at this point for $\phi_e = \phi_M(1)$, where

$$\phi_M(1) = \frac{1 + x}{1 - x} \tag{8.9}$$

and for larger values of the flux one saddle point appears inside the disk between the vortex and the boundary in the interval $x < r < 1$, $\theta = 0$. When $\phi_m(1) < \phi_e < \phi_M(1)$, the definition (8.3) must be generalized to the case of critical point on the boundary [61]. It becomes

$$\chi = N_M - N_s + N_m - \frac{1}{2}N_{sb} \tag{8.10}$$

where $N_{sb}$ is the number of saddle points on the boundary. Thus the index is again equal one.

An efficient way to visualize these transitions is examine the changes in the curve $\Gamma$ as the magnetic flux varies. In the case $\phi_e > \phi_M(1)$, shown in Fig. 8.2a, the curve $\Gamma$ lies inside the disk and separates the paramagnetic (internal) and diamagnetic (external) regions. For $\phi_e = \phi_M(1)$ the saddle point reaches the boundary of the disk and for $\phi_m(1) < \phi_e < \phi_M(1)$ the curve $\Gamma$ starts and ends on the saddle points on the boundary (see Fig. 8.2b). Therefore, in this regime, one cannot define a paramagnetic region inside the disk and there is no closed curve that encloses a unit of flux. There appears an arc of circle on the boundary where the direction of the current flow is opposite to the screening current responsible for the Meissner effect. At $\phi_e = \phi_m(1)$ all the disk becomes paramagnetic and the curve $\Gamma$ disappears.
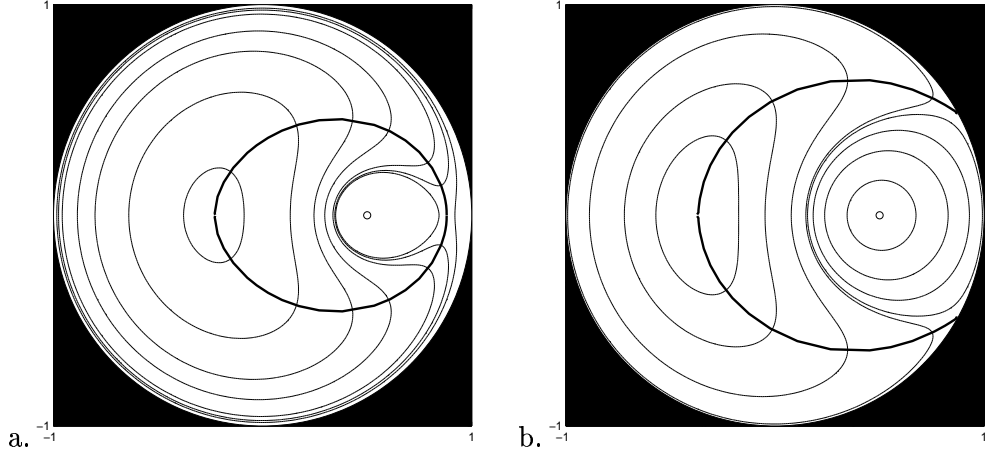
Figure 8.2: The case of one single vortex ($N = 1$). Behavior of the curve $\Gamma$ for a).
$\phi_e > \phi_M(1)$ and b). $\phi_m(1) < \phi_e < \phi_M(1)$

### 8.2.2 Metastable configurations for $N = 2$

For low enough field $\phi_e < \phi_m(2)$, with

$$\phi_m(2) = 2\frac{1 - x^2}{1 + x^2}. \tag{8.11}$$

the only critical point is a saddle point at the center. For $\phi_m(2) < \phi_e < \phi_M(2)$, where

$$\phi_M(2) = 2\frac{1 + x^2}{1 - x^2}. \tag{8.12}$$

there are two minima situated symmetrically on the diameter perpendicular to the line passing through the vortices and two pairs of saddle points on the boundary. This configuration is shown in Fig. 8.3a. Each pair is symmetric with respect to the line passing through the vortices and moves towards the points $r = 1$, $\theta = 0$ or $\theta = \pi$. For $\phi_e > \phi_M(2)$ each pair disappears and gives birth to one single saddle point located between a vortex and the boundary at $\theta = 0$ or $\pi$ as shown in Fig. 8.3c.

Two minima inside the disk move towards the center and at the critical value of the flux $\phi_e = \phi_c(2)$, where $\phi_c(2) = (1 - x^4)/x^2$ they merge with the central point, which becomes a minimum for $\phi_e > \phi_c(2)$. This critical value can be shown to be always greater than $\phi_m(2)$, but it can be greater or less than $\phi_M(2)$ depending on the value of $x$. For $x < \sqrt{2 - \sqrt{3}} \approx 0.52$, one has $\phi_c(2) > \phi_M(2)$, while for $x > \sqrt{2 - \sqrt{3}}$, we have $\phi_c(2) < \phi_M(2)$. The latter case is shown in Fig. 8.3b and 8.3c.

### 8.2.3 The case $N > 2$: topological phase transitions

In that case, the central point is a minimum for all values of $\phi_e$. In addition for low enough external flux there are $N$ saddle points inside the disk situated symmetrically at $\theta = 2\pi(k + 1/2)/N$. As the external flux is increased through $\phi_m(N)$, where

$$\phi_m(N) = N\frac{1 - x^N}{1 + x^N}. \tag{8.13}$$
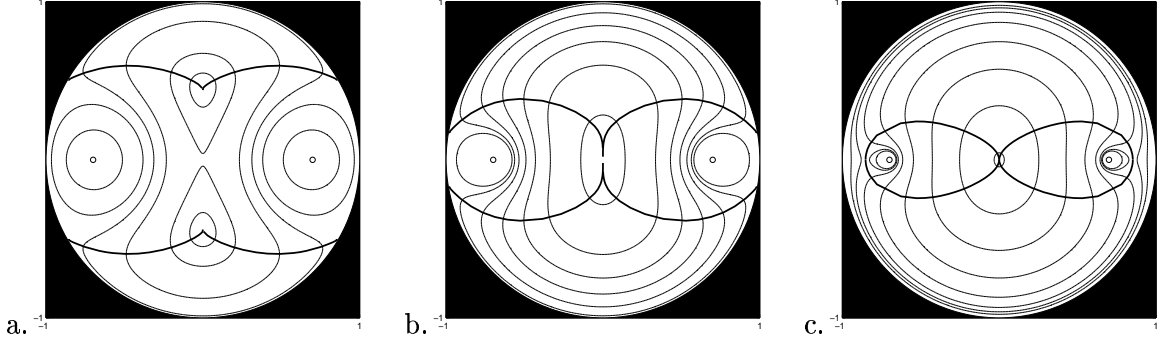
Figure 8.3: The case of $N = 2$ vortices for a). $\phi_m(2) < \phi_e < \phi_c(2)$, b). $\phi_c(2) < \phi_e < \phi_M(2)$ and c). $\phi_e > \phi_M(2)$. The curve $\Gamma$ is shown. The position of the vortices is taken to be $x = 0.7 > \sqrt{2 - \sqrt{3}}$, therefore $\phi_c(2) < \phi_M(2)$.

$N$ pairs of saddle points on the boundary appear together with $N$ minima in the bulk (see Fig. 8.4a). The minima move towards the center along the line defined by $\theta = 2\pi(k+1/2)/N$, $k = 1, \ldots, N$, while two saddle points constituting the $k$-th pair move symmetrically to the points $\theta = 2\pi k/N$ and $\theta = 2\pi(k+1)/N$ as the flux increases in the interval $\phi_m(N) < \phi_e < \phi_M(N)$. When $\phi_e = \phi_M(N)$, with

$$\phi_M(N) = N\frac{1 + x^N}{1 - x^N} \tag{8.14}$$

pairs of saddle points meet at $\theta = 2\pi k/N$ and for larger values of the flux there are $N$ saddle points situated between a vortex and the boundary. In this regime there are $N + 1$ minima and $2N$ saddle points inside the disk as shown in Fig. 8.4b.

At $\phi_e = \phi_c(N)$, where $\phi_c(N)$ is given by the formulae (E.9) and (E.10), each of the $N$ minima coalesce with each of the $N$ saddle points at $r = \rho_c^{1/N}$, $\theta = 2\pi(k+1/2)/N$, where $\rho_c$ is given by (E.9). For $\phi_e > \phi_c(N)$ there remains only one minimum in the center and $N$ saddle points. It can be shown that $\phi_c(N)$ is always greater than $\phi_M(N)$ for $N > 2$.

Then, for $\phi_e = \phi_c(N)$ a topological transition occurs, when a minimum and a saddle point coalesce. This transition and the corresponding curve $\Gamma$ is depicted in Fig. 8.4b and 8.4c. It is seen that the curve $\Gamma$ undergoes itself a topological transition. For $\phi_e < \phi_c(N)$ it does not touch the center and has a topology of a ring, while for $\phi_e > \phi_c(N)$ it has a form of petals of a flower emanating from the center of the disk.

## 8.3  A dynamical interpretation of the curve $\Gamma$

The curve $\Gamma$, defined above as being everywhere normal to the current flow, has a simple interpretation in terms of an effective dynamical system, which gives an alternative method to compute it. Instead of the Hamiltonian flow (8.1), consider the lines of $\vec{\nabla}B$, obtained from those of $\vec{j}$ by a rotation of $90^0$. This flow is clearly non-Hamiltonian and possess fixed points which are not present in the Hamiltonian dynamics, e.g. the positions of the vortices appear in this picture as a point-like sources, though a saddle remain a saddle in this transformation. Then, the curve $\Gamma$ represents a limit cycle of the flow $\vec{\nabla}B$ emanating from the saddle point.
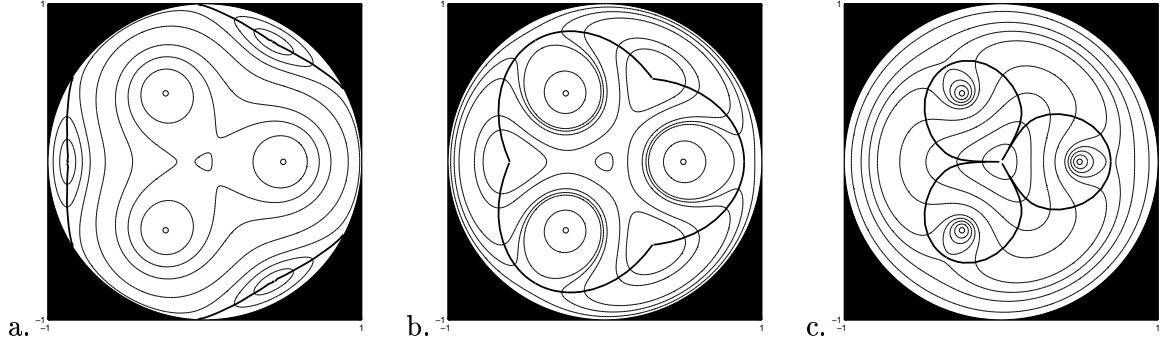
Figure 8.4: The case of $N = 3$ vortices for a). $\phi_m(3) < \phi_e < \phi_M(3)$, b). $\phi_M(3) < \phi_e < \phi_c(3)$ and c). $\phi_e > \phi_c(3)$. The curve $\Gamma$ is shown.
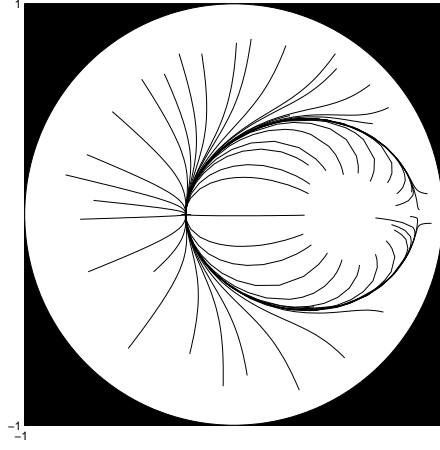


Figure 8.5: The curve $\Gamma$ as the limit cycle of the flow $\vec{\nabla}B$. The parameters are the same as in Fig. 8.2a.

This is illustrated in Fig. 8.5 where it is clearly seen that the same curve as in Fig. 8.2 a) appears as a limit of the lines of $\vec{\nabla}B$.

# Chapter 9

# Hilbert space of Tomonaga-Luttinger model

In this section we review a model exactly solvable for any interaction strength. The simplest model of interacting fermions is the one-branch (chiral) Tomonaga-Luttinger model [48]. Let $n$ label the one-particle orbital with convention that in the ground state $|0\rangle$ of the non-interacting model, $n = 1$ denotes the first unoccupied state. Since a very large number of states is occupied (the number of fermions is large) the number $n$ can be allowed to run from $-\infty$ to $+\infty$. Another consequence is that the one-particle spectrum is assumed to be equidistant: $E_n = n\Delta$. Both the linear dispersion and the fact that the spectrum is unbound are crucial for the solubility of the model. Introducing creation and annihilation operators $c_n^\dagger$, $c_n$ for a fermion on the orbital $n$, with usual anti-commutation relations $\{c_n, c_{n'}^\dagger\} = \delta_{n,n'}$ (other anti-commutators vanish) the Hamiltonian of the problem can be written as

$$\hat{H} = \hat{H}_0 + \hat{U} = E_0 + \sum_{n=-\infty}^{+\infty} E_n : c_n^\dagger c_n : + \sum_{m=1}^{+\infty} \sum_{n,n'=-\infty}^{+\infty} V_m c_{n+m}^\dagger c_n c_{n'-m}^\dagger c_{n'} \tag{9.1}$$

The normal ordering of operators having infinite expectation values is defined as : $\hat{O} := \hat{O} - \langle 0|\hat{O}|0\rangle$. As a result the constant $E_0$ absorbs the (infinite) free ground state energy together with the Hartree term:

$$E_0 = \langle 0|\hat{H}|0\rangle = \sum_{n\leq 0} E_n \langle 0|c_n^\dagger c_n|0\rangle + \frac{V_0}{2} \sum_{n,n'\leq 0} \langle 0|c_n^\dagger c_n c_{n'}^\dagger c_{n'}|0\rangle \tag{9.2}$$

The operator of "total momentum"

$$\hat{P} = \sum_{n=-\infty}^{+\infty} n : c_n^\dagger c_n : \tag{9.3}$$

commutes with the full Hamiltonian. Due to the linear dispersion this operator is proportional to the free part of the Hamiltonian, i.e. the first term on the RHS of (9.1).

Instead of solving this model by the standard method of bosonization using identities among second quantized operators (see for example [48]) we prefer to reformulate our interacting problem in order to relate it to the problems usually discussed within the framework of Anderson localization. We start by labeling the eigenstates of non-interacting problem, which
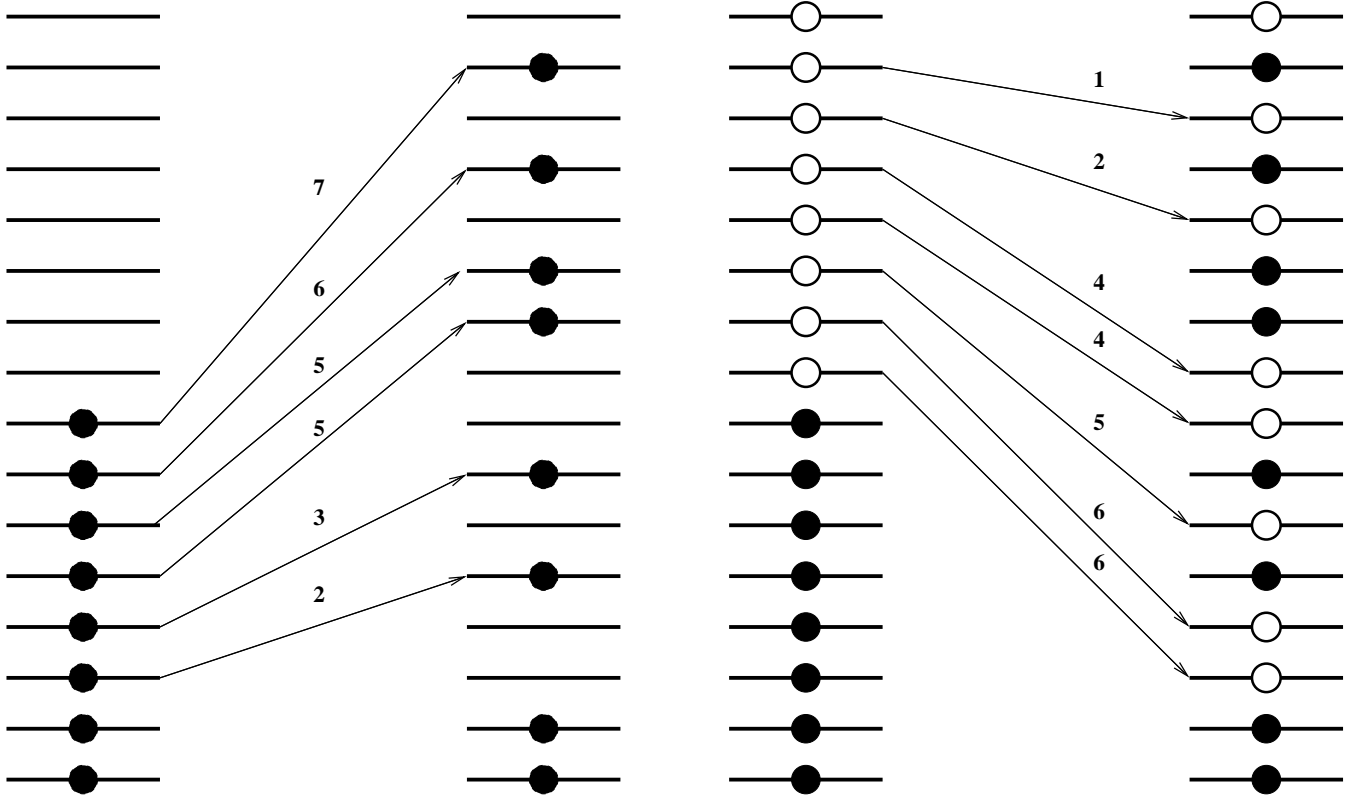
Figure 9.1: Correspondence between Slater determinant and partition $(\lambda) = (7, 6, 5, 5, 3, 2)$. The dual partition $(\tilde{\lambda}) = (6, 6, 5, 4, 4, 2, 1)$ represents shifts of the holes.

are the familiar Slater determinants, by shifts of particles with respect to the non-interacting ground state as shown in the Fig. 9.1: the uppermost particle is shifted up $\lambda_1$ levels, the second one is shifted up $\lambda_2$ levels etc. The numbers $\lambda_i$ are defined to satisfy $\lambda_i \geq \lambda_{i+1}$ for each $i$. If a particle is not shifted it is not recorded. The set $(\lambda)$ of positive integers satisfying $\sum \lambda_i = N$ forms the set of partitions of $N$ and is conveniently displayed by a Young diagram — array with $\lambda_i$ boxes in the $i$-th row. Following the standard notations in the mathematical literature the numbers $\lambda_i$ will be referred to as *parts* in what follows. For example, the partition of $N = 28$, $(\lambda) = (7, 6, 5, 5, 3, 2)$ sometimes written as $(7, 6, 5^2, 3, 2)$ that is displayed in Fig. 9.1 is represented graphically as
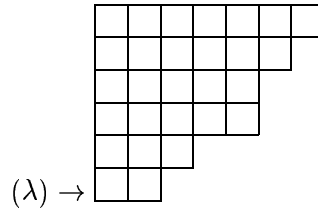


This pictorial representation of Slater determinants has nice properties under particle-hole interchange: recording shifts of the holes (which are moved downwards in energy) rather than particles in Fig. 9.1 yields the partition $(\tilde{\lambda}) = (6, 6, 5, 4, 4, 2, 1)$ whose graphical representation

is just the transpose of the Young diagram for ($\lambda$):

$$(\tilde{\lambda}) \rightarrow$$
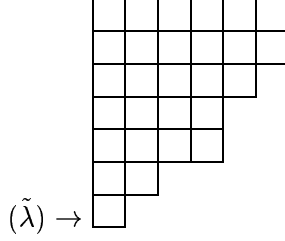
Partition $(\tilde{\lambda})$ is said to be conjugate or dual to $(\lambda)$. This duality results from the fact that each move of a particle upwards is accompanied by a move of a hole downwards.

The eigenstates of the non-interacting Hamiltonian labeled by partitions of $N$ are degenerate and their energy is given by

$$\sum_i \left( E_{1-i+\lambda_i} - E_{1-i} \right) = \Delta \sum_i \lambda_i = N\Delta \qquad (9.4)$$

The interactions conserve this number. The Hamiltonian (9.1) is therefore block-diagonal and does not mix the partitions of different $N$ so we can restrict ourselves to the subspace of the Hilbert space spanned by partitions of $N$.

The dimensionality of this subspace is given by $p(N)$ — the number of partitions of $N$. There is no closed analytical expression for this number but the Euler expression [62] for the generating function

$$p(q) = \sum_{N=1}^{\infty} p(N)\, q^N = \prod_{l=1}^{\infty} \frac{1}{1-q^l} \qquad (9.5)$$

allows to obtain the asymptotic behavior of $p(N)$ for large $N$ and it is given by the formula of Hardy-Ramunajan:

$$p(N) \sim \frac{e^{\pi\sqrt{2N/3}}}{4\sqrt{3}N} \qquad (9.6)$$

It demonstrates that the number of "sites" in the subspace increases rapidly with $N$.

Since for a given subspace $N$ the free part of the Hamiltonian is proportional to the unit matrix the solution consists in diagonalization of the interacting part $U$. The interaction term in (9.1) is conveniently represented in our picture as effective binding between the sites. In order to present the results in a compact and transparent way we drop the requirement on a partition labeling the basis state to be represented by a non-increasing sequence. Instead we extend the notion to any finite sequence of integers (either positive or negative or zero) and use the following rules to relate this sequence to the standard (non-increasing) partition:

1. *In any sequence $(\lambda_1, \lambda_2, \ldots)$ two consecutive parts may be interchanged provided that the preceding part is decreased by unity and the succeeding part increased by unity, the state vector which corresponds to this partition acquires a minus sign*, i.e.

$$|(\lambda_1, \ldots, \lambda_i, \lambda_{i+1}, \ldots)\rangle = -|(\lambda_1, \ldots, \lambda_{i+1}-1, \lambda_i+1, \ldots)\rangle \qquad (9.7)$$

2. *If any part exceeds by unity the preceding part the partition corresponds to zero vector,* i.e.

$$|(\lambda_1, \ldots, \lambda_i, \lambda_i + 1, \ldots)\rangle = 0 \qquad (9.8)$$

3. *If the last part of the sequence is negative the partition corresponds to the zero vector.*

These rules, used in the theory of symmetric functions [63] are in fact nothing but a standard properties of Slater determinants under action of second quantized operators. Rule 1 results from the fact that $i$-th particle is excited to the level $n_i$ such that

$$n_i = \lambda_i + 1 - i$$

with the energy $E_i = n_i \Delta$ while the $(i+1)$-th particle is excited to the level

$$n_{i+1} = \lambda_{i+1} - i$$

and interchanging consecutive rows in a (Slater) determinant results in a sign change. Rule 2 results from the fact that $\lambda_{i+1} = \lambda_i + 1$ implies $n_{i+1} = n_i$ which contradicts the Pauli principle. Rule 3 reflects the fact that negative $\lambda_i$ describe (forbidden) transitions to occupied states inside the Fermi sea.

Let us denote by $\eta_{(\lambda)}$ the factors $-1, 0$ or $+1$ acquired when bringing a partition $(\lambda)$ to its standard form. In these notations the matrix element of the interactions between the partitions $(\lambda)$ and $(\mu)$ can be represented as

$$U_{(\lambda),(\mu)} = \langle(\lambda)|\hat{U}|(\mu)\rangle = \sum_m V_m \sum_{i,j} \langle(\ldots \lambda_i - m \ldots)|(\ldots \mu_j - m \ldots)\rangle. \tag{9.9}$$

Since the basis of Slater determinants is orthonormal the following expression is obtained

$$U_{(\lambda),(\mu)} = \sum_m V_m \sum_{i,j} \eta_{(\ldots \lambda_i - m \ldots)} \eta_{(\ldots \mu_j - m \ldots)} \delta_{(\ldots \lambda_i - m \ldots),(\ldots \mu_j - m \ldots)}. \tag{9.10}$$

The eigenstates of $U$ are

$$|(l)\rangle = \sum_{(\lambda)} \chi_{(l)}^{(\lambda)} |(\lambda)\rangle \tag{9.11}$$

where $\chi_{(l)}^{(\lambda)}$ are the characters of the irreducible representation $(\lambda)$ of an element of the symmetric group $S_N$ belonging to the class $(l)$. For this purpose it is shown in Appendix A that

$$\sum_{i,j} \eta_{(\ldots \lambda_i - m \ldots)} \eta_{(\ldots \lambda_i - m \ldots \lambda_j + m \ldots)} \chi_{(l)}^{(\ldots \lambda_i - m \ldots \lambda_j + m \ldots)} = m n_m \chi_{(l)}^{(\lambda)} \tag{9.12}$$

where $n_m$ is the number of times the cycle $m$ appears in the class $(l)$. This leads to

$$\hat{U}|(l)\rangle = \sum_m V_m m n_m \sum_{(\lambda)} \chi_{(l)}^{(\lambda)} |(\lambda)\rangle = \left( \sum_m V_m m n_m \right) |(l)\rangle. \tag{9.13}$$

The state $|(l)\rangle$ is therefore an eigenstate of the Hamiltonian (9.1) with the eigenvalue

$$E_{(l)} = E_0 + N\Delta + \sum_m V_m m n_m. \tag{9.14}$$

The orthogonality of the characters implies that the states $|(l)\rangle$ form an orthogonal basis, namely:

$$\langle(l)|(l')\rangle = \frac{g}{g_{(l)}} \delta_{(l),(l')} \tag{9.15}$$
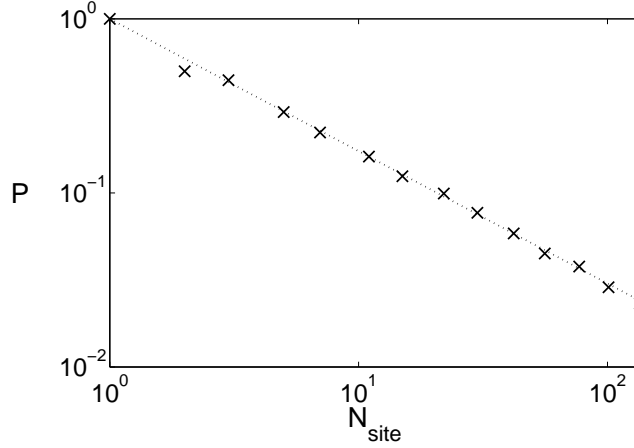
Figure 9.2: The inverse participation ratio (9.19) as function of number of sites $N_{site} = p(N)$. The solid line represents the fit $P = 1/N_{site}^{\alpha}$, where $\alpha \approx 0.8$

where $g = N!$ is the total number of elements in $S_N$ and the number of elements in the class $(l)$ is

$$g_{(l)} = N! \prod_{m=1}^{\infty} \frac{1}{m^{n_m} n_m!}. \tag{9.16}$$

We normalize the states $|(l)\rangle$ as

$$|(l)\rangle = \sqrt{\frac{g_{(l)}}{g}} \sum_{(\lambda)} \chi_{(l)}^{(\lambda)} |(\lambda)\rangle \tag{9.17}$$

so that they form an orthonormal basis. These are standard bosonic states usually labeled by the occupation numbers $n_m$ that are the eigenstates of the interacting Hamiltonian (9.1). The transformation with the matrix

$$\langle (\lambda)|(l)\rangle = \sqrt{\frac{g_{(l)}}{g}} \chi_{(l)}^{(\lambda)} \tag{9.18}$$

is the unitary transformation of the basis vectors in our Hilbert space, which diagonalizes the interacting Hamiltonian (9.1). When the free part of the Hamiltonian is degenerate in the subspace $N$ the states $|(l)\rangle$ play the role of the extended states (in the Hilbert space). In order to verify this statement we calculated numerically the inverse participation ratio $P$, defined as

$$P = \sum_{(\lambda)} |\langle (\lambda)|(l)\rangle|^4 \tag{9.19}$$

for some arbitrary states $(l)$. Although no closed expression is available for the general amplitude (9.18) of the state $|(l)$ on the site $(\lambda)$, the beautiful recurrent relation of the characters of the symmetric group (F.12) (based on the Frobenius formula) was implemented numerically to calculate these amplitudes. The inverse participation ratio averaged over the bosonic states $(l)$ is shown in Fig. 9.2 for different values of $N$. As the number of sites $N_{site} = p(N)$ increases the inverse participation ratio $P$ was found to decay as $P = 1/N_{site}^{\alpha}$,

where $\alpha \approx 0.8$. This allows us to conclude that the bosonic states $(l)$ are indeed extended in the basis of free Slater determinants $(\lambda)$.

# Chapter 10

# Modified Tomonaga-Luttinger model

## 10.1 Interaction matrix elements

The existence of extended states in the chiral Tomonaga-Luttinger model can be attributed to the degeneracy of the diagonal elements of the Hamiltonian (9.1), since the interactions (9.10) have short-range in the space of partitions. In order to define more precisely what we mean by short-range in our Hilbert space we have to order the partitions in some order. Then the interaction can be shown to connect only blocks of elements that are not too far one from the other.

It is natural to order the partitions in the lexicographic order, i.e. if $\lambda_i = 1, 2, 3 \ldots$ numbers the letters in an alphabet the lexicographic order of partitions corresponds to the order of words in Arabic or Hebrew dictionary. For example, the 11 partitions of $N = 6$ in the lexicographic order are:

$$
\begin{aligned}
k = 1 \quad & (1, 1, 1, 1, 1, 1) \\[6pt]
k = 2 \quad & (2, 1, 1, 1, 1) \\[6pt]
k = 3 \quad & (3, 1, 1, 1) \\[6pt]
k = 4 \quad & (2, 2, 1, 1) \\
& (4, 1, 1) \\[6pt]
k = 5 \quad & (3, 2, 1) \\
& (5, 1) \\[6pt]
k = 6 \quad & (2, 2, 2) \\
& (4, 2) \\
& (3, 3) \\
& (6)
\end{aligned}
\tag{10.1}
$$

The partitions are grouped by $k$—the number of 1's (that appear always on the right). The $k$-th group contains partitions of the form

$$
(\lambda_1, \lambda_2, \ldots \lambda_l, 1^{N-k})
\tag{10.2}
$$

with constraint $\lambda_i \geq 2$, with the only exception for the first group containing $(1^N)$. The typical Young diagram of a partition in the $k$-th group is of the form



$$(10.3)$$

To calculate the number of partitions in the $k$-th group we note that exactly $p(k)$ partitions have at least $N - k$ ones. Among them $p(k - 1)$ have at least $N - (k - 1)$ ones and the rest $n(k) = p(k) - p(k - 1)$ have *exactly* $N - k$ ones. Therefore the $k$-th group contains $n(k)$ partitions.

Usually the matrix element of the interaction potential $V_m$ is a decreasing function of the momentum transfer $m$, with some effective range $m_c$. In what follows it will be convenient to analyze a model where the only non-zero matrix element corresponds to $m = 1$ with $V_1 = V$. It will not affect qualitatively our results, since we are primarily interested in the limit of large $N$ subspace. The matrix element of this interaction is given by the simplified version of (9.10)

$$U_{(\lambda),(\mu)} = V \sum_{i,j} \delta_{(\ldots \lambda_i - 1\ldots),(\ldots \mu_j - 1\ldots)}. \qquad (10.4)$$

The factors $\eta$ are omitted since the partitions $(\ldots \lambda_i - 1 \ldots)$ and $(\ldots \mu_j - 1 \ldots)$ are either already in the standard (non-increasing) form or corresponds to zero vector and do not contribute to the sum. Therefore the interaction couples partitions $(\lambda)$ and $(\mu)$ that differ in two of the $\lambda_i$'s, namely $\lambda_i - \mu_i = 1$ and $\lambda_j - \mu_j = -1$. The Young diagram of the partition $(\lambda)$ is obtained from the one of the partition $(\mu)$ by moving one square under the constraint that the new Young diagram is legitimate. Consider the $k$-th group. If $\mu_i > 1$ and $\mu_j > 2$ the coupling is between partitions inside this group. This corresponds to moving a square between $\mu_i > 1$ rows of the Young diagram. In order to couple to neighboring groups a square corresponding to $\mu_i = 1$ should be moved. Moving a square from/to any row with $\mu_j > 1$ to/from the region where $\mu_i = 1$ leads to a coupling to the neighboring group $k \pm 1$. The exception is if a square is moved from $\mu_i = 2$ (that has only two squares and after the move only one is left) and is attached as the last square in the tail of $\mu_j = 1$, or if the last square is moved to $\mu_j = 1$ turning it into a $\mu_j = 2$ row. In this case the length of the tail of $\mu_j = 1$ is changed by two, i.e. the coupling is to the group $k \pm 2$. These are the only moves of one square, therefore only the groups $k'$ such that $|k - k'| \leq 2$ are coupled to the $k$-th group and the interaction between the various blocks of partitions is of short range. Fig. 10.1 shows the structure of the interaction matrix for $N = 14$.

It is therefore natural to expect that the diagonal disorder will destroy the extended states of the chiral Tomonaga-Luttinger model. In the original model in the absence of interactions the eigenenergies $E_{(\lambda)}$ are independent of the partition and take the constant value $E_{(\lambda)} = E_0 + N\Delta$. We introduce a modification and assume that the $E_{(\lambda)}$ are independent random variables. This assumption is made for the sake of simplicity. It cannot be correct
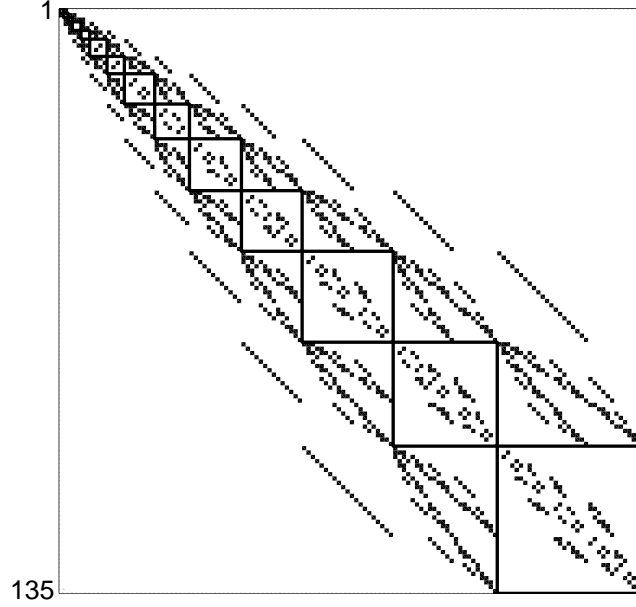
Figure 10.1: The matrix of the interaction (10.4). The blocks corresponding to different groups of partitions are shown.

since there are $p(N)$ values of $E_{(\lambda)}$ that depend on $2N$ level spacings. An assumption that is more physical will be introduced in the following section.

## 10.2 Effective tight-binding model and its solution

In order to be able to solve the model with random energies we simplify further the interaction (10.4). From the experience in research of Anderson localization we expect that the behavior of the eigenvectors will not be affected by the precise form of the short-range off-diagonal matrix elements, so we make the following simplifications. We assume that the effect of transitions inside the same group of partitions is to delocalize the states within the group. The localization within a group is expected only to enhance the overall localization. Next, we neglect the coupling to the $k + 2$-th group. The reason is that for a given partition $(\lambda)$ there exists only one coupling term of this kind. It couples
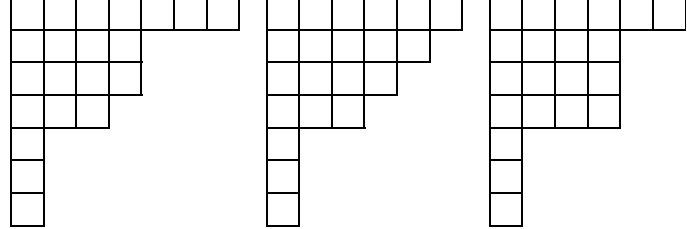
$$\left((\ldots), 1^{N-k}\right) \quad \text{and} \quad \left((\ldots)', 2, 1^{N-k-2}\right) \tag{10.5}$$

This should be compared it with the couplings of $(\lambda)$ to the next group:

$$\left((\ldots), 1^{N-k}\right) \to \left((\ldots)', 1^{N-k-1}\right) \tag{10.6}$$

The number of such couplings is given by the number of different $\lambda_i \geq 2$ in the partition $(\lambda)$, which is generally much larger than 1 for large enough $k$. It is equal to the number of rows with $\lambda_i \geq 2$ in the Young diagram of the partition. Consider for example the partition $(6, 4^2, 3, 1^4)$ of $N = 21$ belonging to he the 17-th group corresponding to the Young diagram

(10.3). It has (apart of ones) three different parts: 6,4,3 and is coupled to 3 partitions in the 18-th group:



$$(7, 4^2, 3, 1^3) \qquad (6, 5, 4, 3, 1^3) \qquad (6, 4^3, 1^3)$$

Another way to visualize the number of coupling is to count the number of concave corners in the Young diagram that is equal to the number of parts namely lines of different length larger than unity.

In Appendix B we show that $d(k)$ — the number of different parts in all partitions of $k$ with $\lambda_i \geq 2$ is exactly $p(k-2)$ — the number of (any) partitions of $(k-2)$. Therefore the mean number of transitions from the $k$-th group to the $k+1$-th group is given by $t(k) = d(k)/n(k) = p(k-2)/\left(p(k) - p(k-1)\right)$.

The Schrödinger equation for our simplified model can be written as a tight-binding form where the groups of partitions are the effective sites:

$$(E - E_{(\lambda)})\psi(\lambda)_k = \sum_{(\mu)} U_{(\lambda),(\mu)}\psi(\mu)_{k-1} + \sum_{(\nu)} U_{(\lambda),(\nu)}\psi(\nu)_{k+1} \qquad (10.8)$$

where $\psi(\lambda)_k$ denotes the value of the wave function on site$(\lambda)$ in the $k$-th group. Let us assume that the wave function is extended within the $k$th group. We introduce a simpler model that is expected to exhibit similar localization properties [64]. We replace the interaction $U_{(\lambda),(\mu)}$ by an average interaction that couples each partition in the $k$-th group to all partitions in the group $k \pm 1$,

$$V_k = \frac{\sum_{(\nu)} U_{(\lambda),(\nu)}}{n(k+1)} \qquad (10.9)$$

In this approximation (10.8) reduces to

$$(E - E_{(\lambda)})\psi(\lambda)_k = V_{k-1}\sum_{(\mu)} \psi(\mu)_{k-1} + V_k \sum_{(\nu)} \psi(\nu)_{k+1} \qquad (10.10)$$

The numerator in (10.9) can be estimated as $V$ times the mean number of couplings with partitions in $(k+1)$-th group:

$$V_k = V \frac{t(k)}{n(k+1)} = V \frac{d(k)}{n(k)n(k+1)} \qquad (10.11)$$

Denoting the sum of the wave-functions over a group by $C_k = \sum_{(\lambda)} \psi(\lambda)_k$ we find with the help of (10.10) that

$$\mathcal{E}_k C_k = V_{k-1}C_{k-1} + V_k C_{k+1} \qquad (10.12)$$

where

$$\frac{1}{\mathcal{E}_k} = \sum_{(\lambda)} \frac{1}{E - E_{(\lambda)}} \qquad (10.13)$$

61

and the sum is over all partitions in the group $k$.

For random independent $E_{(\lambda)}$ all the $\mathcal{E}_k$ are independent random variables and the tight-binding model (10.12) is an Anderson model at zero energy. In the spirit of transfer matrix method it is expected that also for $\mathcal{E}_k$ given by (10.13) similar localization properties will be found. The properties of the solution of this one-dimensional model can be analyzed within the framework of Anderson localization in one-dimensional systems [49].

One can take the uniform distribution of energies that turns out to be convenient for calculations. Remembering that each many-body energy is a sum of $N$ level spacings we assume the following distribution:

$$P(E) = \begin{cases} 1/\sqrt{N}\Delta, & -\sqrt{N}\Delta/2 < E < \sqrt{N}\Delta/2 \\ 0, & \text{otherwise} \end{cases} \qquad (10.14)$$

For a variety of distributions the distribution of $\mathcal{E}_k$ tends to the Cauchy distribution:

$$P(\mathcal{E}_k) = \frac{1}{\pi} \frac{\delta_k(E)}{\mathcal{E}_k^2 + \delta_k(E)^2} \qquad (10.15)$$

where $\delta_k(E) = \delta(E)/n(k)$ and for (10.14) $\delta(E) = \sqrt{N}\Delta/\pi$.

Multiplying the equation (10.12) by $n(k)n(k+1)/(V d(k))$ and observing that in the limit $k \to \infty$ one finds $n(k)/n(k+1) \to 1$ and $d(k)/d(k-1) \to 1$ so that (10.12) takes the form

$$\mathcal{E}_k C_k = C_{k-1} + C_{k+1} \qquad (10.16)$$

It is a Lloyd model with a $k$-dependent distribution of on-site energies characterized by parameter

$$\delta_k(E) = \frac{\delta(E)}{V} \frac{n(k+1)}{d(k)} \qquad (10.17)$$

which in the limit $k \to \infty$ has the property

$$\delta_k(E) \sim \sqrt{\frac{N}{6k}} \frac{\Delta}{V} \qquad (10.18)$$

We generalize the solution of the Lloyd model [49] to the present case of site-dependent distribution of energies. We observe that the distribution parameter depends weakly on the site number $k$ and use the site-dependent localization length ansatz:

$$1/\xi_k = \ln \frac{|C_k|}{|C_{k+1}|} = \cosh^{-1} \sqrt{1 + \frac{\delta_k^2}{4}} \approx \ln \delta_k = \ln \sqrt{\frac{N}{6k}} \frac{\Delta}{V} \qquad (10.19)$$

The last approximation is justified in the weak-coupling limit $V/\Delta \ll 1$.

The validity of the site-dependent localization length assumption is checked numerically. The on-site energies $\mathcal{E}_k$ were generated from the Cauchy distribution (10.15) with parameter $\delta_k$ given by (10.18). The inverse localization length $1/\xi$ (Lyapunov exponent) was calculated using the standard technique of transfer matrices [49] and it was found that the site-dependent ansatz (10.19) describes well (at least qualitatively) the behavior of the localization length. Thus for independently distributed energies the typical behavior of the wave functions is described by coefficients that decay as

$$C_k \sim e^{-k/\xi_k} = \exp\left( -k \log \sqrt{\frac{N}{6k}} \frac{\Delta}{V} \right). \qquad (10.20)$$

In the strong coupling limit similar considerations lead to

$$C_k \sim e^{-k/\xi_k} = \exp\left(-k\sqrt{\frac{N}{24k}\frac{\Delta}{V}}\right) , \qquad (10.21)$$

but in this limit these require some further justification. The importance of this result is that numerical studies of more realistic many-particle energy distributions confirm the validity of (10.20). This will be the subject of the next section.

# Chapter 11

# Effects of energy correlations

In the last section we considered a model in which the diagonal matrix elements $E_{(\lambda)}$ are independent random variables. We did not specify the distribution law of these energies, since the solution does not depend on fine details, but rather on general properties of the distribution. We would like to stress that the assumption of statistical independence of the energies $E_{(\lambda)}$ is not realistic for a many-body system. To illustrate this statement a simple argument can be given. Suppose we are dealing with a disordered mesoscopic system and the one-particle spectrum is random, i.e. consists of levels with independently distributed spacings $\Delta_j = E_j - E_{j-1}$. The generalization of the expression (9.4) for the energy of the partition $(\lambda)$ for this case is

$$E_{(\lambda)} = \sum_i \left( E_{1-i+\lambda_i} - E_{1-i} \right) = \sum_i \sum_{j=2-i}^{\lambda_i+1-i} \Delta_j \tag{11.1}$$

In order to describe the energies $E_{(\lambda)}$ in the subspace $N$ we need $2N$ random quantities $\Delta_j$. On the other hand the number of states in this subspace is given by $p(N)$, the number of partitions of $N$ which grows exponentially for $N \to \infty$. Therefore there exist much more many-body energies $E_{(\lambda)}$ than independent level spacings. Therefore the many-particle energies $E_{(\lambda)}$, which are the sums of the one-particle energies, are statistically dependent.

The analytical calculation of the (joint) distribution of the parameters $\mathcal{E}_k$ defined in (10.13) for the effective tight-binding model (10.12) seems to be hopeless. Nevertheless we expect some features of this distribution, based on the formula (10.13). For an eigenstate the eigenvalue $E$ is in the interval $[-1 + E_{(\lambda)}^{min}, +1 + E_{(\lambda)}^{max}]$, where $E_{(\lambda)}^{min}$ and $E_{(\lambda)}^{max}$ are the minimal and maximal values of $E_{(\lambda)}$. The value of $E$ can be very close one of the $E_{(\lambda)}$. Therefore the terms in the sum on the RHS of (10.13) can be positive or negative and they strongly fluctuate in magnitude. Therefore there is a finite probability that this sum will take a value in the vicinity of zero. Consequently it is expected that the distribution $P(\mathcal{E}_k)$ is broad with a diverging second moment or variance:

$$\Delta \mathcal{E}_k^2 = \langle (\mathcal{E}_k - \langle \mathcal{E}_k \rangle)^2 \rangle \to \infty \tag{11.2}$$

Another important issue is the effective statistical independence of $\mathcal{E}_k$ for different $k$-s. It is known for Anderson localization that the long-range correlations between the on-site energies change dramatically the criteria for the onset of the localization (see [65] and references therein). The measure of statistical dependence of energies in our case is the correlation
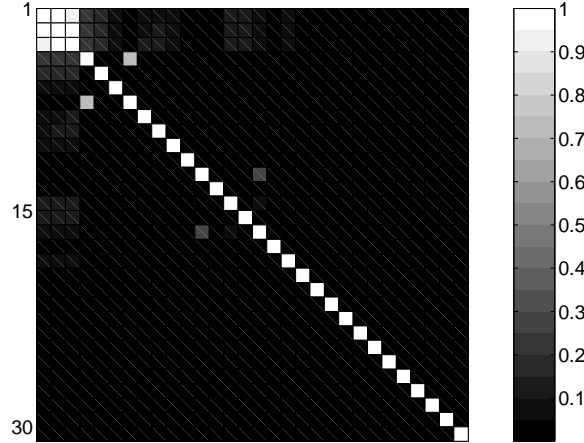
Figure 11.1: The absolute value of correlation matrix elements $C_{kl}$ defined in (11.3) of effective energies $\mathcal{E}_k$ for $N = 30$.

matrix defined as

$$C_{kl} = \frac{\langle (\mathcal{E}_k - \langle \mathcal{E}_k \rangle)(\mathcal{E}_l - \langle \mathcal{E}_l \rangle) \rangle}{\Delta \mathcal{E}_k \Delta \mathcal{E}_l} \tag{11.3}$$

Because of the strong fluctuations between the terms of the sum on the RHS of (10.13), that are different for the various groups, it is reasonable that the off-diagonal terms of the correlation function are much smaller than the diagonal ones. Usually for localization only pair correlations are important [66]. In the view of the diverging variance we assume that $C_{kl} = \delta_{kl}$, an assumption that will be tested numerically.

These facts were checked numerically and in the approximation of independent energies the effective distribution $P(\mathcal{E}_k)$ can be calculated. For this purpose $M = 1000$ realizations of $N = 30$ level spacings $\Delta_j$ were generated from the exponential distribution:

$$P(\Delta) = e^{-\Delta} \tag{11.4}$$

with $\bar{\Delta} = 1$. Then we generated numerically the whole list of $p(30) = 5604$ partitions of $N = 30$ and for each realization of level spacings the energies $E_{(\lambda)}$ were calculated using (11.1). Out of these energies the effective energies $\mathcal{E}_k$ were obtained using the definition (10.13) for $E = 0$. Several statistical tests were performed and results are shown in Fig. 11.1-11.2.

The correlation matrix of the energies $\mathcal{E}_k$ was computed. The $\langle \ldots \rangle$ averages were performed over realizations of the level spacings. The result is shown in Fig. 11.1. It is plausible that the correlations are of short range in the space of indices $k$ and only the diagonal elements of $C_{kl}$ are of appreciable magnitude. This behavior can be attributed to the diverging variance.

Due to the fact that the distribution of the energies $\mathcal{E}_k$ is expected to have a diverging variance the distribution $P(\mathcal{E}_k)$ cannot be calculated from a histogram. Instead its characteristic function

$$X_k(p) = \langle e^{ip\mathcal{E}_k} \rangle \tag{11.5}$$

was computed and plotted for several values of $k$ in Fig. 11.2 as a function of $p$. The diverging second moment due to the fact that $P(x) \propto 1/x^2$ manifests itself in the discontinuity of the
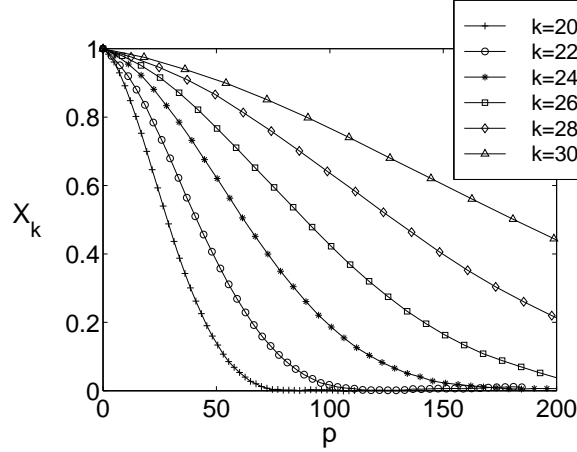
Figure 11.2: Characteristic function $X_k(p)$ of the effective energy distribution for some values of $k$.

derivative at $p = 0$ as can be seen from the Fig 11.3. Therefore we have strong evidence that the energies $\mathcal{E}_k$ have a broad distribution.

Observing the behavior of the characteristic function shown on the Fig. 11.2 and Fig. 11.3 we introduced a scaling ansatz for the distribution function:

$$P(\mathcal{E}_k) = P_k(\mathcal{E}) = \frac{n(k)}{\Delta} \widetilde{P}\left(n(k)\frac{\mathcal{E}}{\Delta}\right). \tag{11.6}$$

The universal function $\widetilde{P}(x)$ is independent of $k$. The scaling of the distribution implies that the characteristic function (11.5) satisfies

$$X_k(p) = \widetilde{X}\left(\frac{p\Delta}{n(k)}\right), \quad \widetilde{X}(q) = \int_{-\infty}^{\infty} dx\, \widetilde{P}(x)e^{iqx} \tag{11.7}$$

which is easy to check by plotting $X_k(p)$ as a function of $q = p\Delta/n(k)$ for different values of $k$. These curves are displayed in Fig. 11.4 and are indeed found to be close to each other in spite of the fact that $n(k)$ ranges from $n(1) = 1$ to $n(30) = 1039$.

We found numerically that the universal characteristic function can be well approximated by the general form

$$\widetilde{X}(q) = \exp\left(-a|q| - \frac{bq^2}{2}\right) \tag{11.8}$$

The value of parameters were found to be $a \approx 1.15$, $b \approx 6.32$. This is the characteristic function of a distribution of a sum of two random variables $x_1$ and $x_2$, where $x_1$ is drawn from Cauchy distribution with probability density

$$p_1(x) = \frac{1}{\pi}\frac{a}{x^2 + a^2} \tag{11.9}$$

and the second is distributed normally according to

$$p_2(x) = \frac{1}{\sqrt{2\pi b}}e^{-\frac{x^2}{2b}}. \tag{11.10}$$

66
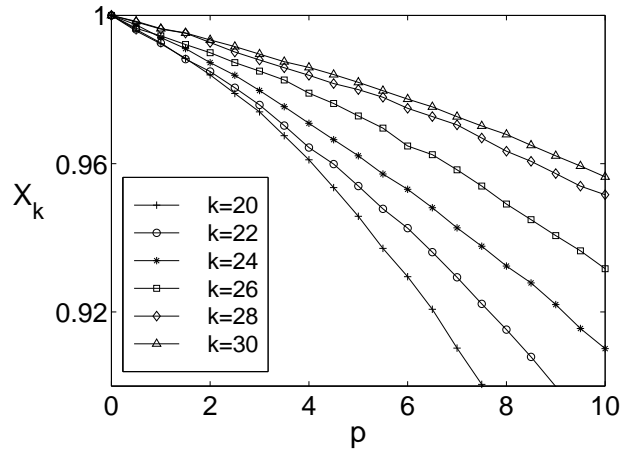
Figure 11.3: The same as on the previous figure for a smaller range of $p$.
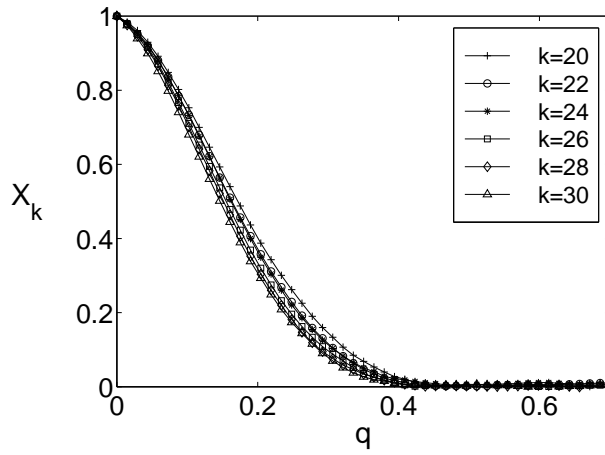


Figure 11.4: The characteristic function $X_k(p)$ as a function of the scaled variable $q = p\Delta/n(k)$ for values of $k$ used in Figs 11.2-11.3

The distribution of $x = x_1 + x_2$ is thus given by

$$\tilde{P}(x) = \int_{-\infty}^{+\infty} dy p_1(x-y) p_2(y) \tag{11.11}$$

and its characteristic function is (11.8). It has a diverging variance due to the fact that $\tilde{P}(x)$ behaves as $\frac{1}{\pi} \frac{a}{x^2}$ for large $|x|$.

The scaling factor $\Delta/n(k)$ and the limiting behavior of the distribution function are the same as those found in the case of mutually independent energies. This allows us to conclude that the behavior of the coefficients $C_k$ given by (10.20), that was obtained in the model with uncorrelated $E_{(\lambda)}$, is satisfied also by the eigenfunctions of the more realistic model of the present section.

# Chapter 12

# Conclusions

Here we present the discussion of the results obtained in this Ph.D work. Then we discuss the possible extensions of our research. The analytical results for the free energy and the magnetization of a mesoscopic super-conductor were derived at the dual point and in the London regimes. We have used a known exact solution for the two dimensional Ginzburg-Landau equations in an infinite plane, valid at the dual point, to study a finite system with boundaries. The infinite system solution approximates well the behavior of the order parameter and the magnetic field in the bulk of the system, while an ansatz was used to approximate the solutions in the boundary region. This division of the system into two regions corresponds to the separation of paramagnetic and diamagnetic behavior of the super-conducting currents. In this way the free energy contains the contributions from the bulk as well as from the boundary region. The diamagnetic boundary region provides the mechanism for selecting the number of vortices as a function of the applied magnetic field. The matching fields for entrance of one additional vortex were calculated and the results show right scaling behavior with the size of the system. This approach enabled us to study thermodynamically stable states but also meta-stable states (to obtain a surface energy barrier).

This model gives theoretical insights into the physical mechanisms involved in the experimental results of [1, 2] and our analytical results agree quantitatively with experimental measurements. In fact, other related thermodynamic quantities such as the surface tension measuring the thermodynamic stability of vortex states can also be computed along this way and could generalize to two-dimensional systems previous results obtained in one dimension [67].

With the help of numerical simulations, we have carried out a perturbative calculation of the free energy in the vicinity of the dual point. The scaling behavior of the free energy was observed. In the limit of large number of vortices some analytical results were obtained in qualitative agreement with the numerical simulations.

More generally, we believe that a theoretical study in the vicinity of the dual point provides a lot of information about the generic solutions of the Ginzburg-Landau equations. We verified that the behavior we found in the vicinity of the dual point, such as the scaling of the free energy, remains valid when $\kappa$ ranges from 0.1 to 10 and this interval of values is indeed relevant for many conventional super-conductors.

Then we studied the properties of a type II super-conductor in the London regime. The main motivation was to obtain analytical results for the properties of a super-conductor at equilibrium and in the meta-stable states. The important goal of our studies was to describe

analytically the topology of the underlying magnetic field profiles and distribution of the order parameter. Once obtained in the London regime, the results concerning the topology hold qualitatively for the whole range of the Ginzburg-Landau parameter. In the London regime, the Ginzburg-Landau equations reduce to a single linear elliptic equation for the magnetic induction that can explicitly be solved in simple geometries. We have derived closed expressions for the free energy and the magnetization of a mesoscopic system which have been obtained as limiting cases of a general calculation valid for a system of any size [38] and not from specific assumptions related to the mesoscopic regime [60]. With these formulae, we have been able to study precisely the matching fields and to compute the paramagnetic Meissner effect, resulting from the existence of meta-stable states.

We devoted much attention to the general and topological study of the meta-stable states using a parallel with the theory of two dimensional dynamical systems. We showed that a vortex pattern can be characterized by as set of topological integers, the number of vortices being one of them. Any change in this set corresponds to a topological transition of the vortex pattern. We calculated the critical fields associated with these transitions and we gave a dual interpretation of these transitions. The simple analytical expressions for the super-conducting currents enabled us to precise the notion of the special curve $\Gamma$, separating the paramagnetic bulk region from the diamagnetic boundary. This curve embodies the main geometric features of a configuration of vortices. Mathematically this curve appears as a limit cycle of the system of currents generated by the vortex pattern.

Our study can be extended in many directions. The scaling results in the vicinity of $\kappa = 1/\sqrt{2}$ were derived from numerical simulations: a systematic perturbative expansion around the dual point would put them on a more rigorous basis. Secondly, a linear stability analysis of the cylindrically symmetrical solution [68] should allow to understand the fragmentation transition between a giant vortex and unit vortices.

The approach that focuses on topological aspects is generic and can be extended, at least in a qualitative manner, to systems beyond the dual or London regime and with different shapes. Here, we considered a circular cylinder to obtain simple analytical expressions. In recent studies, analytic expressions for the free energy of a cylinder with an elliptic cross-section were found in the mesoscopic limit [69] and, more generally, an electrostatic analogy was developed that enables to study mesoscopic super-conductors in the London regime with the help of conformal transformations [70]. In addition, since the separatrix $\Gamma$ exists even for vortex configurations breaking cylindrical symmetry, our approach can be used to analyze hysteretic behavior of meta-stable states, and to study polygonal vortex configurations found numerically in mesoscopic super-conductors [56, 9]. Using such tools, it would be interesting to carry on a quantitative study of topological phase transitions in arbitrary domains.

In this work, only static configurations of vortices have been investigated. A natural extension of the concepts introduced here would be to consider the dynamics of a vortex pattern, where a vortex would move in the field generated by the other vortices. In this context, the study of the deformations of the curve $\Gamma$ would certainly shed some light on the mechanism of vortex nucleation in a super-conducting system.

Now we proceed to the conclusion drawn from the study of quasiparticles in mesoscopic conductors within the framework of Anderson localization in the Hilbert space. The localization properties of the eigenstates of the modified interacting chiral Tomonaga-Luttinger model were studied. For total energy $N\Delta$ subspace we defined an effective lattice of Slater determinants labeled by partitions of $N$ which represent the eigenstates of the system in the absence of interactions. We have observed that in the case of linear dispersion the eigenstates

70

of the interacting model described by the bosons are extended over this lattice. When the random one-particle levels are introduced instead of the equidistant spectrum, the bosons are no more the eigenstates and one has to find another approach to the problem of diagonalizing of the Hamiltonian. In order to achieve this goal we have grouped the different sites (partitions) according to the number of ones, representing the distance of the most excited particle from the Fermi surface in the original Slater determinant. This is to be contrasted with the grouping of many-body states into generations according to the number of excited particles and holes as was firstly done in [20]. Each resulting group of partitions was given a label $k$. The interactions were shown to be of short range in $k$. The interactions were further simplified by assuming that they interconnect only groups of partitions corresponding to the adjacent values of the index $k$ (and the interactions between groups $k$ and $k \pm 2$ were neglected). Assuming further that the states are extended within each group $k$ we obtained an effective tight-binding Anderson model where each group $k$ has an effective random energy and the hopping takes place between the nearest neighbors only. In the assumption of independently distributed on-site energies the model is found to be close to the Lloyd model characterized by a broad distribution of the on-site energies. The main feature of our effective model is that the distribution of energies is $k$-dependent. We employed the site-dependent localization length assumption, which consists in assuming the parameters of distribution change slowly, so locally the localization length is given by the same formula as for the Lloyd model with parameters of the local distribution instead of the uniform global one. Up to an unknown numerical factor this solution describes well the behavior of the localization length as a function of $k$ and it enabled us to show that the eigenstates are localized in the space of groups of partitions, $k$. The weak-coupling and the strong-coupling regimes can be identified according to the value of the parameter $V/\Delta$. In the weak-coupling regime $V \ll \Delta$, the amplitudes decay as $\exp\left(-k \log \sqrt{\frac{N}{6k}} \frac{\Delta}{V}\right)$, namely nearly exponentially. In the strong coupling regime $V \gg \Delta$, this behavior changes to $\exp\left(-\sqrt{\frac{Nk}{24}} \frac{\Delta}{V}\right)$.

One important point which was discussed is the effect of correlations between the many-body energies of the non-interacting system. In the studies devoted to the localization in many-body systems the effective on-site energies corresponding to the eigenstates of the non-interacting system are assumed to be independent random variables, so their spectrum is described by a Poissonian sequence. This is not the case for the true many-body fermionic system, since these energies are sums of independent energies of one-particle excitations. The number of independent random variables is therefore much less than the number of different many-body states. This situation is similar in some sense to one faced in random walk problems, where the increments are distributed independently, while there is a strong correlation between the positions of the random walk at different times. In our work we considered this problem numerically and found that although the correlation between the exact energies corresponding to the eigenstates of the free model are not *a priori* negligible the random energies of the effective sites $k$ are found to be very weakly correlated. Moreover it was found that the parameters of the distribution of the effective energy of the group $k$ scale with the number of the partitions inside the group in the same way as they do in the case of independent many-body energies. This led us to the conclusion that our result for the localization of the eigenstates are valid for more realistic assumptions on the distribution of the many-body energies.

One of the questions arising from our approach to the interacting systems in the mesoscopic

regime is the study of the interacting electrons in dimensions higher than one by the methods of high-dimensional bosonization. In this technique [71, 72, 73, 74, 75] the fermionic system is described as an infinite set of one-dimensional Luttinger models attached to a point on the Fermi surface. Therefore the interactions mix the states belonging to different points in addition to the coupling within the same point (represented by a Luttinger model), which can be treated within the framework developed in the present paper. This possibly can be a mechanism for the delocalization of the states and a resulting localization transition must be compared with the transition encountered in the recent studies [20, 21, 22, 23] of interacting electrons in finite systems.

The nature of localization in the Hilbert space for single-particle dispersions that are more realistic than the random ones is another question to be explored in the future. In addition, the localization properties of the eigenstates exactly solvable one-dimensional models is a problem that can be attacked by analytical methods to provide additional information about interacting systems.

# Appendix A

# The Ginzburg-Landau equations in a cylindrically symmetric system

For a cylindrically symmetric system, we can use $\psi = f(r)e^{in\theta}$ and $\vec{A} = A(r)\hat{e}_\theta$ where $n$ is a non-negative integer which represents the number of vortices at the center of the system. We also define the super-fluid velocity $\vec{v}_s = v_s(r)\hat{e}_\theta$, where

$$v_s(r) = \left(\frac{n}{r} - A(r)\right) \tag{A.1}$$

In this case the Ginzburg-Landau equations are:

$$\frac{d^2 f}{dr^2} + \frac{1}{r}\frac{df}{dr} - v_s^2 f = -2\kappa^2 f(1 - f^2) \tag{A.2}$$

$$\frac{d}{dr}\left(\frac{1}{r}\frac{d}{dr}(rv_s)\right) = 2v_s f^2 \tag{A.3}$$

It is convenient to define the quantity $p(r) = rv_s(r)$. The magnetic field $\vec{B} = B(r)\hat{e}_z$ is given in terms of $p(r)$ by

$$B(r) = -\frac{1}{r}\frac{dp}{dr} \tag{A.4}$$

We obtain finally two coupled ordinary differential equations

$$f'' = -2\kappa^2 f(1 - f^2) + p^2 f/r^2 - f'/r \tag{A.5}$$

$$p'' = 2pf^2 + p'/r \tag{A.6}$$

with the following boundary conditions at $r = a^{-1}$ for $n \neq 0$:

$$\begin{array}{ll} f(0) = 0 & f'(a^{-1}) = 0 \\ p(0) = n & p(a^{-1}) = n - \phi_e \end{array} \tag{A.7}$$

for a disk and

$$\begin{array}{ll} f(0) = 0 & f'(a^{-1}) = 0 \\ p(0) = n & p'(a^{-1}) = -2a\phi_e \end{array} \tag{A.8}$$

for a cylinder. These are the equations we have solved numerically using the relaxation method [76]. From the analysis of the equations (A.6) we deduce the following behaviour in the vicinity of the center of the disk:

$$f \sim r^n \quad \text{and} \quad p \sim r^2 \text{ when } r \to 0$$

The free energy (2.19) is then given in terms of the solution of (A.6) by

$$\frac{\mathcal{F}}{2\pi} = \int_0^{1/a} r\,dr\,\left(\frac{B^2}{2} + \kappa^2\left(1 - f^4\right)\right) \tag{A.9}$$

For the case of infinite system $a = 0$ there are useful identities originating from the radial Ginzburg-Landau equation (A.6). Consider the second equation in (A.6). Its left hand side can be identified with $-B'(r)$ with help of the relation (A.4) for the magnetic field. If we integrate the equation from $r = 0$ to $r = \infty$ and use the boundary conditions which imply that magnetic field vanish at infinity we get

$$B_0 = B(0) = 2\int_0^\infty \frac{dr}{r}\,p(r)f^2(r) \tag{A.10}$$

Next we consider the integral

$$\int_0^\infty r\,dr\,B^2(r) = -\int_0^\infty dr\,r^2 B(r)B'(r) \tag{A.11}$$

where the equality follows from the integration by parts and observation that the contribution from the end-points is zero, as a consequence of the boundary conditions. We use now the second Ginzburg-Landau equation (A.3) to show that

$$BB' = \frac{1}{4r^2}\frac{d}{dr}\left(r^2\frac{B'^2}{f^2}\right) - \frac{B'^2 f'}{2f^3} \tag{A.12}$$

and the first equation (A.2) to express the last term as a derivative plus a term depending on $f(r)$ only:

$$\frac{B'^2 f'}{2f^3} = \frac{1}{r^2}\frac{d}{dr}\left(r^2 f'^2\right) + 4\kappa^2 ff'(1 - f^2). \tag{A.13}$$

Combining this expression with (A.12 we rewrite the integrand in (A.11) as

$$BB' = \frac{1}{4r^2}\frac{d}{dr}\left(r^2\frac{B'^2}{f^2}\right) - \frac{1}{r^2}\frac{d}{dr}\left(r^2 f'^2\right) - 4\kappa^2 ff'(1 - f^2). \tag{A.14}$$

The terms which contain derivatives do not contribute to the integral (A.11) due to the boundary conditions. The only contribution comes from the last term and can be evaluated using the integration by parts:

$$\int_0^\infty r\,dr\,B^2(r) = -\int_0^\infty dr\,r^2 B(r)B'(r) = 2\kappa^2\int_0^\infty r\,dr\,(1 - f^2)^2, \tag{A.15}$$

where the contribution from the end-point vanishes due to the boundary conditions. This identity enables us to rewrite the free energy (A.9) for $a = 0$ (infinite radius) as a functional of $f(r)$ only:

$$\frac{\mathcal{F}}{2\pi} = \kappa^2\int_0^\infty r\,dr\,\left(1 - f^2\right). \tag{A.16}$$

This expression is valid in infinite system for any value of the Ginzburg-Landau parameter, provided $f(r)$ is obtained by solving the equations (A.6). In fact as long as boundary conditions for the order parameter and magnetic field hold approximately at the boundary of a finite domain ( like $\Omega_1$ ) the expression can be used to calculate the thermodynamics of a finite super-conductor.

# Appendix B

# Vector potential of an off-centered configuration with one vortex

In this appendix we measure the distances in units of $R$, so the disk has unit radius.

Suppose that the vortex is located at a distance $x$ from the center of the disk ($0 \leq x < 1$). The phase $\chi(\rho, \theta)$ of the order parameter satisfies $\Delta \chi = 0$ everywhere on the disk except on the vortex with boundary condition $\hat{\mathbf{n}}.\vec{\nabla}\chi = 0$

Using the image method, the phase $\chi(\rho, \theta)$ at a point located at a distance $\rho$ from the center of the disk (with $0 \leq \rho \leq 1$) is given by [40]:

$$\chi(\rho, \theta) = \mathrm{Im}\, \ln \left( \frac{\rho\, e^{i\theta} - x}{\rho\, e^{i\theta} - 1/x} \right) \tag{B.1}$$

where Im denotes the imaginary part part of a complex-valued function. Or equivalently:

$$\tan \chi(\rho, \theta) = \frac{1 - x^2}{1 + x^2} \frac{\theta}{\cos \theta - (\rho + \rho^{-1})/(x + x^{-1})} \tag{B.2}$$

On the boundary of the disk, $\rho = 1$, and one finds that

$$\frac{\partial \chi}{\partial \theta} = \frac{1 - x^2}{1 + x^2} \frac{1}{1 - 2x \cos \theta/(1 + x^2)}, \quad \frac{\partial \chi}{\partial \rho} = 0 \tag{B.3}$$

therefore

$$\int \frac{d\theta}{2\pi} |\vec{\nabla}\chi(1, \theta)|^2 = a^2 \frac{1 + x^2}{1 - x^2} \tag{B.4}$$

The vector-potential $\vec{A}(R)$ at the boundary of the sample is a function of the polar angle $\theta$ since the vortex is not at the center of the disk. We determine $\vec{A}(R)$ from the following conditions:

$$\vec{\nabla} \cdot \vec{A} = 0, \quad \oint_{\partial\Omega} \vec{A}(R) \cdot d\vec{l} = \phi_e$$

and on the boundary $\vec{A}(R) \cdot \hat{\mathbf{n}} = 0$. The following choice,

$$\vec{A}(R) = \phi_e \vec{\nabla}\chi \tag{B.5}$$

valid near boundary of the system, satisfies these requirements.

# Appendix C

# Magnetic induction in a cylinder

We present the solution of the London equation (6.6) for the magnetic induction

$$\nabla^2 B(\vec{r}) - 2B(\vec{r}) = -4\pi \sum_{k=1}^{N} \delta(\vec{r} - \vec{r}_k) \tag{C.1}$$

with the boundary condition $B(R, \theta) = H_e$. The polar coordinates are convenient for this geometry. The equation (C.1) with a vanishing right hand side describes the Meissner regime in the absence of vortices. The corresponding solution of the homogeneous equation is given by the $\theta$-independent function

$$B_M(r) = H_e \frac{I_0(\sqrt{2}r)}{I_0(\sqrt{2}R)}. \tag{C.2}$$

where the functions $I_n(x)$, $K_n(x)$ are modified Bessel functions of first and second kind of order $n$ which provide the regular and singular solutions respectively of (C.1). The solution of the inhomogeneous equation (C.1) for $N$ vortices is written as a sum of the solution of the homogeneous equation and a particular solution:

$$B(r, \theta) = B_M(r) + B_V(r, \theta) + B_{\bar{V}}(r, \theta) \tag{C.3}$$

where $B_V(r, \theta)$ is the solution for $N$ vortices in the unbound domain

$$B_V(r, \theta) = 2 \sum_{k=1}^{N} K_0(\sqrt{2}|\vec{r} - \vec{r}_k|) \tag{C.4}$$

and the term $B_{\bar{V}}(r, \theta)$ is introduced to take care of the boundary conditions:

$$B_{\bar{V}}(R, \theta) = -B_V(R, \theta) = -2 \sum_{k=1}^{N} K_0 \left( \sqrt{2 \left( R^2 + r_k^2 - 2Rr_k \cos(\theta - \theta_k) \right)} \right) \tag{C.5}$$

On the other hand, the field $B_{\bar{V}}$ can be written as a superposition of solutions of (C.1) regular in the interior of the boundary:

$$B_{\bar{V}}(R, \theta) = \sum_{n=-\infty}^{+\infty} c_n I_n(\sqrt{2}r) e^{in\theta} \tag{C.6}$$

76

where, since the field is real, the relation $c_{-n} = c_n^*$ holds. Expanding the lhs of (C.5) into Fourier series using standard identities of Bessel functions [77] we get

$$K_0 \left( \sqrt{2 \left[ R^2 + r_k^2 - 2Rr_k \cos(\theta - \theta_k) \right]} \right) = \sum_{n=-\infty}^{+\infty} K_n(\sqrt{2}R) I_n(\sqrt{2}r_k) e^{in(\theta - \theta_k)}. \qquad \text{(C.7)}$$

Equating the coefficients of the expansion of both sides of equation (C.5) one obtains

$$c_n = \frac{K_n(\sqrt{2}R) I_n(\sqrt{2}r_k)}{I_n(\sqrt{2}R)} e^{-in\theta_k} \qquad \text{(C.8)}$$

from which the expression (6.11) follows immediately.

# Appendix D

# Expression of the Gibbs energy for a cylinder

One takes advantage of the vector identity $(\nabla \times \vec{B}) \cdot (\nabla \times \vec{B}) = \nabla \cdot (\vec{B} \times \nabla \times \vec{B}) + \vec{B} \cdot (\nabla \times \nabla \times \vec{B})$ to rewrite $(\nabla \times \vec{B}) \cdot (\nabla \times \vec{B}) = \nabla \cdot (\vec{B} \times \nabla \times \vec{B}) - \vec{B} \nabla^2 \vec{B}$, since $\nabla \cdot \vec{B} = 0$. Then one uses the London equation (6.6) to rewrite the expression (6.3) for the free energy as

$$\mathcal{F} = \pi \sum_{k=1}^{N} \int_{\Omega} d^2 r \, B(\vec{r}) \delta(\vec{r} - \vec{r}_k) + \frac{1}{4} \int_{\Omega} d^2 r \, \nabla \cdot (\vec{B} \times \nabla \times \vec{B}) \tag{D.1}$$

The singular part $\mathcal{F}_{\infty}$ is obtained from the contribution of $B_V$ to the first integral. The regular contribution to the free energy can be written using Stokes theorem:

$$\mathcal{F} - \mathcal{F}_{\infty} = \pi \sum_{k=1}^{N} B_M(\vec{r}_k) + \pi \sum_{k=1}^{N} B_{\bar{V}}(\vec{r}_k) + \frac{R}{4} \int_0^{2\pi} d\theta \, B(R,\theta) B_r(R,\theta) \tag{D.2}$$

where $B_r$ denotes the partial derivative of $B(r,\theta)$ with respect to $r$ and the fields $B_M$ and $B_{\bar{V}}$ are given by (6.9) and (6.11). In the last term $B(R,\theta) = H_e$ can be taken out of the integration sign and the integral becomes

$$2\pi \frac{dB_M(R)}{dR} + 2\pi \frac{\partial}{\partial R} \int_0^{2\pi} d\theta \, (B_V(R,\theta) + B_{\bar{V}}(R,\theta))$$

$$= 2\sqrt{2}\pi H_e \frac{I_1(\sqrt{2}R)}{I_0(\sqrt{2}R)} - 4\sqrt{2}\pi \sum_{k=1}^{N} \frac{I_0(\sqrt{2}r_k)}{I_0(\sqrt{2}R)} \left( I_0(\sqrt{2}R)K_1(\sqrt{2}R) + K_0(\sqrt{2}R)I_1(\sqrt{2}R) \right)$$

$$\tag{D.3}$$

To prove the last equality the properties of the Bessel functions $I_0'(x) = I_1(x)$, $K_0'(x) = -K_1(x)$ and the expansion (C.7) were used. Only $n = 0$ term contributes to the angular integral. Using another property of Bessel functions $I_0(x)K_1(x) + K_0(x)I_1(x) = 1/x$ and one obtains that:

$$\frac{H_e R}{4} \int_0^{2\pi} d\theta \, B_r(R,\theta) = \frac{\sqrt{2}\pi R H_e^2}{2} \frac{I_1(\sqrt{2}R)}{I_0(\sqrt{2}R)} - \pi \sum_{k=1}^{N} H_e \frac{I_0(\sqrt{2}r_k)}{I_0(\sqrt{2}R)} \tag{D.4}$$

We notice that the contribution from the Meissner field $B_M$ in (D.1) exactly cancels with the second term in the last equation. Hence, the regular part of free energy becomes:

$$\mathcal{F} - \mathcal{F}_\infty = \sqrt{2}\pi R H_e^2 \frac{I_1(\sqrt{2}R)}{I_0(\sqrt{2}R)} - 2\pi \sum_{n=-\infty}^{+\infty} \sum_{j,k=1}^{N} \frac{K_n(\sqrt{2}R)I_n(\sqrt{2}r_j)I_n(\sqrt{2}r_k)}{I_n(\sqrt{2}R)} \cos n(\theta_j - \theta_k)$$

$$(D.5)$$

The term containing the average magnetic induction over the cross section of the cylinder is evaluated along the same lines, using the London equation (6.6):

$$H_e \int_\Omega B(\vec{r})d^2r = 2\pi N H_e + \frac{H_e}{2} \int_\Omega \nabla\cdot\nabla B(\vec{r})d^2r = \sqrt{2}\pi R H_e^2 \frac{I_1(\sqrt{2}R)}{I_0(\sqrt{2}R)} + 2\pi H_e \sum_{k=1}^{N} \left(1 - \frac{I_0(\sqrt{2}r_k)}{I_0(\sqrt{2}R)}\right)$$

$$(D.6)$$

Using the expressions (D.5) and (D.6) in the definition (6.13) of the Gibbs energy completes the derivation of (6.15).

# Appendix E

# Study of the critical points

In order to study critical points of the Hamiltonian system defined in section 5.1, one has to solve the equations (8.6) and (8.7) for a given number $N$ of vortices.

## E.1 Existence and location of the critical points

We first look for critical points which are neither on the boundary of the disk nor at the center, *i.e.* we concentrate on the generic position $0 < r < 1$. When $0 < r < 1$, one deduces that the equation (8.7) is satisfied if $N\theta = 0$, *i.e.* when $\theta = k\pi/N$ for $k = 0, 1, \ldots, 2N - 1$. These values of the angle can be subdivided into two groups according to the sign of $\cos N\theta$. We now discuss the solution of the equation (8.6) for the two cases separately.

### E.1.1 Bulk critical points such that $\cos N\theta = +1$

In this case, we are looking for 'parallel' critical points that lie in the same direction as the vortices. And we shall prove that for any $N$, there exists a critical field $\phi_M(N)$, defined as follows,

$$\phi_M(N) = N(1 + x^N)/(1 - x^N) \tag{E.1}$$

such that when $\phi_e > \phi_M(N)$ there is always a critical point between each vortex and the boundary, and no such point exists if $\phi_e < \phi_M(N)$.

Using the new variables $\xi = x^N$ and $\rho = r^N$ the equation (8.6) reduces to

$$\frac{\phi_e}{N} \rho^{\frac{2}{N}-1} = \frac{\xi^2 - 1}{(1 - \xi\rho)(\xi - \rho)} \tag{E.2}$$

Looking at this equation, it is clear that systems with $N = 1$, $N = 2$ or $N > 2$ should be discussed separately.

- For $N = 1$, the plots of the left and right hand sides of this equation are represented in Fig. E.1. They cross for $\rho < 1$ only if the rhs evaluated at $r = 1$ is less than $\phi_e$, *i.e* for $\phi_e > \phi_M = (1 + \xi)/(1 - \xi) = (1 + x)/(1 - x)$. In this case the solution of (E.2) can be shown to exist using the continuity of the functions. The position of the critical point corresponding to this solution satisfies $\xi < r < 1$, *i.e* the point resides between the vortex and the boundary. For $\phi_e < \phi_M$ there is no solution.
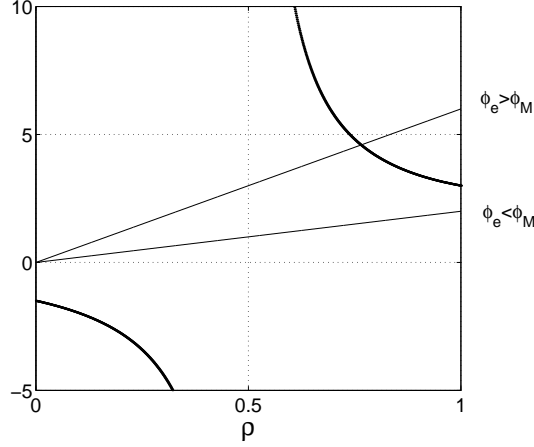
Figure E.1: Graphical solution of the equation (E.2) for one single vortex ($N = 1$). The position of the vortex is taken to be $x = 0.5$.

- For $N \geq 2$, it is worthwhile to consider the reciprocal of (E.2) which rewrites as

$$\frac{N}{\phi_e}\rho^{1-\frac{2}{N}} = \frac{1}{\xi^2 - 1}(1 - \xi\rho)(\xi - \rho) \qquad (E.3)$$

The right hand side is a convex parabola with zeros at $\xi < 1$ and $1/\xi > 1$. For $N = 2$ the lhs is a constant function and it is clear that if $\phi_e > \phi_M = 2(1+\xi)/(1-\xi) = 2(1+x^2)/(1-x^2)$ there is always a solution for $\xi < \rho < 1$, therefore there exists a critical point between the vortex and the boundary, while $\phi_e < \phi_M$ no solution exists. For $N > 2$ the lhs is an increasing fractional power of $\rho$ (see Fig. E.2). The equation (E.3) always has a solution between $\xi$ and 1 if $\phi_e > \phi_M = N(1+\xi)/(1-\xi) = N(1+x^N)/(1-x^N)$ and no solution if $\phi_e < \phi_M$.

### E.1.2  Bulk critical points such that $\cos N\theta = -1$

We are now looking for 'anti-parallel' critical points that lie in a direction bisecting the angle between two neighboring vortices. Here the discussion is more involved:

- when $N = 1$ there appears a critical field $\phi_m(1) = (1 - x)/(1 + x)$ such that: when $\phi_e > \phi_m(1)$ there exists a critical point in the direction opposite to the vortex whereas when $\phi_e < \phi_m(1)$ no such point exists.

- when $N = 2$, there are two critical fields $\phi_m(2)$ and $\phi_c(2)$ such that: when $\phi_m(2) < \phi_e < \phi_c(2)$ there are exactly two anti-parallel critical points and there are no such points when $\phi_e < \phi_m(2)$ or $\phi_e > \phi_c(2)$.

- when $N > 2$, one has again two critical fields $\phi_m(N)$ and $\phi_c(N)$ such that: when $\phi_e < \phi_m(N)$ there exist $N$ anti-parallel critical points, when $\phi_m(N) < \phi_e < \phi_c(N)$, there are $2N$ such points, and when $\phi_e > \phi_c(N)$, there are no anti-parallel critical points.
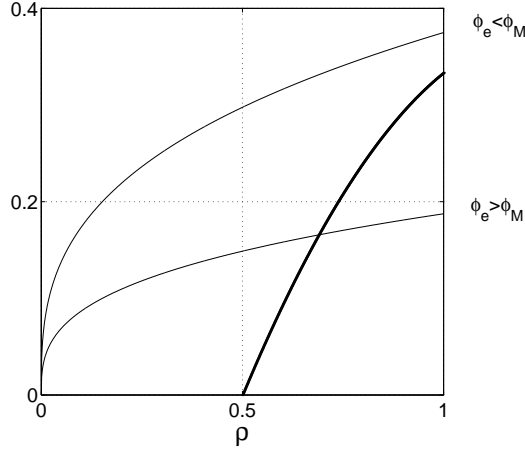
81

Figure E.2: Graphical solution of the equation (E.3) for $N > 2$ vortices. The position of the ring of vortices is taken to be $x = 0.5$.

We now prove these assertions and calculate the corresponding critical fields.

Consider first that $N = 1$; then the equation (8.6) in terms of the variables $\rho$ and $\xi$ becomes

$$\phi_e \rho = \frac{1 - \xi^2}{(1 + \xi\rho)(\xi + \rho)} \qquad (E.4)$$

And a solution exists in the interval $0 < \rho < 1$ if the value of the lhs at $\rho = 1$ exceeds the value of the rhs at the same point, as shown in Fig. E.3. This happens for $\phi_e > \phi_m(1) = (1 - x)/(1 + x)$;

Now, when $N \geq 2$, the equation (8.6) can be rewritten as

$$\frac{N}{\phi_e} \rho^{1 - \frac{2}{N}} = \frac{1}{1 - \xi^2}(1 + \xi\rho)(\xi + \rho) \qquad (E.5)$$

- $N = 2$: this case is illustrated in Fig. E.4. For $\phi_e < \phi_m(2) = 2(1 - \xi)/(1 + \xi) = 2(1 - x^2)/(1 + x^2)$ there is no solution, for $\phi_e = \phi_m(2)$ one solution appears at $\rho = 1$ and it persists for the range of the flux $\phi_m(2) < \phi_e < \phi_c(2) = 2(1 - \xi^2)/\xi = 2(1 - x^4)/x^4$. For higher flux, $\phi_e > \phi_c(2)$, this solution disappears at $\rho = 0$.

- The case $N > 2$ is the most interesting: Fig. E.5 shows the behavior of both sides of the equation (E.5). Comparing the value of the lhs at $\rho = 1$ with that of the rhs and using the fact that $\rho^{1 - \frac{2}{N}}$ has a negative curvature, while that of the rhs is always positive, we can state that for $\phi_e < \phi_m(N)$, where

$$\phi_m(N) = N(1 - \xi)/(1 + \xi) = N(1 - x^N)/(1 + x^N) \qquad (E.6)$$

there is only one solution. Another solution appears at $\rho = 1$ for $\phi_e = \phi_m(N)$ and these two solution move towards each other when the flux is increased in the interval $\phi_m(N) < \phi_e < \phi_c(N)$, whereas at the critical value of the flux $\phi_e = \phi_c(N)$ these two solutions coalesce. For $\phi_e > \phi_c(N)$, the equation (E.5) has no solutions in the interval $0 < \rho < 1$.
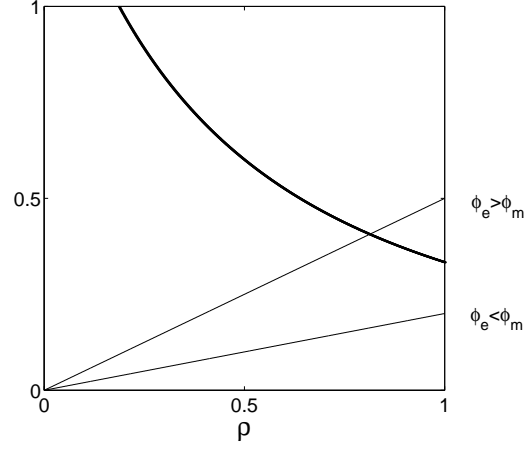
82

Figure E.3: Graphical solution of the equation (E.4) for one single vortex ($N = 1$). The position of the vortex is taken to be $x = 0.5$.
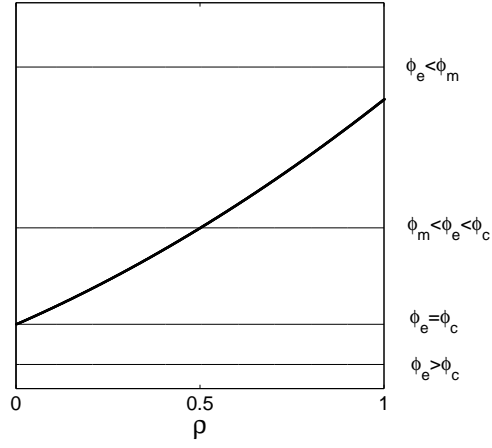


Figure E.4: Graphical solution of the equation (E.5) for $N = 2$ vortices. The position of each vortex is taken to be $x = 0.5$.
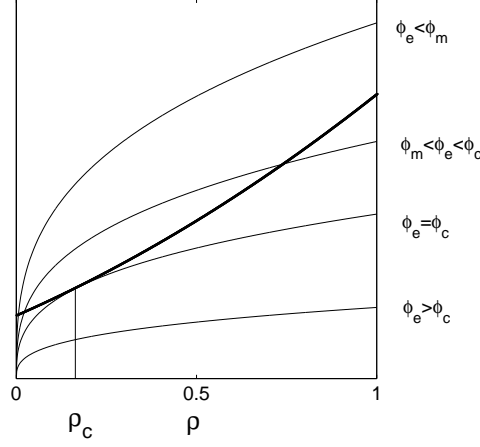
Figure E.5: Graphical solution of the equation (E.5) for $N > 2$ vortices. The position of each vortex is taken to be $x = 0.5$.

Calculation of the critical flux $\phi_c$:

For $\phi_e(N) = \phi_c$ the function $f_{lhs}(\rho) = \frac{N}{\phi_e}\rho^{1-\frac{2}{N}}$ and $f_{rhs}(\rho) = (1 + \xi\rho)(\xi + \rho)/(1 - \xi^2)$ are tangent at some point $\rho = \rho_c$ as shown in Fig. E.5. Equating the value of these functions and the value of their derivatives at $\rho = \rho_c$ we obtain the following equations:

$$\begin{cases} \phi_c(\rho_c + \xi)(1 + \xi\rho_c) & = & N(1 - \xi^2)\rho_c^{1-\frac{2}{N}} \\ \phi_c(2\xi\rho_c + \xi^2 + 1) & = & (N - 2)(1 - \xi^2)\rho_c^{-\frac{2}{N}} \end{cases} . \tag{E.7}$$

Dividing the first equation by the second leads to the quadratic equation for $\rho_c$:

$$(N + 2)\xi\rho_c^2 + 2(\xi^2 + 1)\rho_c - (N - 2)\xi = 0 \tag{E.8}$$

which has the unique positive solution

$$\rho_c = \frac{-(1 + \xi^2) + \sqrt{(1 - \xi^2)^2 + N^2\xi^2}}{(N + 2)\xi} \tag{E.9}$$

The critical flux is obtained by substituting the value of $\rho_c$ into the first equation of (E.7):

$$\phi_c = \frac{N(1 - \xi^2)\rho_c^{1-\frac{2}{N}}}{(\rho_c + \xi)(1 + \xi\rho_c)} \tag{E.10}$$

We notice that for $N = 2$ the formula (E.9) yields the correct value $\rho_c = 0$. Although topologically the cases $N = 2$ and $N > 2$ are different, the critical flux $\phi_c(2) = (1 - \xi^2)/\xi$, as we shall see later, comes out correctly.

### E.1.3 Central and boundary critical points

So far we did not discuss the two cases, $r = 0$ and $r = 1$. For $N = 1$ the center, $r = 0$, of the disk does not satisfy the equations (8.6),(8.7) and therefore is not a critical point. For

$N > 1$ the value $r = 0$ is always a solution of the equations (8.6),(8.7). For the points on the boundary, $r = 1$, the equation (8.7) is always satisfied and substituting the value $r = 1$ into (8.6) we find that there are $2N$ critical points on the boundary with an angle given by the following relation:

$$\cos N\theta = \frac{1}{2x^N} \left[ 1 + x^{2N} - \frac{N(1 - x^{2N})}{\phi_e} \right] \tag{E.11}$$

which is meaningful only for values of the flux between $\phi_m(N)$ and $\phi_M(N)$.

## E.2 The nature of the critical points

We now discuss the topological nature of the critical points and classify them by linearizing the stability exponents near each of these points. The problem is then reduced to the study of the Hessian matrix of the second derivatives

$$H = \begin{pmatrix} \partial_r^2 B & \partial_r \partial_\theta B \\ \partial_\theta \partial_r B & \partial_\theta^2 B \end{pmatrix} \tag{E.12}$$

Since at the critical points inside the disk we have $N\theta = 0$ the mixed derivative vanish and the Hessian matrix is diagonal in polar coordinates. The second derivative with respect to $\theta$ is given at the critical points by

$$\partial_\theta^2 B = -2N^2 \rho \frac{(1 - \rho^2)(1 - \xi^2)}{(1 - \xi\rho)^2(\xi - \rho)^2} < 0 \tag{E.13}$$

for $\cos N\theta = +1$ and by

$$\partial_\theta^2 B = +2N^2 \rho \frac{(1 - \rho^2)(1 - \xi^2)}{(1 + \xi\rho)^2(\xi + \rho)^2} > 0 \tag{E.14}$$

for $\cos N\theta = -1$. The value of the second derivative with respect to $r$ can be obtained by looking at the way the first derivative $\partial_r B$ changes sign near each solution of the equation (8.6). We shall now discuss separately the nature of the critical points in the 'parallel', 'anti-parallel', 'central' and 'boundary' cases.

### E.2.1 Bulk critical points with $\cos N\theta = +1$.

For $\phi_e > \phi_M$, there is only one critical point at $\rho_1$ in the interval $\xi < r < 1$. The results for the second derivatives at this point are summarized in the following table:

| | $0 < \rho < \rho_1$ | $\rho_1 < \rho < 1$ |
|---|---|---|
| $\partial_r B$ | $-$ | $+$ |
| $\partial_r^2 B$ | $+$ | |
| $\partial_\theta^2 B$ | $-$ | |
| Crit. point | Saddle | |

### E.2.2   Bulk critical points with $\cos N\theta = -1$.

The following tables provide a classification of critical points in a variety of regimes.

<u>$N = 1$</u>  $\phi_e < \phi_m$  No critical points.

$\phi_e > \phi_m$  One critical point at $\rho_1$

|  | $0 < \rho < \rho_1$ | $\rho_1 < \rho < 1$ |
|---|---|---|
| $\partial_r B$ | – | + |
| $\partial_r^2 B$ | + | |
| $\partial_\theta^2 B$ | + | |
| Crit. point | Minimum | |

<u>$N = 2$</u>  $\phi_e < \phi_m$  No critical points.

$\phi_m < \phi_e < \phi_c$  One critical point at $\rho_1$

|  | $0 < \rho < \rho_1$ | $\rho_1 < \rho < 1$ |
|---|---|---|
| $\partial_r B$ | – | + |
| $\partial_r^2 B$ | + | |
| $\partial_\theta^2 B$ | + | |
| Crit. point | Minimum | |

$\phi_e > \phi_c$  No critical points.

<u>$N > 2$</u>  $\phi_e < \phi_m$  One critical point at $\rho_1$

|  | $0 < \rho < \rho_1$ | $\rho_1 < \rho < 1$ |
|---|---|---|
| $\partial_r B$ | + | – |
| $\partial_r^2 B$ | – | |
| $\partial_\theta^2 B$ | + | |
| Crit. point | Saddle | |

$\phi_m < \phi_e < \phi_c$  Two critical points at $\rho_1 < \rho_2$

|  | $0 < \rho < \rho_1$ | $\rho_1 < \rho < \rho_2$ | $\rho_2 < \rho < 1$ |
|---|---|---|---|
| $\partial_r B$ | + | – | + |
| $\partial_r^2 B$ | – | | + |
| $\partial_\theta^2 B$ | + | | + |
| Crit. point | Saddle | | Minimum |

$\phi_e > \phi_c$  No critical points.

### E.2.3   Central and boundary critical points.

Consider now the point $r = 0$. Expanding the field $B(r, \theta)$ given by (8.5) for small $r$ we obtain

$$B(r, \theta) \approx -(\phi_e - 2N \ln x) + \phi_e r^2 + 2\cos(N\theta) \left( \frac{1 - \xi^2}{\xi} \right) r^N \qquad \text{(E.15)}$$

As we mentioned before, for $N = 1$ the point $r = 0$ is not a critical point (due to the presence of a term linear in $r$ ). For $N = 2$, two last terms are quadratic in $r$ and the character of the critical point depends on the value of the flux $\phi_e$. For $\phi_e < \phi_c = (1 - \xi^2)/\xi$ the center, $r = 0$, is a saddle, while for $\phi_e > \phi_c$ it turns to be to a minimum. This is to be compared with the prediction of formula E.10. It is interesting to notice that this happens when the minimum located along the line $\cos 2\theta = -1$ disappears at the center. For $N > 2$, the last term in the equation (E.15) is negligible and the center is always a minimum.

When $\phi_m < \phi_e < \phi_M$ we must consider the critical points on the boundary. Since for $r = 1$ the condition $\partial_\theta B = 0$ is satisfied for all $\theta$, we obtain $\partial_\theta^2 B = 0$ and $\partial_r \partial_\theta B \neq 0$ if $\cos^2 N\theta \neq 1$, which is always satisfied for $\phi_e$ in the interval between $\phi_m$ and $\phi_M$. Thus the determinant of the Hessian matrix (E.12), given by $\det H = -(\partial_r \partial_\theta H)^2$, is negative and the eigenvalues are of opposite sign. We conclude that the critical points at the boundary are saddles.

# Appendix F

# A property for characters of $S_N$

In this appendix we show that the property (9.12)

$$\sum_{i,j} \eta_{(...\lambda_i-m...)}\eta_{(...\lambda_i-m...\lambda_j+m...)}\chi_{(l)}^{(...\lambda_i-m...\lambda_j+m...)} = mn_m\chi_{(l)}^{(\lambda)}$$

is satisfied for the characters of the symmetric group $S_N$. We did not find this property in any textbook on the representations of groups, but its validity follows from the known properties of the characters of $S_N$ found, for example, in [63] and [78]. We present the proof of this property here for the sake of completeness of the discussion.

The Frobenius formula as it is written in the classic textbooks on group theory [78, 63] states the following identity between two antisymmetric functions of $N$-dimensional vector $z = (z_1, z_2, \ldots, z_N)$:

$$S_{(l)}(z)D(z) = \sum_{(\lambda)} \chi_{(l)}^{(\lambda)}\Psi_{(\lambda)}(z) \tag{F.1}$$

where $\chi_{(l)}^{(\lambda)}$ is the character of the class $(l)$ of the symmetric group $S_N$ in the irreducible representation $(\lambda)$. With the partition $(\lambda)$ one associates the totally antisymmetric function:

$$\Psi_{(\lambda)}(z) \equiv \sum_P \mathrm{sgn}(P)\, z_{P(1)}^{\lambda_1+N-1} z_{P(2)}^{\lambda_2+N-2} \ldots z_{P(N)}^{\lambda_N} \tag{F.2}$$

where the sum runs over all the permutations of $1, 2, \ldots, N$, the sign of permutation being $\pm$ for an even/odd permutation. This is, up to a normalization constant, a Slater determinant constructed out of one-particle wave-functions $z^{n_i} = z^{\lambda_i+N-i}$, where $z = e^{i\theta}$. The factor $D(z)$ in (F.1) is the Vandermonde determinant:

$$D(z) = \begin{vmatrix} 1 & 1 & \cdots & 1 \\ z_1 & z_2 & \cdots & z_N \\ z_1^2 & z_2^2 & \cdots & z_N^2 \\ \vdots & \vdots & \ddots & \vdots \\ z_1^{N-1} & z_2^{N-1} & \cdots & z_N^{N-1} \end{vmatrix} = \prod_{i<j}(z_i - z_j) \tag{F.3}$$

representing the ground state of $N$ fermions. Let $S_m$ be a power sum of variables $z_j$ defined as follows:

$$S_m(z) = \sum_j z_j^m \tag{F.4}$$

The function $S_m(z)$ is totally symmetric function of the $z_j$-s. These functions are linearly independent as can be checked by calculating the Jacobian:

$$\left| \frac{\partial S_m}{\partial z_j} \right| = N! D(z). \tag{F.5}$$

The class $(l)$ is characterized by $n_1, n_2, \ldots, n_m, \ldots$ cycles of length $1, 2, \ldots, m, \ldots$. For this class the totally symmetric function $S_{(l)}$ is defined as a product of power sums

$$S_{(l)}(z) = S_1^{n_1} S_2^{n_2} \ldots S_N^{n_N} = \prod_{m=1}^{\infty} S_m^{n_m} \tag{F.6}$$

Since for different $m$-s the power sums $S - m$ are linearly independent so are the monomials $S_{(l)}$ for different partitions $(l)$.

The Frobenius formula (F.1) can be inverted with help of the orthogonality relation of the characters:

$$\Psi_{(\lambda)}(z) = \frac{1}{g} \sum_{(l)} g_{(l)} \chi_{(l)}^{(\lambda)} S_{(l)}(z) D(z) \tag{F.7}$$

where $g = N!$ is the order of the $S_N$ and $g_{(l)}$ is the number of elements of $S_N$ in the class $(l)$ given by (9.16).

We turn now to develop a recurrence relation between the characters. For this purpose it is instructive to consider the product of the antisymmetric function $\Psi_{(\mu)}(z)$ and a power sum $S_m(z)$. Since the power sum is totally symmetric the summands can be rearranged in the order set by each permutation and one obtains

$$
\begin{aligned}
S_m(z)\Psi_{(\mu)}(z) &= \sum_P \text{sgn}(P) \left( \sum_i z_{P(i)}^m \right) z_{P(1)}^{\mu_1+N-1} z_{P(2)}^{\mu_2+N-2} \ldots z_{P(N)}^{\mu_N} = \\
&= \sum_i \eta_{(\ldots\mu_i+m\ldots)} \Psi_{(\ldots\mu_i+m\ldots)}(z)
\end{aligned}
\tag{F.8}
$$

where $\eta_{(\ldots\mu_i+m\ldots)} = -1, 0$ or $+1$ is determined accordingly to the rules of Section 2.

Having established the relation between the Slater determinants $\Psi_{(\mu)}$ for various partitions we turn to develop a recurrence relation between the characters. Consider class $(l)$ with at least one $m$-cycle. Let us denote by $(l'_m)$ the class obtained by removing one $m$-cycle from $(l)$. It is then clear that

$$S_{(l)} = S_m S_{(l'_m)} = \left( \sum_j z_j^m \right) S_{(l'_m)} \tag{F.9}$$

The partition $(l'_m)$ defines a class in the symmetry group $S_{N-m}$. The Frobenius formula (F.1) for this class reads

$$S_{(l'_m)} D(z) = \sum_{(\mu')} \chi_{(l'_m)}^{(\mu')} \Psi_{(\mu')} \tag{F.10}$$

while for $(l)$ it can be rewritten with the help of (F.8) in the form

$$
\begin{aligned}
S_{(l)} D(z) &= S_m S_{(l'_m)} D(z) = \sum_{(\mu')} \chi_{(l'_m)}^{(\mu')} S_m \Psi_{(\mu')} = \\
&= \sum_{(\mu')} \chi_{(l'_m)}^{(\mu')} \sum_i \eta_{(\ldots\mu'_i+m\ldots)} \Psi_{(\ldots\mu'_i+m\ldots)}
\end{aligned}
\tag{F.11}
$$

89

Comparing the coefficients of the $\Psi_{(\mu')}$ in (F.11) with those in (F.1) we find the recurrence relation of the characters

$$\chi_{(l)}^{(\lambda)} = \sum_i \eta_{(...\lambda_i - m...)} \chi_{(l'_m)}^{(...\lambda_i - m...)} \tag{F.12}$$

This relation yields the characters of $S_N$ in terms of the characters of the symmetric group $S_{N-m}$.

In order to derive (9.12) take some particular $m$ and let each partition $(l)$ contain $m$ as its part $n_m^{(l)}$ times. For each $(\lambda)$ consider the following sum over partitions:

$$F_{(\lambda)}(z) = \frac{1}{g} \sum_{(l)} g_{(l)} m n_m^{(l)} \chi_{(l)}^{(\lambda)} S_{(l)}(z) \tag{F.13}$$

If $(l)$ has no parts equal to $m$, $n_m^{(l)} = 0$ and $(l)$ does not contribute to this sum. We want to factor out $S_m(z)$ from the sum and for this purpose we can write $S_{(l)}(z) = S_m(z) S_{(l'_m)}(z)$, so that the sum is over $(l'_m)$. With the help of (9.16) we see that the expansion coefficients satisfy

$$g_{(l)} m n_m / g = m n_m \prod_{k=1}^{\infty} \frac{1}{k^{n_k} n_k!} = \frac{m n_m}{m^{n_m} n_m!} \prod_{k \neq m} \frac{1}{k^{n_k} n_k!}$$

$$= \frac{1}{m^{n_m - 1} (n_m - 1)!} \prod_{k \neq m} \frac{1}{k^{n_k} n_k!} = g_{(l'_m)} / g' \tag{F.14}$$

where $g' = (N - m)!$. The sum in (F.13) takes the form

$$F_{(\lambda)}(z) = \left( \sum_j z_j^m \right) \frac{1}{g'} \sum_{(l'_m)} g_{(l'_m)} \chi_{(l)}^{(\lambda)} S_{(l'_m)}(z) \tag{F.15}$$

Application of the recurrence relation (F.12) to the characters in the sum together with the inverse Frobenius formula (F.7) yields

$$
\begin{aligned}
F_{(\lambda)}(z) D(z) &= S_m(z) \sum_i \eta_{(...\lambda_i - m...)} \frac{1}{g'} \sum_{(l'_m)} g_{(l'_m)} \chi_{(l'_m)}^{(...\lambda_i - m...)} S_{(l'_m)}(z) D(z) = \\
&= \sum_i \eta_{(...\lambda_i - m...)} S_m(z) \Psi_{(...\lambda_i - m...)}(z) \tag{F.16}
\end{aligned}
$$

The relation (F.8) is applied to show that

$$F_{(\lambda)}(z) D(z) = \sum_{i,j} \eta_{(...\lambda_i - m...)} \eta_{(...\lambda_i - m...\lambda_j + m...)} \Psi_{(...\lambda_i - m...\lambda_j + m...)}(z) \tag{F.17}$$

Application of the inverse Frobenius formula (F.7) yields

$$F_{(\lambda)}(z) = \frac{1}{g} \sum_{ij} \sum_{(l)} \eta_{(...\lambda_i - m...)} \eta_{(...\lambda_i - m...\lambda_j + m...)} g_{(l)} \chi_{(l)}^{(...\lambda_i - m...\lambda_j + m...)} S_{(l)}(z) \tag{F.18}$$

Making use of the linear independence of $S_{(l)}$ for different partitions $(l)$ and equating the coefficients of the $S_{(l)}(z)$ with the corresponding coefficients in (F.13) results in the required relation (9.12).

# Appendix G

# Number of distinct parts of partitions

In this appendix we show that $d(N)$ – the number of distinct parts in the partitions of $N$ with parts $\lambda_i \geq 2$ equals $p(N-2)$ – the number of unrestricted partitions of $N-2$. Together with the generating function (9.5) for the number of partitions let us introduce the generating function

$$\tilde{p}(z,q) = \sum_{N=1}^{\infty} \sum_{d=1}^{\infty} \tilde{p}(N,d) q^N z^d \tag{G.1}$$

for the number $\tilde{p}(N,d)$ of partitions of $N$ having entries that satisfy $\lambda_i \geq 2$ and having exactly $d$ distinct parts. For example for $N = 6$ and $d = 2$ this number is $\tilde{p}(N,d) = 1$, corresponding to the partition $(4,2)$ as can be seen from the list (10.1). The number of distinct parts $d(N)$ in all partitions of $N$ with parts $\geq 2$ is then given by

$$d(N) = \sum_{d=1}^{N} d\tilde{p}(N,d) \tag{G.2}$$

It is generated by the following function

$$d(q) = \sum_{N=1}^{\infty} d(N) q^N = z \frac{d}{dz} \tilde{p}(z,q) \Big|_{z=1} \tag{G.3}$$

The explicit expression for $\tilde{p}(z,q)$ can be found easily summing directly over all the appropriate partitions:

$$\tilde{p}(z,q) = \sum_{(\lambda),\lambda_i \geq 2} q^{|(\lambda)|} z^{d(\lambda)} \tag{G.4}$$

where $d(\lambda)$ is the number of distinct parts in $(\lambda)$ and $|(\lambda)| = \sum_i \lambda_i$. It is convenient to use the sets of "occupation numbers" $\{n_m\}$, where $n_m$ – the number of times $m$ appears in the partition $(\lambda)$. Noting that $|(\lambda)| = \sum_i \lambda_i = \sum_m m n_m$ and $d(\lambda) = \sum_m \theta(n_m)$, where $\theta(x)$ is the Heavyside step function we rewrite (G.4) as a sum over all the configurations $\{n_m\}$, with $m \geq 2$

$$
\begin{aligned}
\tilde{p}(z,q) &= \sum_{\{n_m\},m \geq 2} q^{\sum_{m=2}^{\infty} m n_m} z^{\sum_{m=2}^{\infty} \theta(n_m)} = \prod_{m=2}^{\infty} \sum_{n_m=0}^{\infty} q^{m n_m} z^{\theta(n_m)} = \\
&= \prod_{m=2}^{\infty} \left( 1 + \frac{z q^m}{1 - q^m} \right)
\end{aligned}
\tag{G.5}
$$

Differentiating this expression with respect to $z$ at $z = 1$ we get

$$d(q) = z\frac{d}{dz} \prod_{m=2}^{\infty} \left(1 + \frac{zq^m}{1 - q^m}\right)\bigg|_{z=1} = q^2 \prod_{m=1}^{\infty} \frac{1}{1 - q^m} = q^2 p(q) \qquad \text{(G.6)}$$

where $p(q)$ is given by (9.5). The function $q^2 p(q)$ is the generating function for $p(N - 2)$. The equality of the generating functions $d(q)$ and $q^2 p(q)$ implies the equality of the coefficients: $d(N) = p(N - 2)$, i.e. the number of different parts in all partitions of $N$ with entries $\geq 2$ is given by the number of unrestricted partitions of $N - 2$. Applying this argumentation to all partitions ending with $N - k$ ones yields $d(k) = p(k - 2)$.

# Appendix H

# Distribution of harmonic sum of independent random variables

We consider the harmonic mean $X$ defined as

$$\frac{1}{X} = \frac{1}{N} \sum_{n=1}^{N} \frac{1}{x_n} \tag{H.1}$$

of $N$ independent random variables $x_1, x_2, \ldots x_N$ drawn from the common distribution with probability density $P(x)$. The only requirement we impose on $P(x)$ is that

$$\lim_{x \to 0} P(x) = C > 0 \tag{H.2}$$

Consider the random variable $y = 1/x$. Its distribution function $Q(y)$ can be calculated by the standard methods. For $y \to \pm\infty$ it has the asymptotic behavior

$$Q(y) \to \frac{C}{y^2} \tag{H.3}$$

and its second moment diverges. The general theory of broad distributions [79, 80, 81] predicts that in the limit $N \to \infty$ the probability density of the sum (H.1) $Y = 1/X$ is Lorenzian

$$Q_N(Y) = \frac{1}{\pi} \frac{\pi C}{(\pi C)^2 + Y^2} \tag{H.4}$$

and consequently the probability density $P_N(X))$ of variable $X = 1/Y$ is again a Lorenzian:

$$P_N(X) = \frac{1}{\pi} \frac{\delta}{\delta^2 + X^2} \tag{H.5}$$

characterized by the parameter $\delta$ related to the original distribution $P(x)$ by the formula:

$$\delta = \frac{1}{\pi C} \tag{H.6}$$

In particular for the uniform distribution (10.14) it takes the value $\delta = \Delta/\pi$.

93

# References

[1] A.K. Geim, I.V. Grigorieva, S.V. Dubonos, J.G.S. Lok, J.C. Maan, A.E. Filippov and F.M. Peeters, Nature, **390**, 259 (1997).

[2] A.K. Geim, S.V. Dubonos, J.G.S. Lok, M. Henini and J.C. Maan, Nature, **396**, 144 (1998).

[3] J. Pearl, Appl. Phys. Lett. **5**, 65 (1964).

[4] G.J. Dolan, J. Low. Temp. Phys. **15**, 111 (1974).

[5] A.K. Geim, S.V. Dubonos, and J.J. Palacios Phys. Rev. Lett. **85**, 1528-1531 (2000).

[6] P. Singha Deo, F.M. Peeters and V.A. Schweigert, Superlattices Microstruc. **25**, 1195 (1999).

[7] V.A. Schweigert, F.M. Peeters, and P. Singha Deo, Phys. Rev. Lett. 81, 2783 (1998).

[8] P. Singha Deo, V.A. Schweigert and F.M. Peeters Phys. Rev. B **59**, 6039 (1999).

[9] J.J. Palacios, Phys. Rev. B **58**, R5948 (1998).

[10] J.J. Palacios, Phys. Rev. Lett. **84**, 1796 (2000).

[11] V.A. Schweigert, P. Singha Deo and F.M. Peeters, Phys. Rev. Lett. **81**, 2783 (1998).

[12] V.V. Moshchalkov, L. Gielen, C. Strunk, R. Jonckheere, X. Qiu, C. Van Haesendonck and Y. Bruynseraede, Nature, **373**, 319 (1995).

[13] O. Buisson, P. Gandit, R. Rammal, Y.Y. Wang and B. Pannetier, Phys. Lett. A **150**, 36 (1990).

[14] W. A. Little and R.D. Parks, Phys. Rev. Lett. **9**, 9 (1962).

[15] R. P. Groff and R.D. Parks, Phys. Rev **176**, 567 (1968).

[16] R. Benoist and W. Zwerger, Z. Phys. B **103**, 377 (1997).

[17] U. Sivan, F.P. Milliken, S. Rishton, Y. Lee, J.M. Hong, V. Boegli, D. Kern, and M. de Franza, Europhys. Lett. **25**, 605 (1994).

[18] B.L. Altshuler and A.G. Aronov, Pis'ma Zh. Eksp. Teor. Fiz. **30**, 514 (1979) [Sov. Phys. JETP Lett. **30**, 482 (1979)]

[19] U. Sivan, Y. Imry, and A.G. Aronov, Europhys. Lett. **28**, 115 (1994)

[20] B. L. Altshuler, Y. Gefen, A. Kamenev, L. S. Levitov, Phys. Rev. Lett. **78**, 2803 (1997).

[21] A.D. Mirlin and Y.V Fyodorov, Phys. Rev. B **56**, 13393 (1997).

[22] R. Berkovitz and Y. Avishai, Phys. Rev. Lett. **80**, 568 (1998).

[23] M. Pascaud, G. Montambaux, cond-mat/9810211.

[24] P.G. Silvestrov, Phys. Rev. Lett. **79**, 3994 (1997).

[25] P. W. Anderson, Phys. Rev. **109**, 1492 (1958).

[26] See, for example, M. Blann, Annu. Rev. Nucl. Sci **25**, 123 (1975); D. Agassi, H.A. Weidenmuller, and G. Mantzouranis, Phys. Rep. **21C**, 1451 (1975); H. Feshbach, A. Kerman, and S. Koonin, Ann. Phys. (N.Y.) **125**, 429, (1980); H. Nishioka, H.A. Weidenmuller, and S. Yoshida, Ann. Phys. (N.Y.) **183**, 166 (1988); A. Bohr and B.R. Mottelson, *Nuclear Structure* (W.A. Benjamin, Inc., New York, Amsterdam, 1969); A.J. Konig and J.M. Akkermans, Ann. Phys. (N.Y.) **208**, 216 (1991), and references therein.

[27] R. Abou-Chacra, P.W. Andeson, D.J. Thouless, J. Phys. C **6**, 1734 (1973).

[28] H. Kunz and B. Souillard, J. Phys. (France) Lett. **44**, 411 (1983).

[29] B. Shapiro, Phys. Rev. Lett. **50**, 747 (1983).

[30] E. Abrahams, P.W. Anderson, D.C. Licciardello and T.V. Ramakrishnan, Phys. Rev. Lett. **42**, 673 (1979).

[31] H. Kunz and B. Souillard, J. Phys. (France) Lett. **44**, L-503 (1983).

[32] Carlos Mejfa-Monasterio, Jean Richert, Thomas Rupp, and Hans A. Weidenmüller, Phys. Rev. Lett. **81**, 5189 (1998).

[33] D. Saint-James, E.J. Thomas and G. Sarma, *Type II Superconductivity* (Pergamon Press, Oxford 1969).

[34] E.B. Bogomol'nyi, Yad. Fiz. **24**, 861 (1976) [Sov. J. Nucl. Phys. **24**, 449 (1977)].

[35] J.L. Harden and V. Arp, Cryogenics **3**, 105 (1963).

[36] C. Taubes, Comm. Math. Phys. **72**, 277 (1980).

[37] L. Jacobs and C. Rebbi, Phys. Rev. B **19**, 4486 (1979).

[38] G. Böbel, Nuovo Cimento **38**, 6320 (1965).

[39] E.A. Shapoval, JETP Letters **69**, 577 (1999).

[40] A.L. Fetter, Phys. Rev. B **22**, 1200 (1980).

[41] P.G. de Gennes, *Superconductivity of metals and alloys* (Addison-Wesley, New York, 1989).

[42] C.P. Bean and J.D. Livingston, Phys. Rev. Lett. **12**, 14 (1964).

[43] A.S. Krasilnikov, L.G. Mamsurova, N.G. Trusevich, L.G. Shcherbakova and K.K Pukhov, Supercond. Sci. Technol **8**, 1 (1995).

[44] P.A. Venegas and E. Sardella, Phys. Rev. B **58**, 5789 (1998)

[45] J.J. Palacios, Phys. Rev. B **58**, R5948 (1998).

[46] E. Akkermans and K. Mallick, J.Phys. **A32**, 7133 (1999); E. Akkermans, D.M. Gangardt and K. Mallick, Phys. Rev. B **62**, 12427 (2000).

[47] E.H. Lieb and D. C. Mattis *Mathematical physics in one dimension : exactly soluble models of interacting particles* (Academic Press , 1966)

[48] For general references see: M. Stone, editor, *Bosonization* (World Scientific, 1994), F. D. M. Haldane, J. Phys. C **14**, 2585, (1981).

[49] K. Ishii, Progr. Theor. Phys. Suppl. **53**, 77 (1973).

[50] F. London, *Superfluids, Vol. 1: Macroscopic theory of superconductivity* (Dover, New York, 1960).

[51] V.A. Schweigert and F.M. Peeters, Phys. Rev. B **57**, 13817 (1998).

[52] E. Akkermans and K. Mallick, J. Phys. A. **32**, 7133 (1999).

[53] G. Dunne, private communication.

[54] For a discussion of topological aspects, see E. Akkermans and K. Mallick, in *Topological Aspects of Low dimensional systems*, Les Houches Lecture Notes, July 1998, Interéditions (Springer-Verlag, Berlin, 2000).

[55] V.A. Schweigert and F.M. Peeters, Phys.Rev.Lett. **83**, 2409 (1999); V.A. Schweigert and F.M. Peeters, Physica C **332**, 266 (2000).

[56] P. Singha Deo, V.A. Schweigert, F.M. Peeters and A.K. Geim, Phys. Rev. Lett. **79**, 4653 (1997).

[57] E. Akkermans, D. Gangardt and K. Mallick, Phys. Rev. B **63**, 64523 (2001).

[58] A.A. Abrikosov, *Fundamentals of the theory of metals* (North-Holland, Amsterdam, 1988).

[59] P.A. Venegas and E. Sardella, Phys.Rev. B **58**, 5789 (1998).

[60] A.I. Buzdin and J.P. Brison, Phys. Lett. A **196**, 267 (1994).

[61] M. Morse, *Topological methods in the theory of functions of a complex variable* (Princeton University Press, Princeton, NJ, 1947).

[62] G. E. Andrews, *The Theory of Partitions* (Addison-Wesley, Reading, 1976).

[63] D. E. Littlewood, *The Theory of Group Characters and Matrix Representations and Groups*, 2nd ed. (Oxford, 1950).

[64] J.-L. Pichard and G. Sarma, J. Phys. C **18**, 3457 (1985).

[65] F.M. Izrailev and A.A. Krokhin, Phys. Rev. Lett. **82** 4062 (1999).

[66] N. Brenner and S. Fishman, Nonlinearity **4**, 211 (1992).

[67] A.T. Dorsey, Ann. Phys. **233**, 248 (1994).

[68] E.B. Bogomol'nyi and A.I. Vainshtein, Sov. J. Nucl. Phys. **23**, 588 (1976).

[69] C. Meyers and M. Daumens, Phys.Rev. B **62**, 9762 (2000).

[70] A. Buzdin and M. Daumens, Physica C **332**, 108 (2000).

[71] A.H. Castro Neto and Eduardo H. Fradkin, Phys. Rev. B. **51**, 4084 (1995).

[72] A. Houghton, J.B. Marston, Phys. Rev. B. **48**, 7790 (1993).

[73] A. Houghton, H.-J. Kwon, and J.B. Marston, Phys. Rev. B. **50**, 1351 (1994).

[74] P. Kopietz, J. Hermisson, and K.Schönhammer, Phys. Rev. B **52**, 10877 (1995).

[75] P. Kopietz and K.Schönhammer, Z. Phys. B **100**, 259 (1996).

[76] W.H. Press, B.P. Flannery, S.A. Teukolsky and W.T. Vetterling, *Numerical Recipes: The Art of Scientific Computing* (Cambridge University Press, Cambridge, 1992).

[77] M. Abramowitz and I.A. Stegun, *Handbook of mathematical functions*, (Dover, New York 1965).

[78] M. Hammermesh, *Group Theory and its Application to Physical Problems* (Addison-Wesley, 1962).

[79] J.-P. Bouchaud and A. Georges, Phys. Rep. **195**, 127 (1990).

[80] P. Levy, *Théorie de l'Addition des Variables Aléatoires* (Gauthier Villars, Paris 1954).

[81] B.V. Gnedenko and A.N. Kolmogorov, *Limit Distributions for Sums of Independent Random Variables* (Addison-Wesley, Reading, MA 1954).